NASA CR 182142

[redacted]

NASA

LARGE SCALE ADVANCED PROP-FAN (LAP) TECHNOLOGY ASSESSMENT REPORT

By: C.L. DeGeorge

HAMILTON STANDARD DIVISION
UNITED TECHNOLOGIES CORPORATION

Prepared for

National Aeronautics and Space Administration
NASA-Lewis Research Center
Contract NAS3-23051

NASA CR 182142

NASA

LARGE SCALE ADVANCED PROP-FAN (LAP) TECHNOLOGY ASSESSMENT REPORT

By: C.L. DeGeorge

HAMILTON STANDARD DIVISION
UNITED TECHNOLOGIES CORPORATION

Prepared for

National Aeronautics and Space Administration
NASA-Lewis Research Center
Contract NAS3-23051

TABLE OF CONTENTS

TABLE OF CONTENTS
(Continued)

LIST OF ILLUSTRATIONS

LIST OF ILLUSTRATIONS
(Continued)

LIST OF TABLES

1.0 SUMMARY

This report describes the technologically significant findings and accomplishments of the Large Scale Advanced Prop-Fan (LAP) Program in the areas of aerodynamics, aeroelasticity, acoustics, and materials and fabrication. The extent to which the design goals related to these disciplines were achieved by the SR-7L and SR-7A Prop-Fans is also discussed. Finally, recommendations are made for additional research in those disciplines that would advance the technology readiness of Prop-Fans.

In the area of aerodynamics, the SR-7L performance, measured statically and in a wind tunnel, is discussed and compared with predictions. Reasons for discrepancies between measured and predicted static performance are hypothesized and means of improving the ability to predict static performance are suggested. Extensive measurement of the steady and unsteady pressure distribution on the surface of the SR-7L blades was accomplished for a range of Prop-Fan operating conditions. The measured pressure distributions are employed to explain the observed Prop-Fan performance and the usefulness of the surface pressure data is considered.

The discussion of aeroelasticity concentrates on blade natural frequencies, stalled and unstalled Prop-Fan stability and Prop-Fan forced response. Methods used to predict the natural frequencies of Prop-Fan blades are correlated with test data. A stall buffet phenomena was observed during Prop-Fan static operation. The high blade vibratory stress encountered during stall buffet prevented the SR-7L Prop-Fan from absorbing design power statically. The characteristics of the stall buffet are analyzed. No indications of unstalled flutter were found for the Prop-Fan operating points run during the LAP program, which was as predicted. The methods used to predict Prop-Fan blade forced response are discussed, and measured and predicted forced vibratory responses of the SR-7L and SR-7A Prop-Fans are compared.

No significant acoustic work was conducted during the LAP program. The acoustic design of the Prop-Fan was conducted in the preliminary design contract (NAS3-22394) which preceded the LAP program. Measurement of Prop-Fan acoustic performance and comparison of prediction with data will be accomplished in the follow-on Prop-Fan Test Assessment (PTA) Program. However, some of the blade surface steady pressure data acquired during the LAP program has significant implications for Prop-Fan noise predictions. The application of this data to Prop-Fan noise prediction is discussed.

In the LAP program, Prop-Fan aerodynamic technology was implemented without resorting to the use of exotic materials or the development of new manufacturing techniques. The procedures used in the fabrication of the SR-7L and SR-7A Prop-Fans are outlined.

2.0 INTRODUCTION

National energy demand has outpaced domestic supply, creating an increased U.S. dependence on foreign sources. As one element in the overall solution to this problem, NASA in 1975 established the Aircraft Energy Efficiency (ACEE) Program, directed at reducing the fuel consumption of commercial subsonic air transports. One component of the ACEE program showing significant potential for fuel saving was the development of advanced technology turboprops. State of the art turboprop propulsion systems provide excellent fuel efficiency at speeds to Mach .6. Analytical studies and research with wind tunnel models have indicated that the inherent fuel efficiency of the turboprop can be extended to the Mach .8, 35,000 foot altitude operating regime of todays commercial turbofan-powered airlines. These efforts have resulted in projections that a 30 to 40 percent fuel savings, relative to current in service turbofan-powered aircraft, could be realized by the use of an advanced turboprop.

The term Prop-Fan has come to be accepted as the nomenclature for advanced turboprop systems designed for speeds up to Mach .8. Prop-Fans achieve high efficiency in this speed range by the application of thin swept wing technology to the design of propeller blades and by achieving high disc loading through the use of a greater number of blades. In 1983 the Hamilton Standard Division of United Technologies Corporation, under contract to the NASA Lewis Research Center, undertook the task of designing, fabricating and testing a near full scale Prop-Fan which was designated the Large Scale Advanced Prop Fan or LAP. The design parameters for the LAP included 8 blades and a 9 foot diameter disk with a blade tip speed of 255 m/sec (800 ft/sec). The LAP was to be designed for a maximum takeoff power of 4413KW (6000 H.P.) and a design cruise power of 1906 KW (2592 H.P.) at 35,000 ft and Mach .8. The desired net propulsive efficiency at the design cruise condition was 78.6%. The acoustic requirements were a near field noise level of 144 dB at the design cruise condition and a far field noise level on takeoff meeting FAR 36 minus 10 dB. The Large Scale Advanced Prop-Fan is depicted in Figure 2.1.

The specific objectives undertaken by Hamilton Standard under the LAP program were as follows:

1. Design and fabricate large-scale, flightworthy, advanced technology Prop-Fan blades for testing and evaluation.

2. Evaluate Prop-Fan blade structural characteristics (natural frequencies and modes, strength, fatigue life, and FOD tolerance) through specimen and large-scale blade tests.

3. Design and fabricate flightworthy hub, pitch change mechanism, and pitch control hardware for use in Prop-Fan system testing.

4. Experimentally determine the operating characteristics of the hub, blade retention, pitch change mechanism, and pitch control at simulated operating conditions.

5. Experimentally determine the Prop-Fan performance, overspeed characteristics, and stall flutter boundaries at static (zero forward speed) conditions.

6. Experimentally evaluate the Prop-Fan high speed flutter characteristics.

7. Design, fabricate and test an aeroelastic model Prop-Fan having the same aerodynamic characteristics and similar aeroelastic characteristics as the Large Scale Advanced Prop-Fan.

8. Deliver Prop-Fan assemblies for planned testing with a drive system.

Based on the functional requirements for the Large Scale Advanced Prop-Fan and the overall objectives of the program, significant technical investigation and development were required in the areas of aerodynamics, aeroelasticity and aeroacoustics. This report presents the significant work performed and results obtained in each of the areas under the Large Scale Advanced Prop-Fan contract. The results obtained are also compared with the program objectives and recommendations are made for additional research and development. Because of funding limitations, various tests which were originally planned were not conducted. These tests were the static and rotating blade FOD; higher stress level hub and blade fatigue; spinner ESA and fatigue; aeroelastic model spin pit, nacelle wing and acoustic flight.

The LAP program was accomplished without having to advance the state of the art in the area of materials and fabrication. However, the materials and manufacturing techniques used in the creation of the SR-7L and SR-7A Prop-Fans are described.

A number of Contractor Reports covering the design of the SR-7L and SR-7A have been published. They are:

* CR-174786 Hub/Blade Retention Design - M. Soule

* CR-174788 Pitch Change Actuator and Control Design - R. Schwartz, P. Carvalho, M. Cutler

* CR-174790 Blade Design - W. Sullivan, J. Turnberg, J. Violette

* CR-174791 Aeroelastic Model Design - D. Nagle, S. Auyeung, J. Turngerg

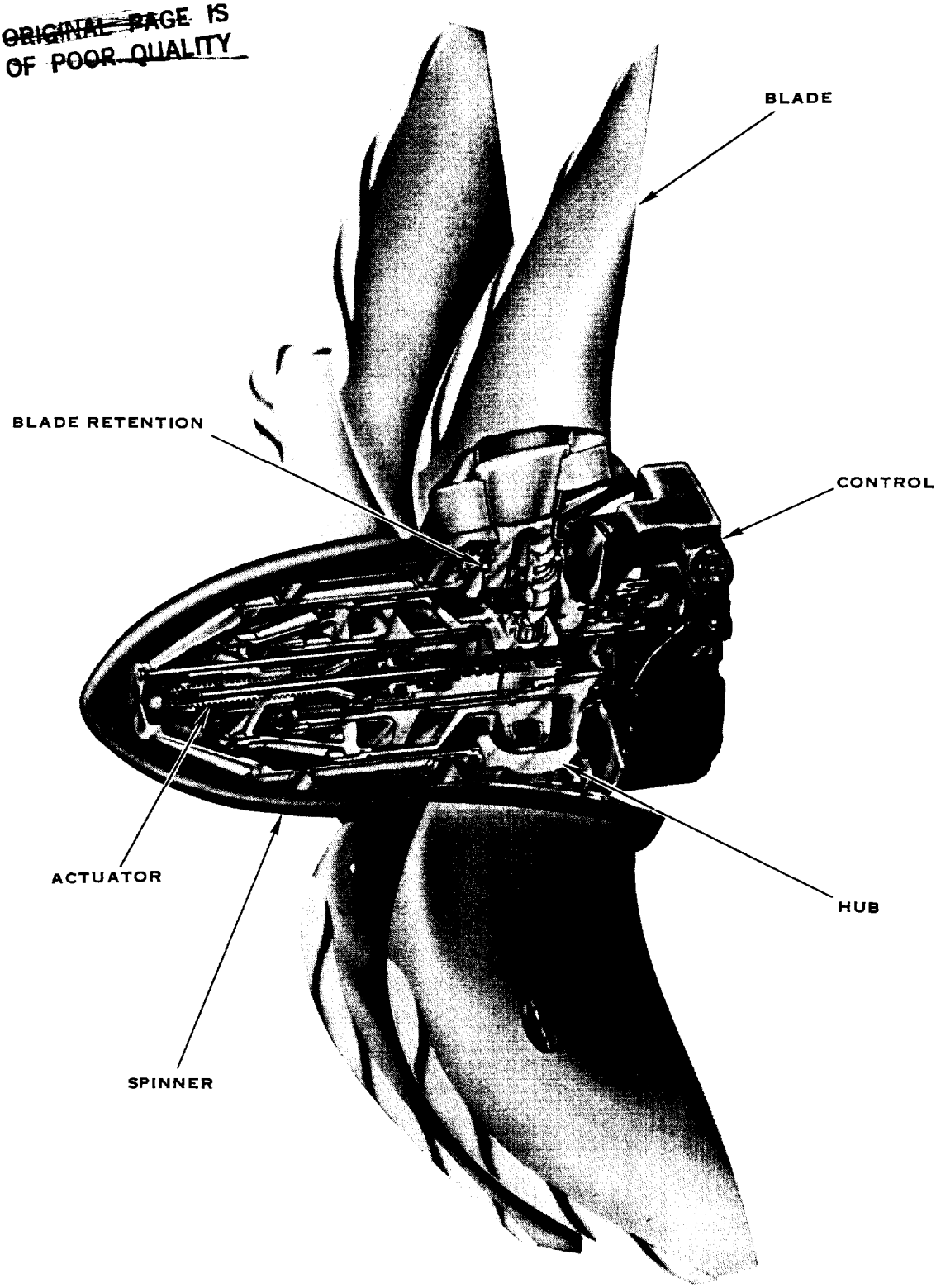

FIGURE 2.1 LARGE SCALE ADVANCED PROP-FAN

E-37990

3.0 AERODYNAMICS

The aerodynamic design of the Large Scale Advanced Prop-Fan (designated the SR-7L) was conducted during the course of a NASA preliminary design study contract (NAS3-22394), which preceded the initiation of the LAP program. The results of the design study are presented in detail in reference 1. However the procedure and results are summarized here as background for the aerodynamic research conducted during the LAP program.

The aerodynamic design of the SR-7L Prop-Fan blade was accomplished using a proprietary Hamilton Standard Compressible Vortex Computer Program (H409) for the blade sections outboard of the 50% radius. This program accounts for the effects of the supersonic Mach number zone of influence and the swept lifting line on the induced velocities at the blades. The program utilizes two dimensional, compressible airfoil data which is corrected for blade sweep, cascade interference and the blade tip Mach cone. The inboard blade sections were designed using a proprietary Pratt & Whitney Streamline Computer Program (A654). This program utilizes a cascade program which accounts for compressibility.

The first step in the design process was to determine the effect of various parameters on the aerodynamic performance. The parameters that were examined included the number of blades, the blade sweep, thickness ratio, planform, twist and stacking. In the vicinity of the design cruise operating point (.8 Mn, 35000 ft), the aerodynamic efficiency of the Prop-Fan was found to increase with the number of blades for a constant solidity. Efficiency also increased with blade sweep up to 40°. Efficiency was found to be very sensitive to thickness ratio, efficiency increasing with decreasing thickness ratio. The planform studies showed that a narrow tip planform was optimum for aerodynamic efficiency. The parameter study was able to determine an optimum twist distribution, and any variation from this optimum that was studied caused significant degradation in efficiency. Blade stacking was found to have essentially no effect on aerodynamic performance.

The SR-7L aerodynamic design was the result of compromises between optimizing aerodynamic, acoustic and mechanical factors. The Prop-Fan design employed eight blades. The blade design makes use of a NACA Series 16 airfoil outboard and a Series 65 circular arc airfoil inboard. Each blade has an activity factory of 227 with 37° of sweep at the tip. The blades were designed with predeflection so that they assume the optimum twist distribution when subjected to the aerodynamic and centrifugal loads of the design cruise condition.

All of the aerodynamic data obtained for the SR-7L during the course of the Large Scale Advanced Prop Fan Program was derived from two tests; the Static Rotor Test conducted at Wright Patterson Air Force Base in Dayton, Ohio and the High Speed Wind Tunnel test conducted in the ONERA S1 atmospheric wind tunnel in Modane, France. The combination of the test facilities and operating conditions prevented the achievement of the design performance conditions. For the Static Rotor Test the SR-7L Prop Fan was mounted on a 10,000 HP electric motor driven whirl rig. No relative air velocity was supplied to

the Prop-Fan rotor. The Prop-Fan was operated over a wide range of rotational speeds and blade angles. The Prop-Fan is shown installed on the static whirl rig in Figure 3.1. The High Speed Wind Tunnel Test was conducted at Mach numbers from .2 to .83 and over a wide range of blade pitch angles and Mach numbers. The drive system on which the Prop Fan was mounted was rated for 1000 kw (1341 hp), which was well below the rated power of the Prop-Fan. Therefore, the Prop-Fan was run in two and four blade configurations as well as with eight blades so that power loadings per blade approaching the design value could be obtained, however without cascade effects. The two, four and eight blade Prop-Fan configuration are shown installed in the wind tunnel in Figure 3.2. The drive system also allowed the axis of rotation of the Prop-Fan to be canted, creating an inflow angle at the Prop-Fan disc and unsteady flow in the reference frame of the rotating blades.

Three types of aerodynamic investigations were conducted during both the Static Rotor and High Speed Wind Tunnel Tests. First the aerodynamic performance was mapped over the range of test points runs. This was accomplished by measuring the net thrust produced and power absorbed at each test point, correcting the data to standard atmospheric conditions and reducing it to coefficient form ($C_{T_{net}}$, C_p). The thrust and power measurement were made using instrumentation integral to the test facilities. Mapping of the pressure distribution over the entire SR-7L blade surface was accomplished for a series of Prop-Fan operating points for which the flow over the blade surface was essentially steady. This was accomplished by installing a specially fabricated pressure tap blade in the Prop-Fan. The locations of the pressure taps on the surface of this blade are illustrated in Figure 3.3. It is believed that this was the most extensive instrumenting of a full size propeller blade ever accomplished. Measurement of surface pressure at several blade surface locations was also accomplished for operating conditions resulting in unsteady flow on the blade surface. This was achieved by installing pressure transducers on the blade surface. The transducer locations are illustrated in Figure 3.4. Details of how these tests were conducted and of the data reduction procedure employed are discussed in references 2 and 3.

3.1 Aerodynamic Performance

3.1.1 Static Performance

Curves of the corrected power absorbed and corrected thrust produced versus blade angle for a constant RPM are presented in Figures 3.5 and 3.6 for static operation of the SR-7L Prop Fan. Figure 3.7 presents the predicted curve of static power coefficient versus blade pitch angle. Figure 3.8 presents the predicted curve of thrust coefficient versus power coefficient. Thrust coefficient data and power coefficient data are overlayed on the predicted curves. The predicted curves were generated using Hamilton Standard Computer Program H444 (Reference 4). Figure 3.6 shows a smooth increase in thrust between blade angles of -6° and 30°. Thrust then decreases slightly between blade angle of 30° and 34° and then is essentially constant from 34° to 60°. Figures 3.7 and 3.8 show good agreement between data and predictions at blade

angles below 30°, however a divergence between data and predictions is observed above 30°. Both thrust produced and power absorbed by the Prop-Fan are lower than predicted above blade angles of 30°.

In view of the shapes observed in the performance curves, the data from previous static tests of single rotation Prop-Fan wind tunnel models was carefully reviewed. Under close examination it was found that similar shapes of the C_P versus 3/4 and C_T versus C_P curves were present to some degree in all prior test data for single rotation Prop-Fan wind tunnel models including the SR-2, SR-3 and SR-5. Data illustrating this behavior for the SR-3 Prop-Fan is presented in Figures 3.9 and 3.10. Of the models tested, the SR-3 is most aerodynamically like the SR-7L. In general, the performance curves for all Prop-Fans are similar and tend to have a maximum thrust coefficient of .6 to .7 at a power coefficient greater than .7.

The reason for the shortfall in static performance at high blade angle is not clear from the data presented here. Referring to the thrust versus blade angle data in Figure 3.6, the deviation of the measured performance occurs at the same blade angle, independent of the RPM. Since the performance shortfall is observed at rotational speeds as low as 900 RPM, it is unlikely that it was caused by shock separation or compressibility. The 900 RPM rotational speed results in blade tip speeds in the Mach .3 to Mach .4 range. This type of behavior may be indicative of stall. However, calculations made with computer program H444 indicate angles of attack well below stall at the outboard blade sections for blade angles beyond 34°. The H444 program uses a classical undistorted wake model to obtain variable inflow distributions for performance predictions. This model may not accurately represent the actual physical wake geometry for the highly loaded SR-7L Prop-Fan operating statically at high blade angle. Therefore the angle of attack distribution along the blade may be different than was predicted.

Aerodynamic analysis programs have been developed that make use of empirical wake description formulae which define the distorted wake based on flow visualization studies. This method utilizes lifting line theory and incorporates a wake model consisting of a finite number of trailing vortex filaments. The trajectories and positioning of these filaments must be prescribed based on the empirical formulae. Once the position of the wake is fixed, a matrix solution is generated utilizing the Kutta-Joukouski and Biot-Savart relations and the airfoil lift properties. This solution yields the blade circulation distribution and the corresponding induced velocities. The blade element velocity diagram is then constructed and the loading distribution is obtained. One such program is the Hamilton Standard program PANPER. Because of the discrepancies that were noted between the static aerodynamic data and the predictions made using H444, the curve of static thrust coefficient versus power coefficient was recomputed using PANPER. The results obtained using PANPER are compared with the H444 predictions as well as with the test data in Figure 3.11. The comparison shows that the PANPER calculations are a better match to test data than the H444 prediction above a power coefficient of .7. However, H444 more closely matches the data below a Cp of .7. Furthermore, there is still a 13% discrepancy between the data and the PANPER calculation

at power coefficients higher than .7. Therefore PANPER does not appear to be a significant improvement over H444 in predicting the static performance of Prop-Fans. One reason for this may be that the empirical wake description formulae used in the program were derived from wake visualization studies conducted for a standard propeller. The wake configuration for a Prop Fan may be substantially different. This suggests that flow visualization studies need to be performed on Prop-Fans to determine their wake geometry and thus improve the tools available for calculating their static performance.

3.1.2 Performance, Mn > 0

The net thrust determined during wind tunnel testing was the uninstalled thrust of the Prop Fan, operating in the presence of a spinner and centerbody. In order to determine the net thrust, the measured thrust was corrected for spinner drag, backpressure and buoyancy force.

The spinner drag causes a force which acts in a direction opposite to the thrust produced by the blades. The spinner drag force was computed by multiplying the spinner drag coefficient by the free stream dynamic pressure at each test point and the spinner reference area. The spinner drag coefficient was experimentally determined as a function of Mach number in preliminary wind tunnel testing. The spinner drag force is added to the measured thrust to obtain net thrust.

The spinner back pressure causes an increase in measured thrust due to the differential, between the pressure behind the spinner and the freestream pressure, acting on the spinner bulkhead. The back pressure force is determined by the integration of the measured pressure distribution behind the spinner and is subtracted from the measured thrust to obtain net thrust.

The buoyance force is the apparent increase in measured thrust caused by the interaction between the Prop-Fan rotor and the centerbody or nacelle downstream of the rotor. The buoyancy force is equal to the difference between the centerbody drag measured at the operating point of interest and the centerbody drag measured at the same Mach number without the rotor present. The centerbody drag is determined by the integration of the measured centerbody surface pressures. The buoyancy force is subtracted from the measured thrust to obtain net thrust.

Curves of the net thrust coefficient versus power coefficient are presented for a range of advance ratios and Mach numbers in Figures 3.12 and 3.13. The data represents the performance obtained with both the four blade and eight blade Prop-Fan configurations which were run in the wind tunnel. These curves show that the net thrust coefficient exhibits smooth consistent variation with power coefficient and advance ratio.

Figures 3.14 and 3.15 show comparisons of the calculated and experimentally determined performance of the four blade and eight blade Prop-Fan configurations. The predicted and measured performance agree very well in both cases. It may be concluded from this that the H444 analysis program provides good results for flight operating conditions where the angle of attack at all the blade stations is well away from the stall point.

3.2 Blade Surface Steady Pressure Testing

3.2.1 Static Performance

Blade surface steady pressure data acquired during the static rotor test provided some insights into the peculiar behavior of static thrust as blade angle was increased beyond 30°. Figures 3.16 and 3.17 describe the variation of blade surface pressure with blade angle at the innermost (r/R = .287) and outermost (r/R = .963) blade stations at which data was taken., At the inboard blade station, the area between the face side and camber side pressure distribution curves increase continuously as blade angle is varied from 22° to 38°. This demonstrates that the airfoil section normal force coefficient also increases continuously with blade angle from 22° to 38°. At the outboard most blade station, the opposite trend is observed. The area between face and camber side pressure distribution curves decreases steadily with increasing blade angle. The implication of this data is that for static operating conditions, a loss of lift occurs at the blade tip as blade angle is increased beyond 30°. Since the Prop-Fan thrust coefficient was found not to increase as blade angle was increased beyond 30°, it is concluded that the increase in loading in the inboard portion of the blade is being offset by the decrease in loading of the blade tip. Figure 3.18 shows the distribution of the airfoil section normal force coefficient versus percent span on the blade for 900 RPM and a range of blade angles. The normal force coefficient was determined by integration of the pressure distribution data. For a blade angle of 22° a sharp rise in section normal force coefficient is noted near the tip of the blade ($.93 < r/R < 1.0$). For blade angles of 32° and 38° a decrease in normal force coefficient is noted in the tip region. Since thrust does not increase as the blade angle advances beyond 30°, it is concluded that the increase in loading in the inboard portion of the blade is being offset by the decrease in loading of the blade tip. The normal force coefficient distribution for 1300 RPM and a 32° blade angle is also compared to the 32° blade angle data taken at 900 RPM. This comparison shows minor variation of the section normal force coefficient with RPM as would be expected.

Since the Static Rotor Test results showed that the SR-7L blade pressure distribution near the tip was significantly different than expected, three additional rows of pressure taps were added to the steady pressure measurement blade outboard of the r/R = .963 blade station. This allowed a much more thorough investigation of aerodynamic phenomena at the blade tip. Data was recorded for some nominal static operating conditions during wind tunnel testing. Mach numbers in the range from .01 to .04 were obtained for this testing due to flow induced in the tunnel by the action of the Prop-Fan. The data of Figure 3.19 reveals a suction peak on the camber surface of the blade tip. The suction peak was observed to move forward on the blade surface as blade pitch angle was increased and then disappeared. The suction peak disappeared as blade angle was increased from 26° to 30°. This corresponds closely with the blade angle at which static thrust ceased to increase with blade angle as was depicted in Figure 3.6. The suction peak was possibly the result of roll up of the blade tip vortex onto the camber surface of the blade. This causes increased lift due to the lower pressures on the suction surface of the blade resulting from the vortex. The absence of the suction peak at blade

angles above 26° could be the result of the vortex collapsing due to flow separation. The data of Figure 3.19 indicates that vortex flow was also present on the leading edge of the Prop-Fan blade. This is evidenced by the negative pressure peaks at the leading edge of the blade which is present at all the blade stations where pressure data was measured. The leading edge vortex is driven by blade sweep and also generates additional lift due to low pressure in the vortex acting on the camber surface.

As previously mentioned, the static cases run in the ONERA wind tunnel were actually quasi-static cases because flow induced in the tunnel by the Prop-Fan resulted in Mach numbers between .01 and .04. It was noted that when attempting to duplicate operating conditions, Mach number varied in this range even though Prop-Fan RPM and power coefficient were matched identically. The reasons for this variation were attributed to changes in ambient atmospheric conditions and mechanical factors within the wind tunnel. The effects of this variability in Mach number were investigated by comparing the pressure data taken at the same blade station for two operatng conditions where RPM and power coefficient were matched but the Mach number differed. The results of this investigation revealed that these small changes in Mach number had a very large effect on blade surface pressure distribution, at least on the suction surface of the blade. This is illustrated in Figure 3.20. A change in Mach number from .02 to .04, power coefficient and RPM held constant, caused the leading edge loading hump, which was indicative of leading edge vortex flow, to disappear. It is concluded from this data that the SR-7L blade surface pressure distribution is extremely sensitive to variations in Mach number about $M_n = 0$.

3.2.2 Operation at $M_n > 0$

Blade surface steady pressure data was acquired during wind tunnel testing at Mach numbers in the range from .2 to .78. All of this testing was accomplished using the two blade Prop-Fan configuration.

Some of the aerodynamic effects that are apparent in Figures 3.21 through 3.27 are leading edge vortex loading at 0.20 Mach number for the take-off power case (Figure 3.22), inverted leading edge pressure distributions for the low power cases at high Mach numbers (Figures 3.23, 3.24, 3.25, 3.26 and 3.27) and evidence of trailing edge shock waves at the outboard stations at high Mach numbers (evident by the trailing edge pressure jump in Figures 3.25, 3.26 and 3.27). The inverted leading edge pressure distributions, as noted above, are typial for cambered airfoil sections operating at incidence the design angle of attack value.

The significance of this blade surface pressure data is that it is extensive enough to provide a thorough picture of the complex three dimensional flow that occurs on highly swept Prop-Fan blades. The data is also sufficient to provide an understanding of how these flows vary with such parameters as power loading, advance ratio and Mach number. If sufficient analysis of this data is conducted and the data is correlated with predictions made with state of the art analytical tools, it should be possible to make significant improvements in aerodynamic design techniques for Prop-Fan blades. This should hasten the evolution of the Prop-Fan to a commercially viable product.

3.3 Blade Surface Unsteady Pressure Testing

3.3.1 Static Conditions

The purpose of employing the unsteady pressure measurement blade during the static rotor test was to determine the feasibility of measuring time varying pressures on the surface of the SR-7L blade. The method chosen to create the unsteady pressure was the placement of a 10 cm (2.5 inch) diameter obstruction approximately .6 meters (24 inches) in front of the blade pitch axis. The obstruction spanned from the blade root to well beyond the blade tip. It was believed that the inflow to the Prop-Fan rotor disc, passing over the obstruction, would create a pressure pulse that could be sensed by transducers installed in the blade surface.

Initial testing accomplished with the unsteady pressure measurement blade revealed that none of the transducers were sensing a pressure pulse at blade angles from 22° to 38° and at rotational speeds from 600 RPM to 1700 RPM. Tufts were then attached to the flow obstruction and at other locations near the plane of rotation of the Prop-Fan in an attempt to visualize the inflow. The motion of the tufts indicated that the inflow to the Prop-Fan was more radial than had been expected and therefore the wake created by the obstruction was not being intersected by the blade stations containing the transducers. By attaching flat plates to the cylindrical obstruction, a wake was generated that intersected the pressure transducers at the inboard blade station. The pressure variation measured by one of the transducer at the 35.0 inch blade station is shown in Figure 3.28. A pressure pulse with an amplitude of 1034 Pascal (.15 psi) is detected once per revolution. This demonstrated that the measurement of time varying pressures on the surface of a Prop-Fan blade was viable.

3.3.2 Operation at Mn > 0

Blade surface unsteady pressure data was acquired during wind tunnel testing at Mach numbers in the range from .02 to .70. All of this testing was accomplished using the two blade Prop-Fan configuration. Data was acquired both with and without a wake generator in the Prop-Fan inflow.

Figure 3.29 presents examples of the measured unsteady pressures. The data shown is for a representative take-off condition (Mn=0.2, J=0.883, Cp=0.250 and B3/4=32°), and is for a transducer located on the camber side of the blade, at the 90% radius and at 56% chord.

The pressure versus time plots at the left in Figure 3.29 were obtained from a signal enhancing waveform analyzer. Sampling was initiated by the recorded once per revolution pip signal and waveforms from 1024 revolutions were averaged. Thus the repetitive portion of the pressure waveform is enhanced and the random part is suppressed. The spectra, shown at the right in Figure 3.29, were obtained via digital Fourier transform analysis. Successive time slices were transformed and averaged for 4.8 seconds. Each spectrum contains 400 frequency points spaced linearly from 0 to 500 Hertz.

Preliminary interpretation of the data shows:

In the waveforms, a transducer can be considered to be scanning the inlet flow as it rotates. Since the blade position is known as a function of time, the time axis can be converted to angular position. For the trace at the top, representing clean inflow, the signal level should be low, corresponding to a low distortion level. However, a small sinusoidal component can be seen in the waveform and spectrum that must be caused by a residual flow angularity in the tunnel. This can be considered a background level and must be subtracted from the data for the 3° angular inflow and for the cylinder wakes.

In the data for the 3° angular flow, the angle of attack seen by the instrumented blade should be nearly a pure sinewave at the once per revolution (1P) frequency. Simplistic analysis would indicate that the blade pressure response should also be sinusoidal. The waveform and spectrum show that this is far from true. Figure 3.30 illustrates the terms "advancing" and "retreating" for angular inflow. Further evaluation of the data at other positions on the blade is required to identify the source of this non-sinusoidal behavior.

For the data with the cylinder wake, the blade pressure should respond with a pulse each time the blade passes through a wake at the top and bottom of the revolution. This behavior is observed in the bottom trace, but the pulse magnitudes are surprisingly different at the top and bottom positions. Another interesting feature of the data for cylinder wakes is the oscillating response after the wake pulse.

Sinusoidal response was observed on the pressure (face) side of the blade in all cases examined for angular inflow conditions.

Sinusoidal response was also observed on the suction (camber) side of the blade under low loading conditions. However, under high loading conditions, non-sinusoidal behavior is present. The non-sinusoidal response appears to be a result of leading edge and tip vortices which may be distorting the response. Another possibility is the formation and breakdown of the vortices as the angular inflow or wake inflow modulates the angle of attack.

The significance of this blade surface pressure data is that it is extensive enough to provide a thorough picture of the complex three dimensional flow that occurs on highly swept Prop-Fan blades. The data is also sufficient to provide an understanding of how these flows vary with such parameters as power loading, advance ratio and Mach number. If sufficient analysis of this data is conducted and the data is correlated with predictions made with state of the art analytical tools, it should be possible to make significant improvements in aerodynamic design techniques for Prop-Fan blades. This should hasten the evolution of the Prop-Fan to a commercially viable product.

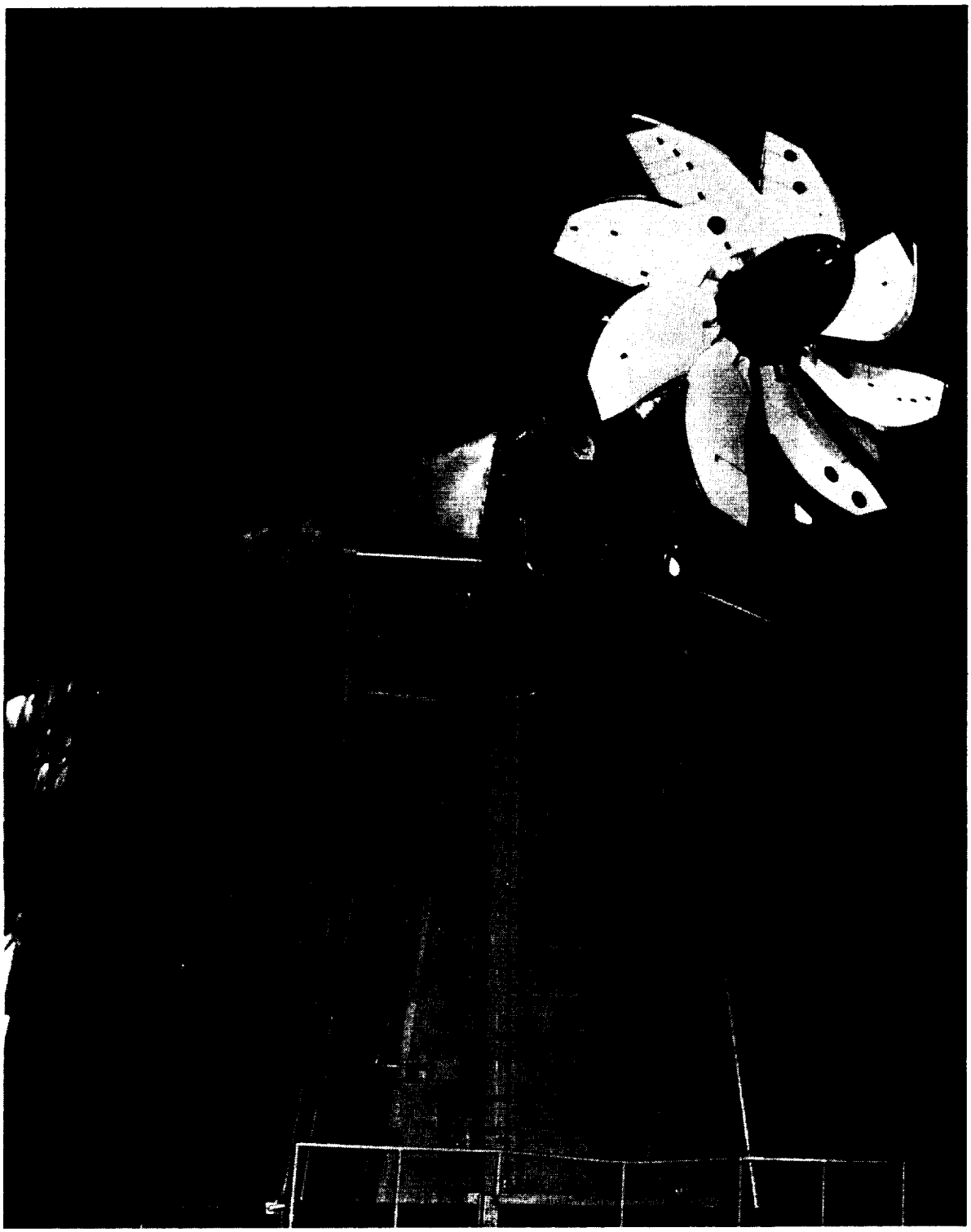

FIGURE 3.1 SR–7L PROP–FAN ON WPAFB WHIRL RIG E-37994

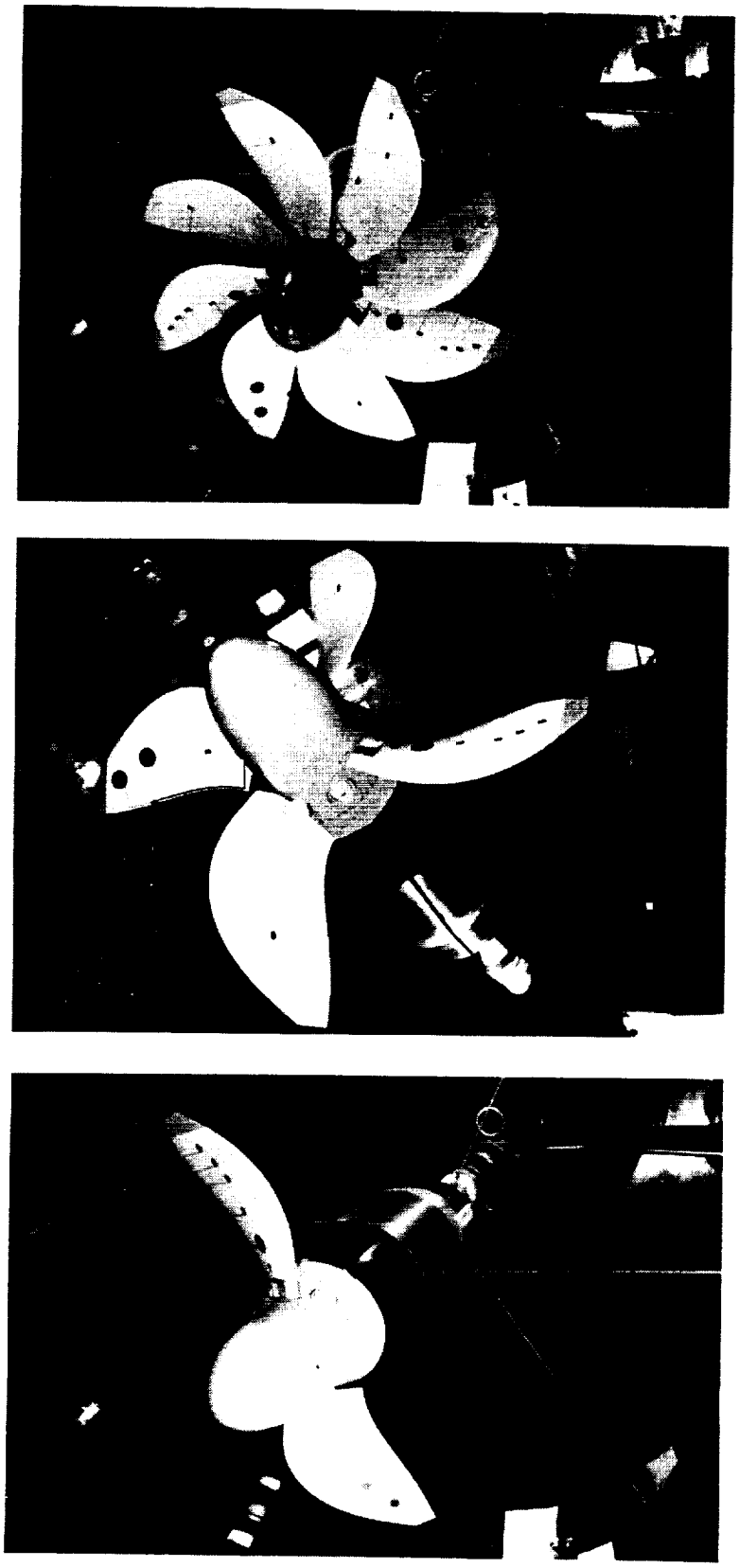

E-37987

FIGURE 3.2 PROP FAN TWO, FOUR AND EIGHT BLADE CONFIGURATIONS, HIGH SPEED WIND TUNNEL TESTS

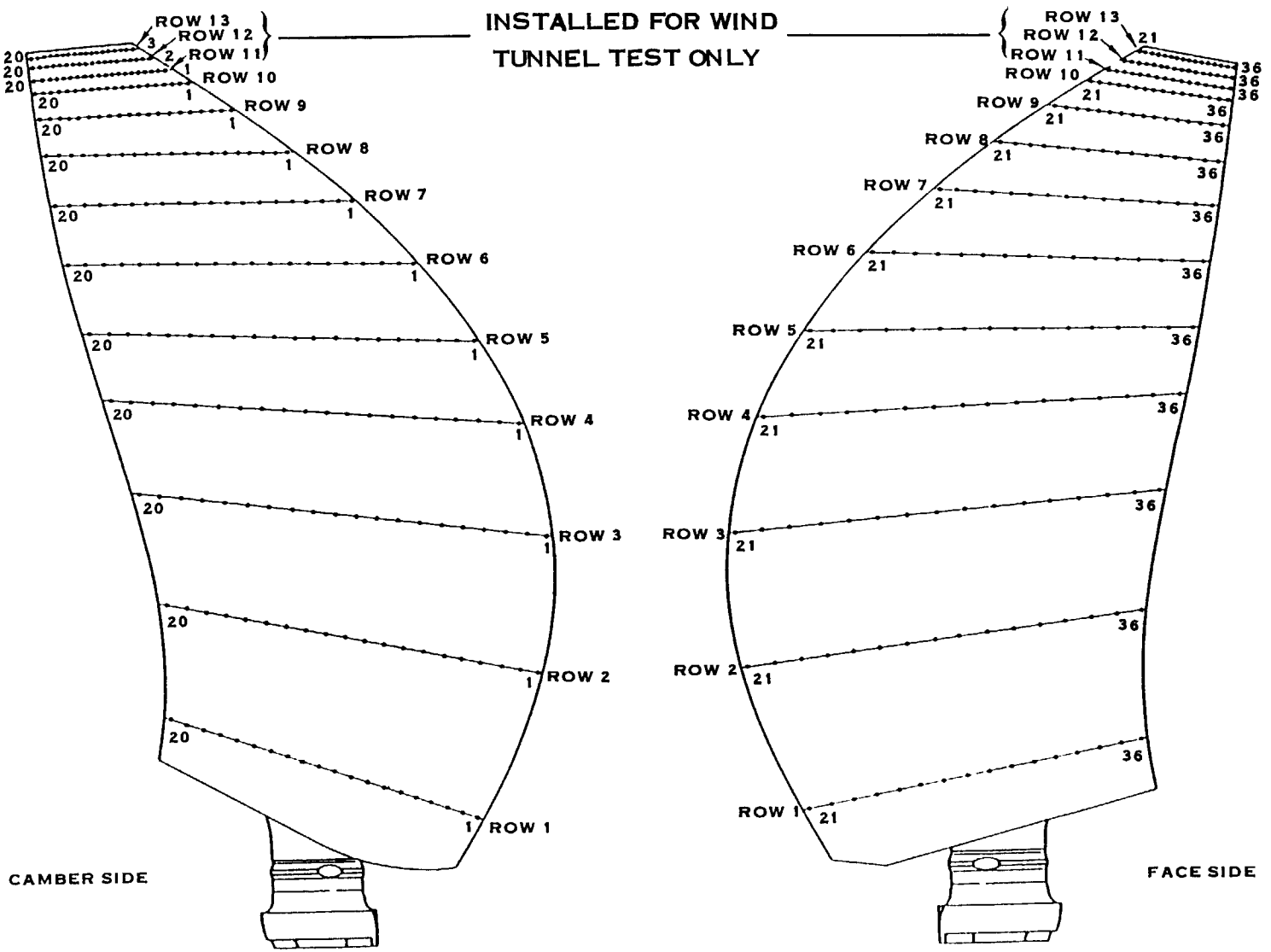

FIGURE 3.3 TAP LOCATIONS, STEADY PRESSURE BLADE, HIGH SPEED WIND TUNNEL TEST

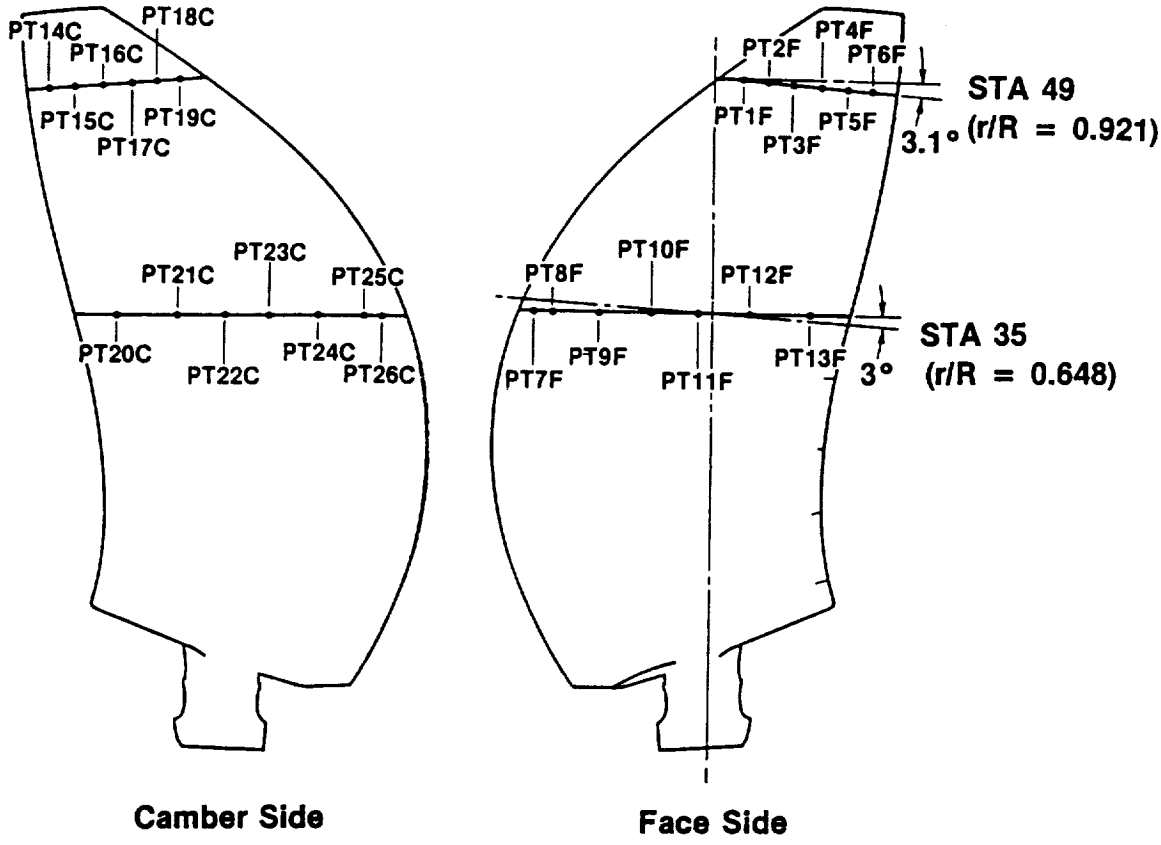

Locations — % Chord	
PT1F & PT19C	16.58
PT2F & PT18C	29.85
PT3F & PT17C	43.11
PT4F & PT16C	56.38
PT5F & PT15C	69.64
PT6F & PT14C	89.54
PT7F & PT26C	4.93
PT8F & PT25C	10.00
PT9F & PT24C	23.33
PT10F & PT23C	36.66
PT11F & PT22C	49.99
PT12F & PT21C	63.32
PT13F & PT20C	83.33

FIGURE 3.4 UNSTEADY PRESSURE BLADE, TRANSDUCER LOCATIONS

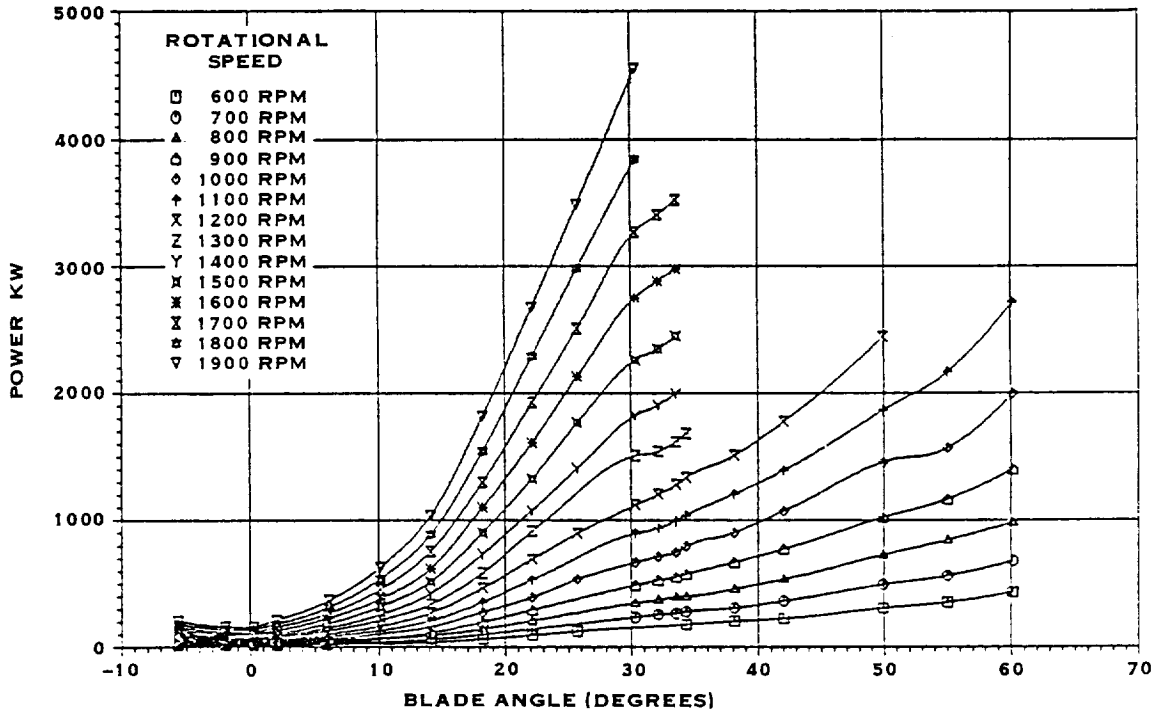

FIGURE 3.5 SR–7L CORRECTED STATIC POWER VS. BLADE ANGLE

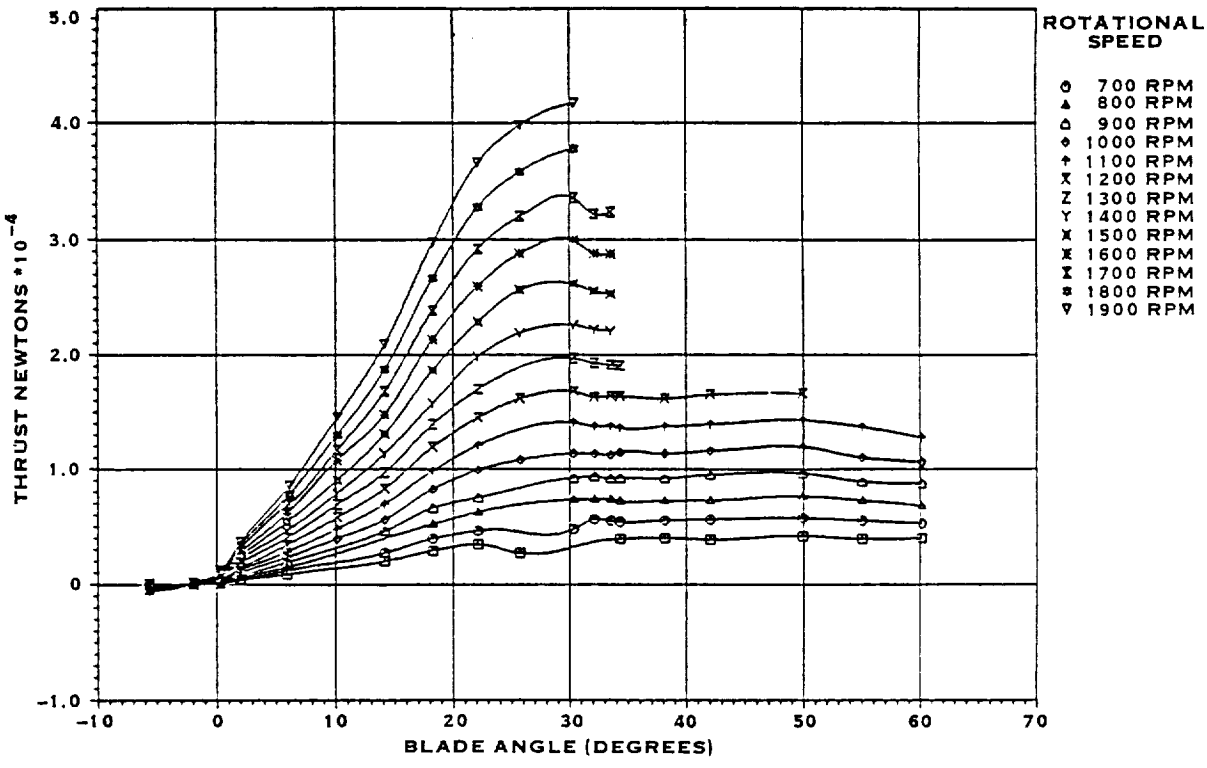

FIGURE 3.6 SR–7L CORRECTED STATIC THRUST VS. BLADE ANGLE

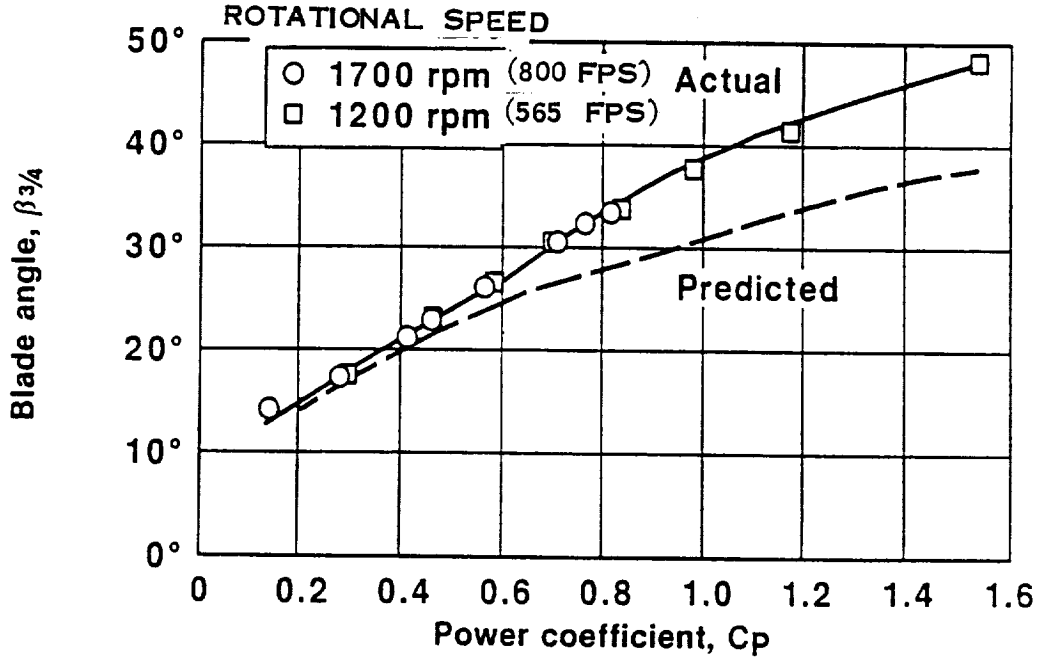

FIGURE 3.7 SR-7L PROP FAN, COMPARISON OF MEASURED AND PREDICTED CURVES OF BLADE ANGLE VS. POWER COEFFICIENT

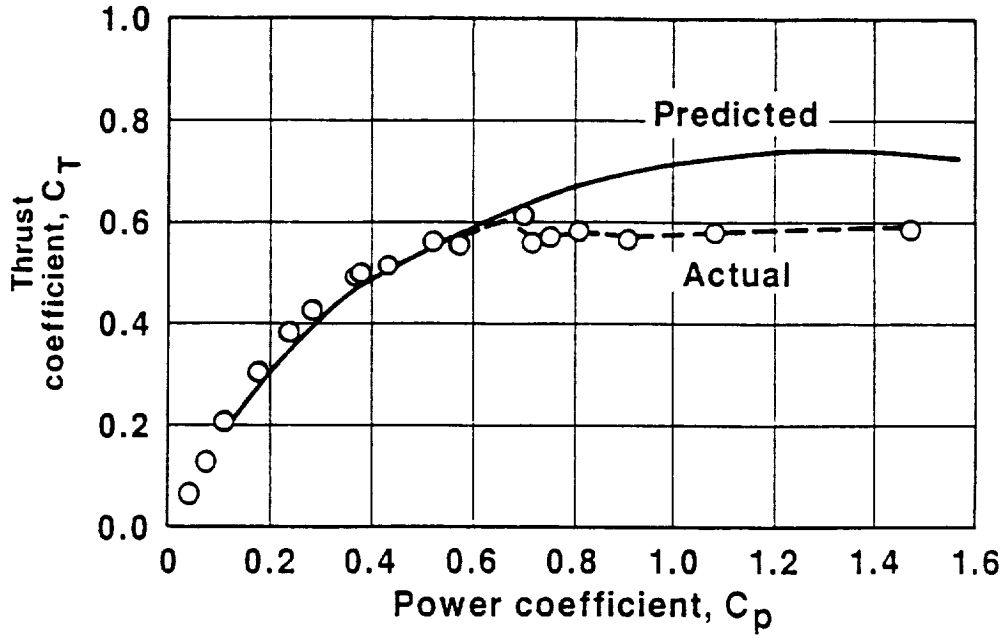

FIGURE 3.8 SR-7L PROP-FAN, COMPARISON OF MEASURED AND PREDICTED CURVES OF THRUST COEFFICIENT VS. POWER COEFFICIENT

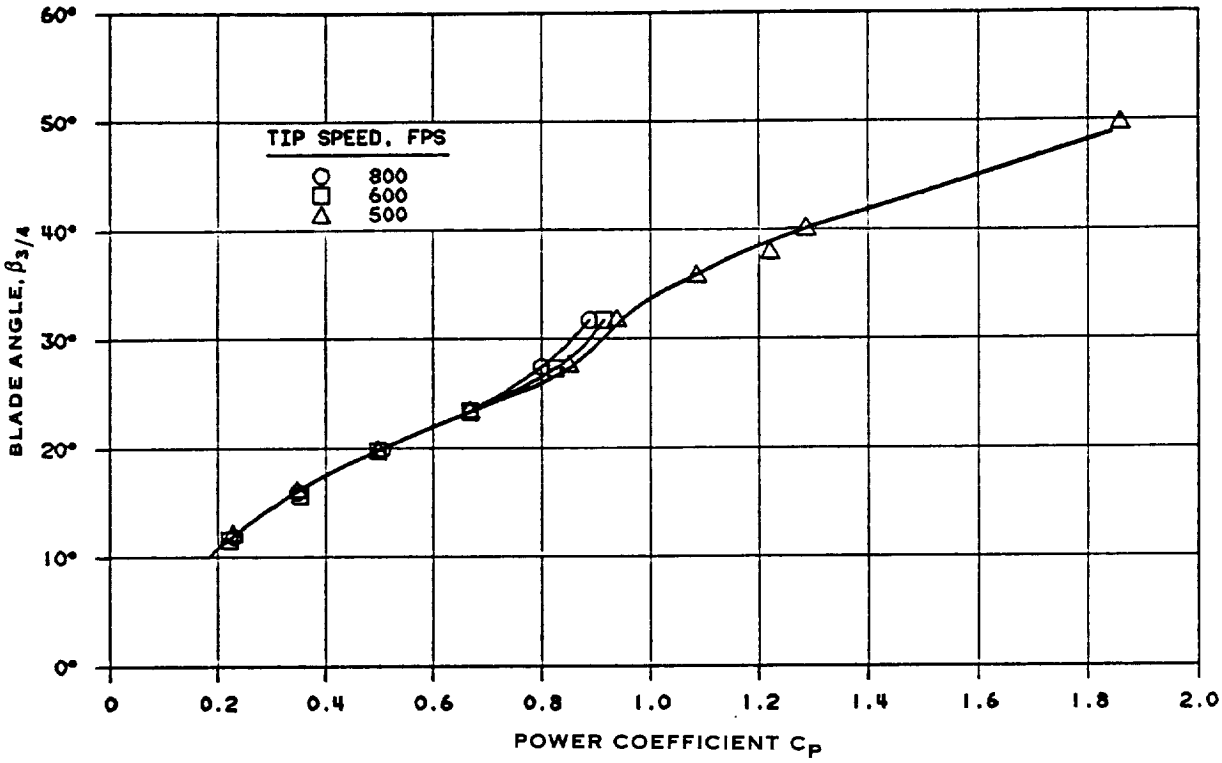

FIGURE 3.9 SR-3 PROP-FAN, BLADE ANGLE VS. MEASURED POWER COEFFICIENT, $V_\infty = 0$

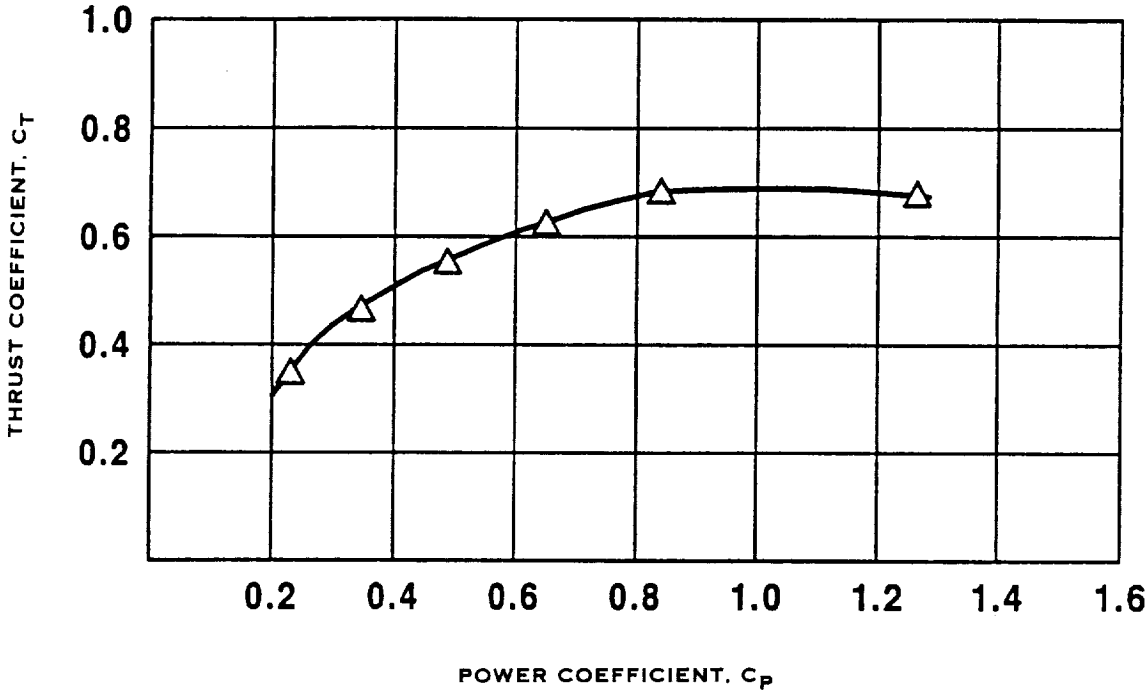

FIGURE 3.10 SR-3 PROP-FAN, MEASURED COEFFICIENT VS. POWER COEFFICIENT, V_∞

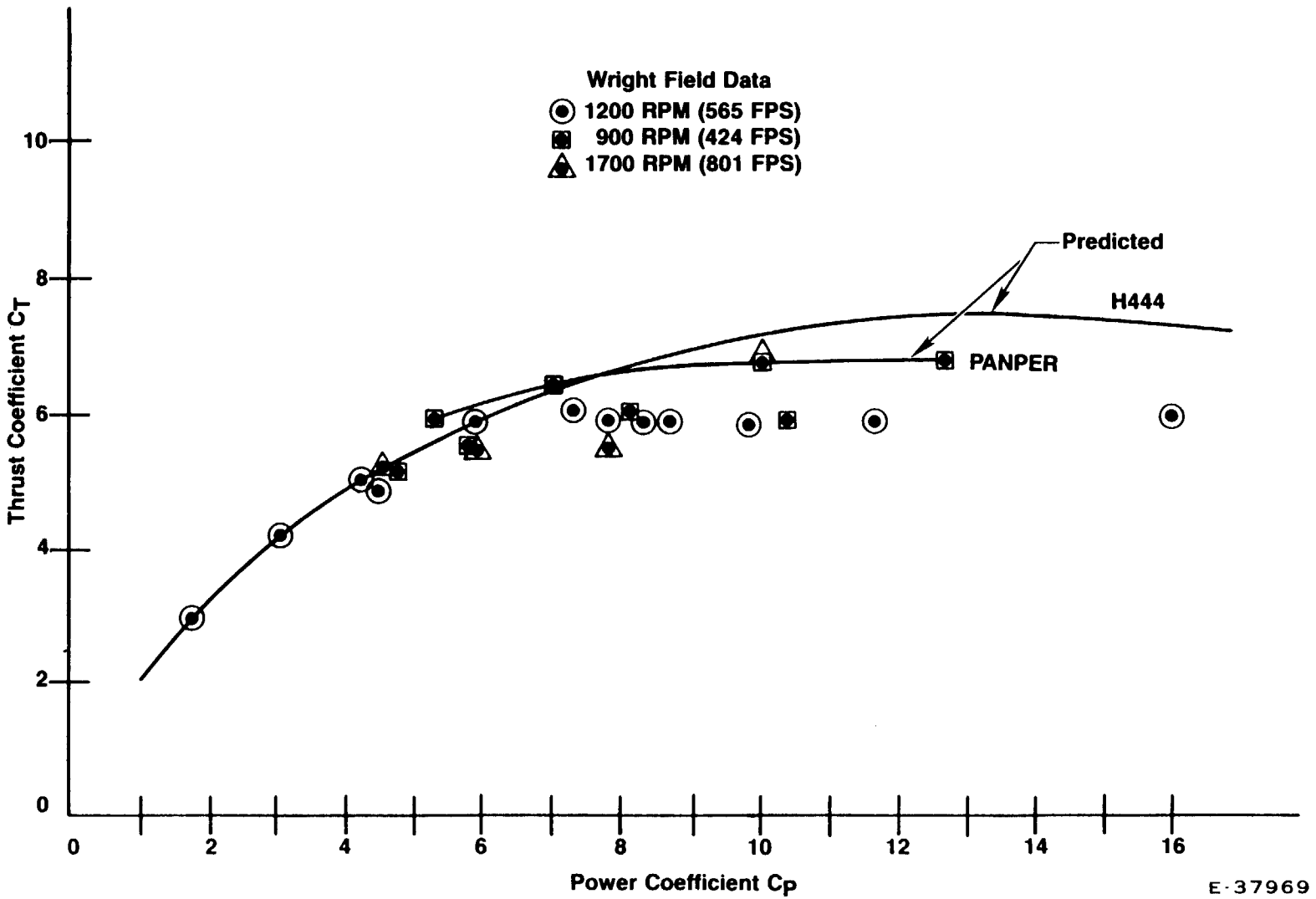

FIGURE 3.11 COMPARISON OF PANPER AND H444 PREDICTIONS OF SR-7L STATIC AERODYNAMIC PERFORMANCE WITH DATA

ONERA S-1 WIND TUNNEL

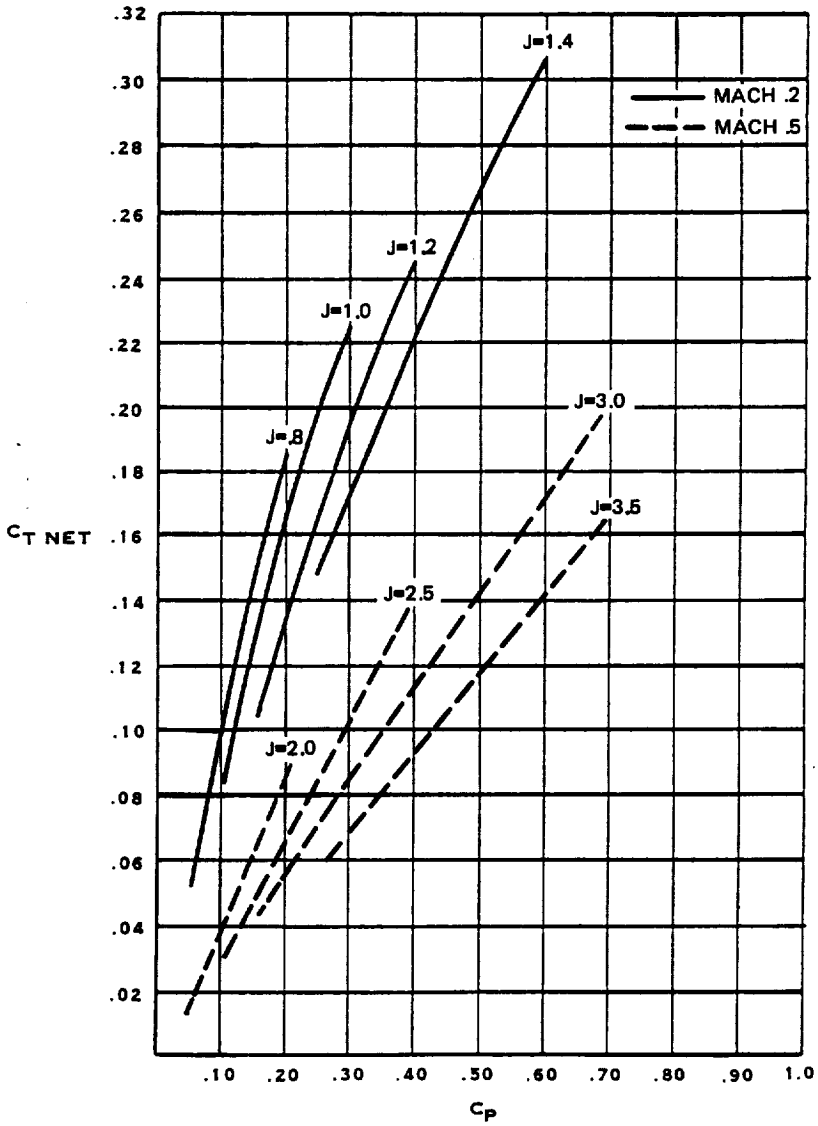

FIGURE 3.12 C_{TNET} VS C_P, CONSTANT ADVANCE RATIO, 4 BLADES

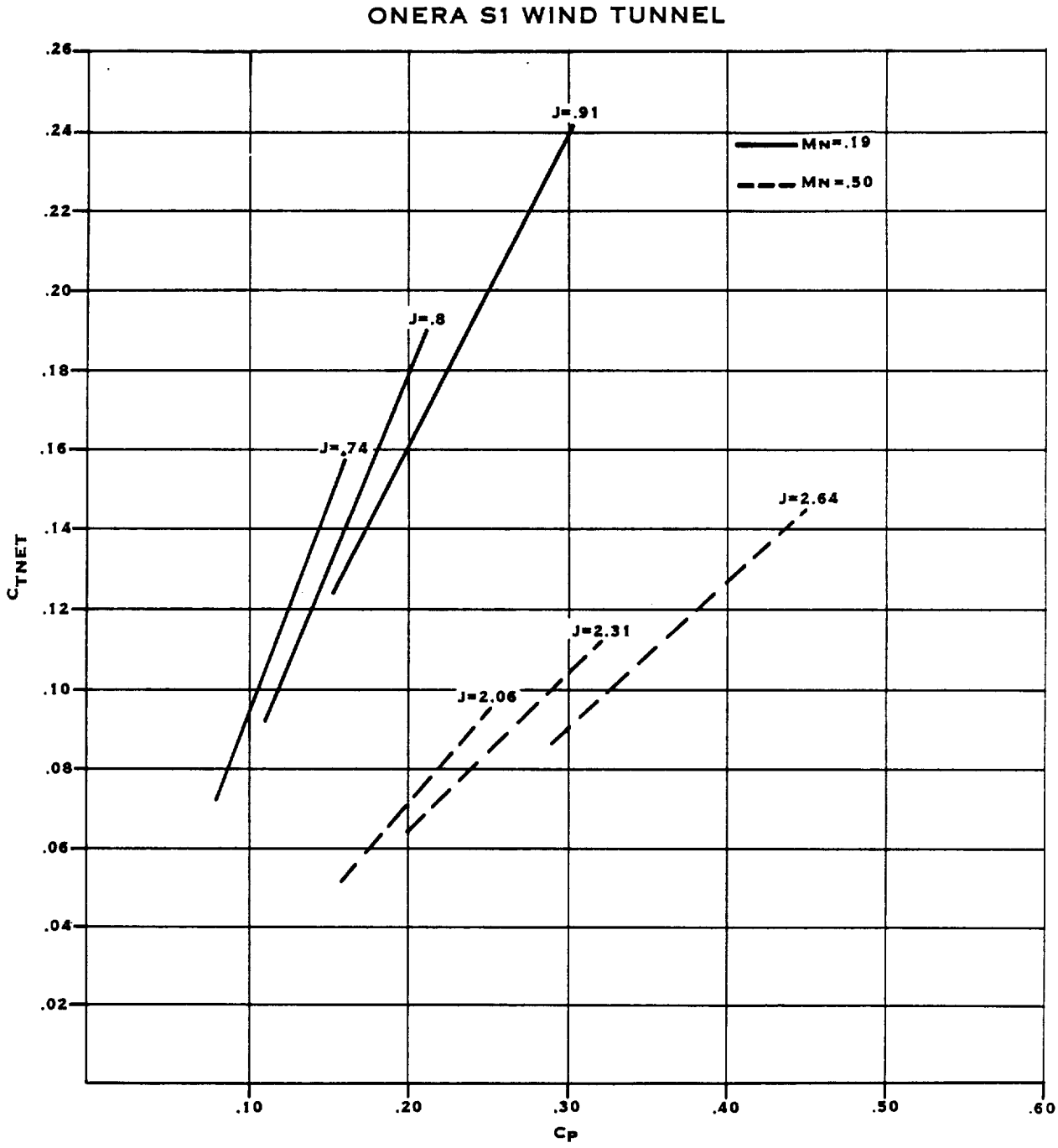

FIGURE 3.13 C_{TNET} VS. C_P CONSTANT ADVANCE RATIO, 8 BLADES

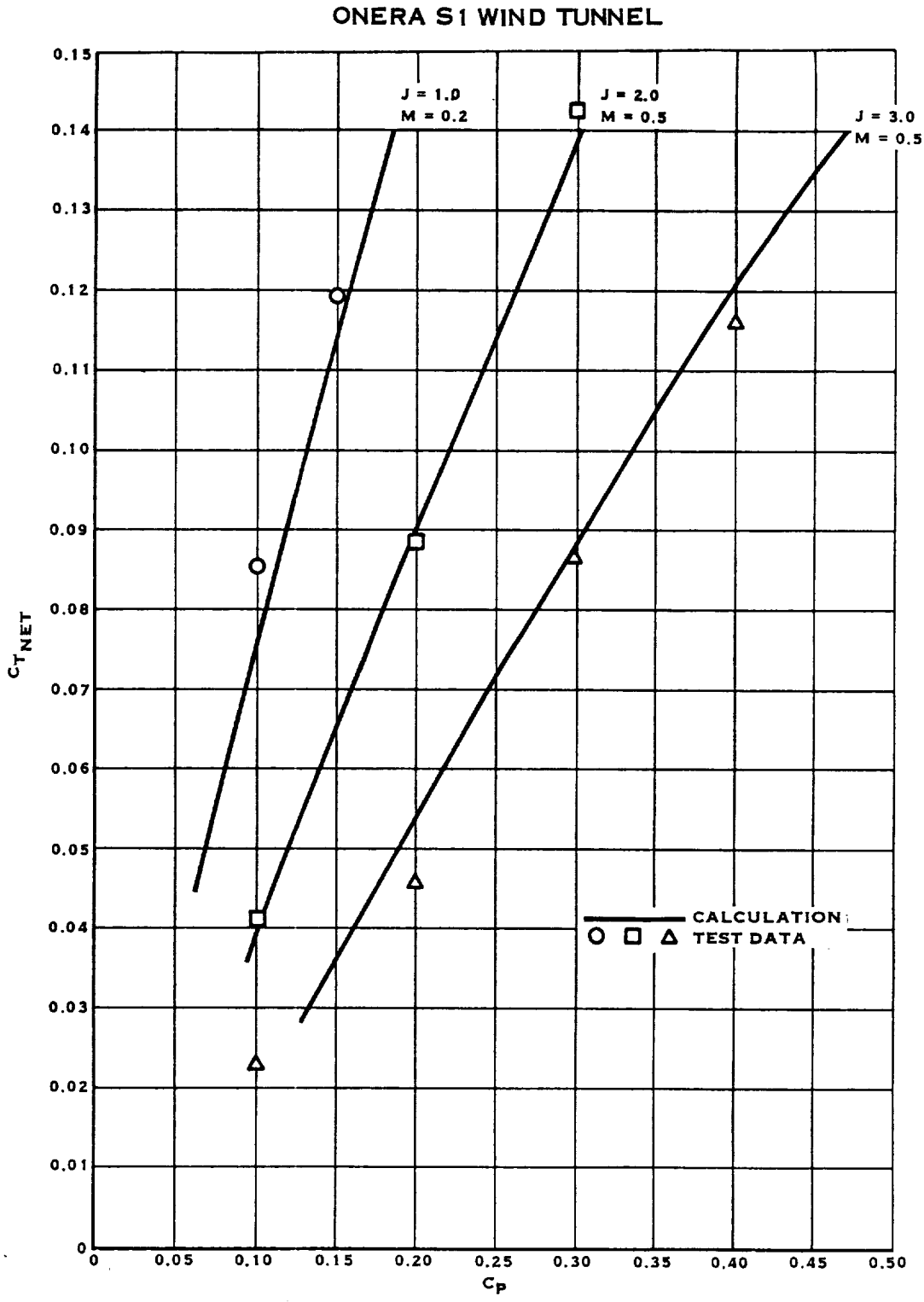

FIGURE 3. 14 COMPARISON OF MEASURED AND PREDICTED SR–7L PERFORMANCE 4 BLADES

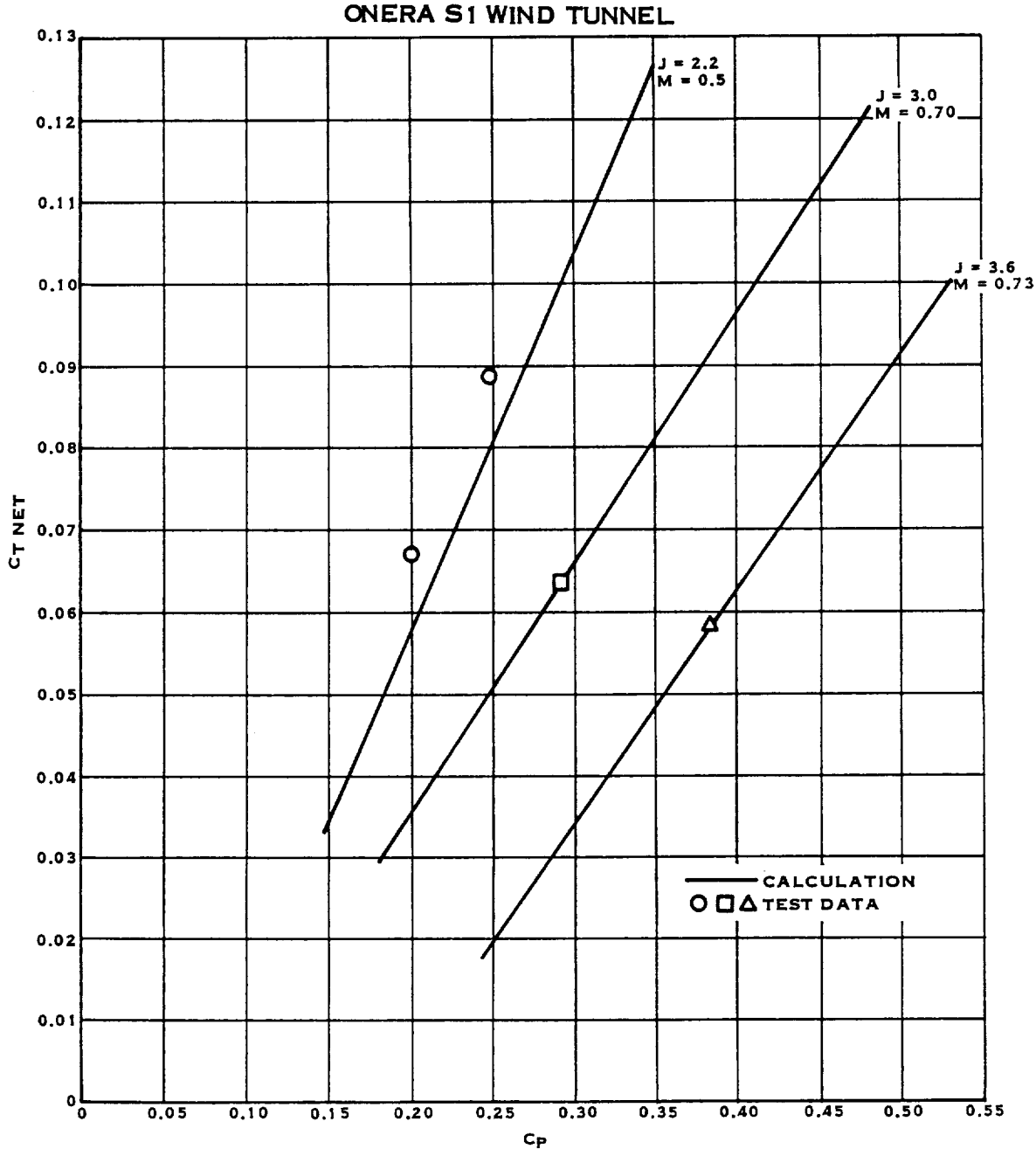

FIGURE 3. 15 COMPARISON OF MEASURED AND PREDICTED SR–7L PERFORMANCE, 8 BLADES

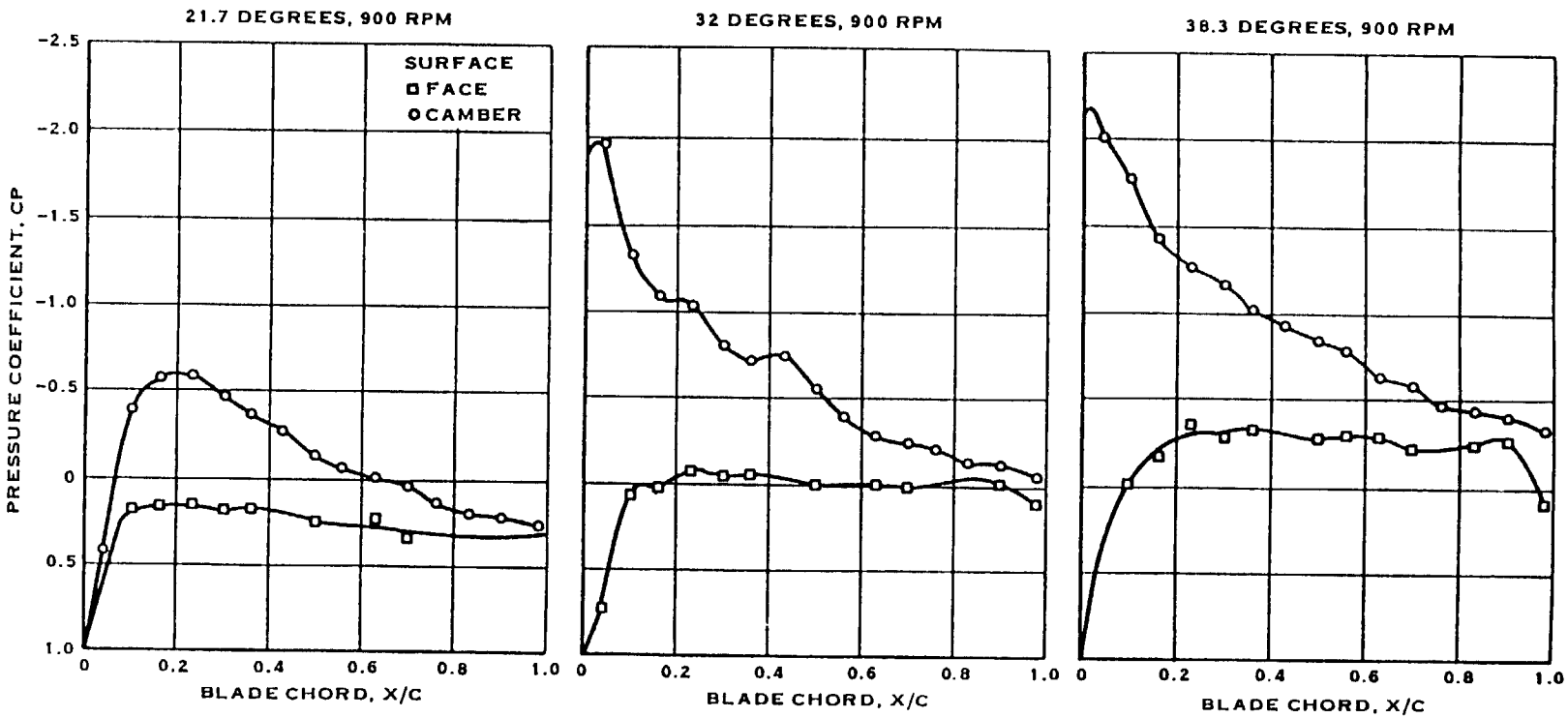

FIGURE 3.16 SR–7 PRESSURE DISTRIBUTION, $r/R = 0.287$

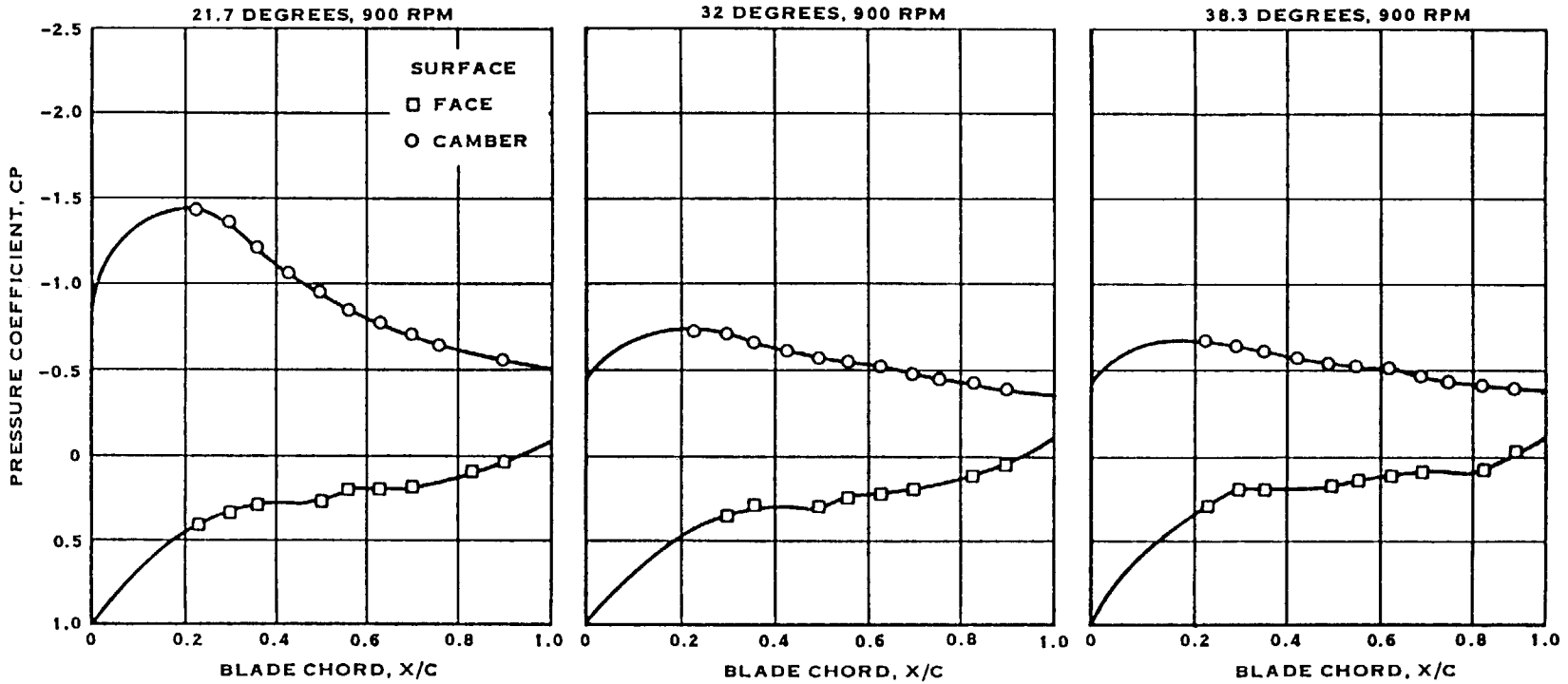

FIGURE 3.17 SR–7 PRESSURE DISTRIBUTION, $r/R = 0.963$

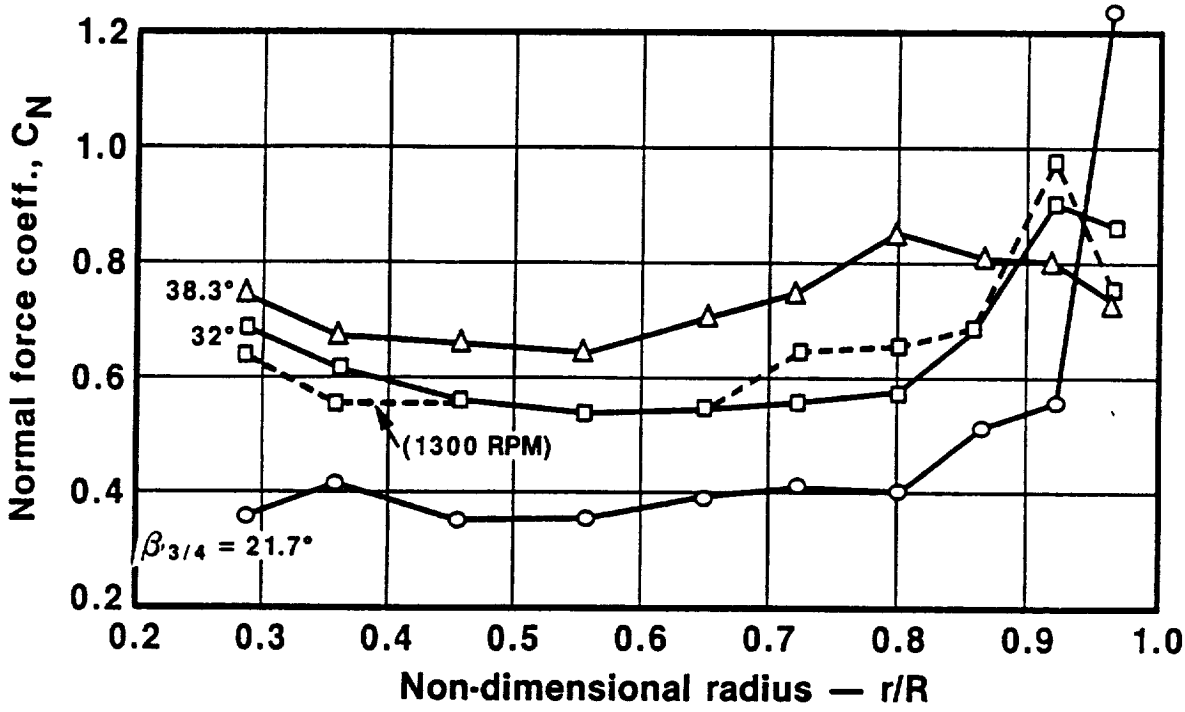

FIGURE 3. 18 SR–7L BLADE NORMAL FORCE COEFFICIENT VS. RADIUS RATIO, $RPM_{CORR} = 900$

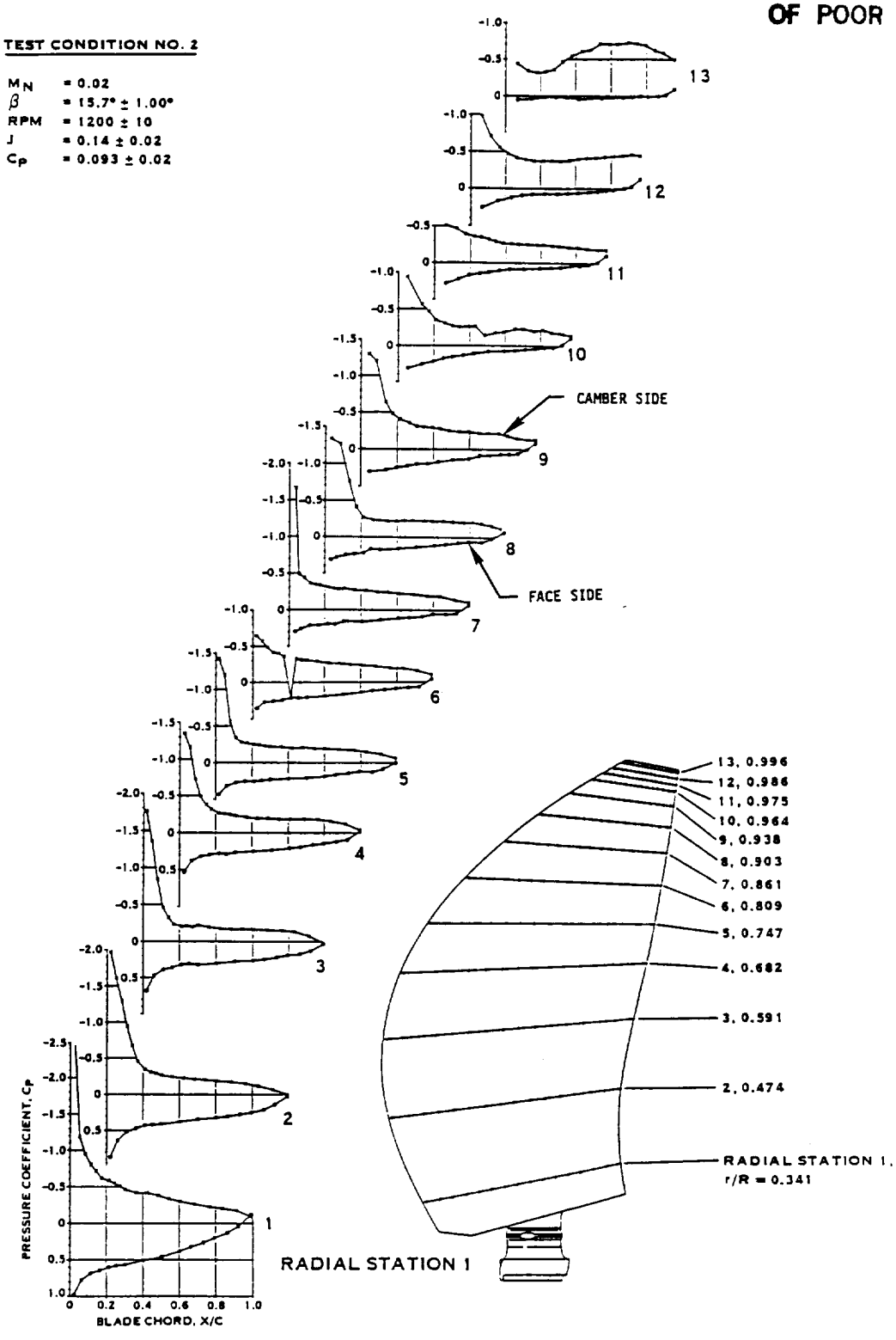

FIGURE 3. 19 PRESSURE DISTRIBUTION, WIND TUNNEL QUASI –STATIC CASE

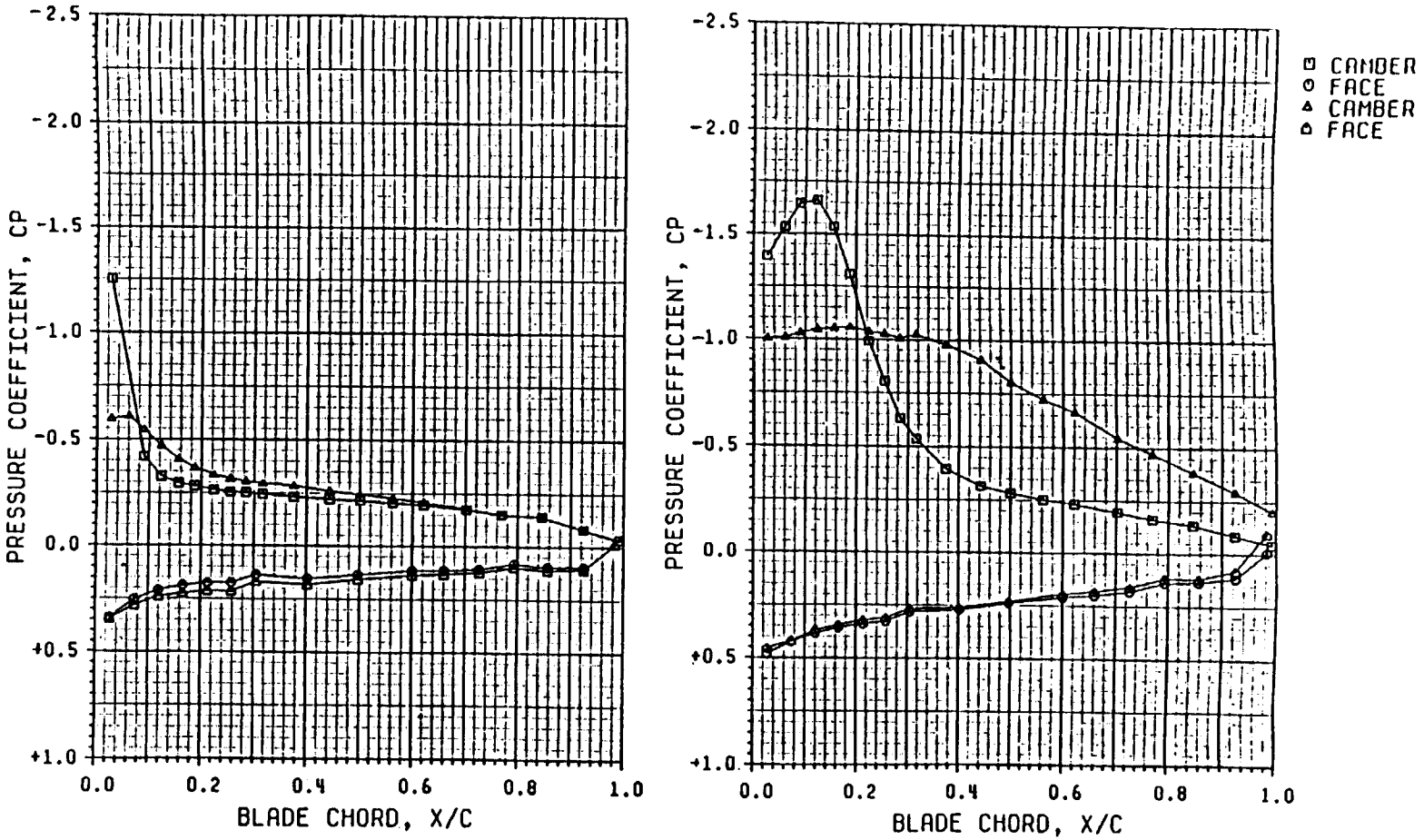

□, ◇ **Original Data, Record No. 100**
M∞ = 0.01, J = 0.061, CP = 0.08

△, △ **Repeat Run Data, Record No. 204**
M∞ = 0.03, J = 0.155, CP = 0.096

□, ◇ **Original Data, Record No. 103**
M∞ = 0.02, J = 0.124, CP = 0.202

△, △ **Repeat Run Data, Record No. 205**
M∞ = 0.04, J = 0.247, CP = 0.201

FIGURE 3.20 DEMONSTRATION OF MACH NUMBER VARIATION EFFECT ON PRESSURE COEFFICIENTS AT LOW MACH NUMBERS (STATIC ROTOR CASES).

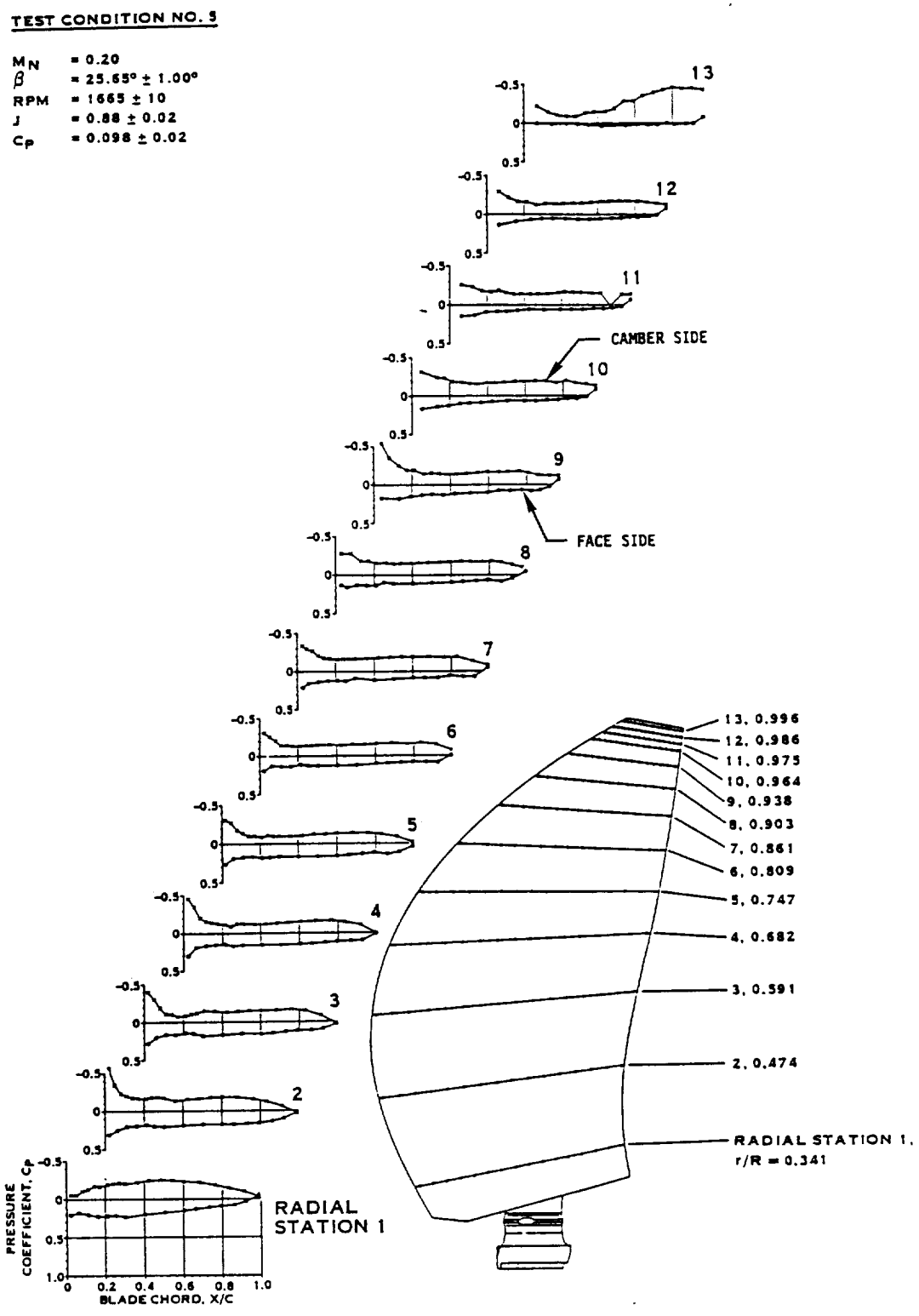

FIGURE 3.21 PRESSURE DISTRIBUTION, MACH. 2, LOW POWER

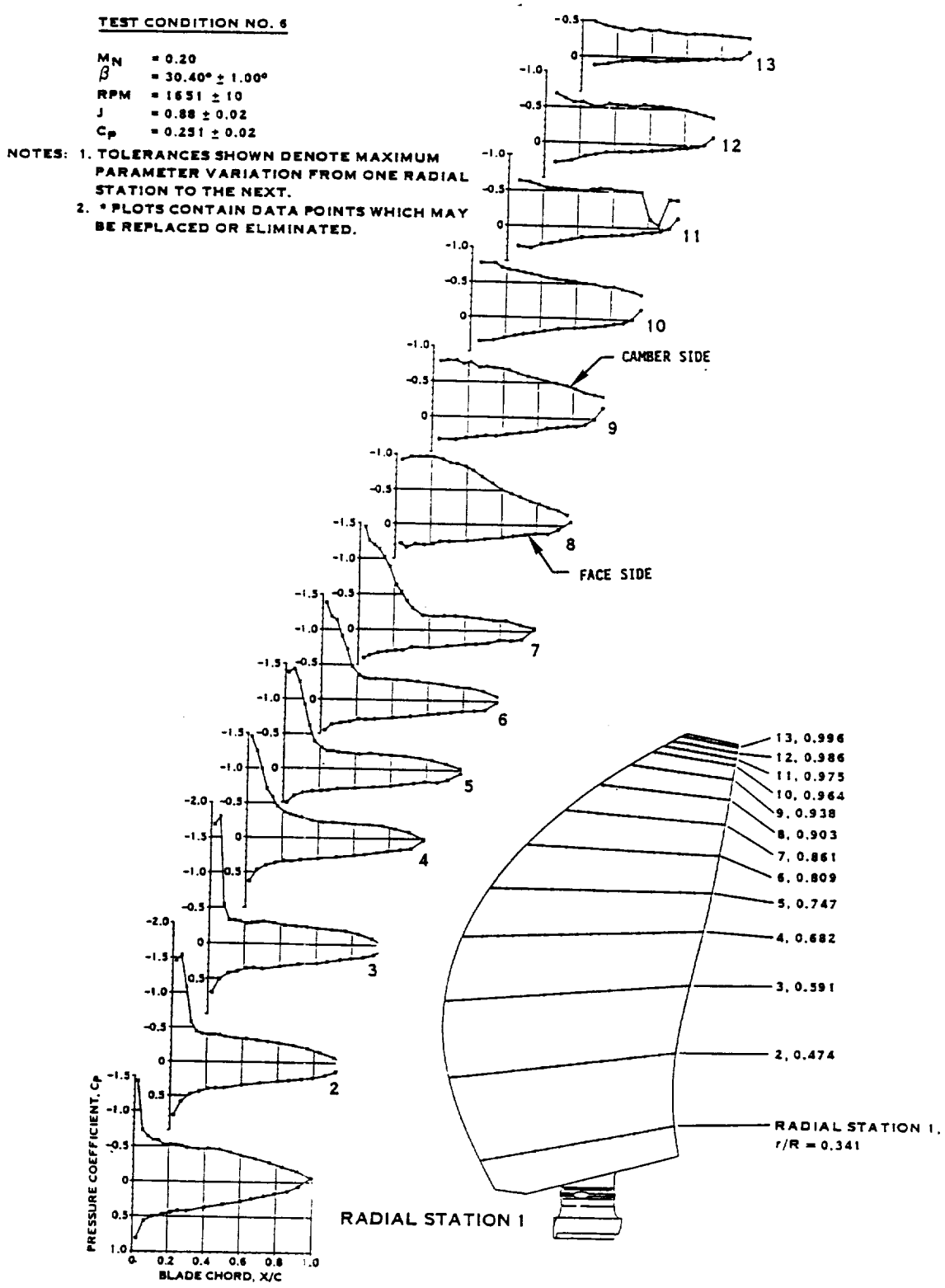

FIGURE 3.22 PRESSURE DISTRIBUTION, MACH. 2, HIGH POWER

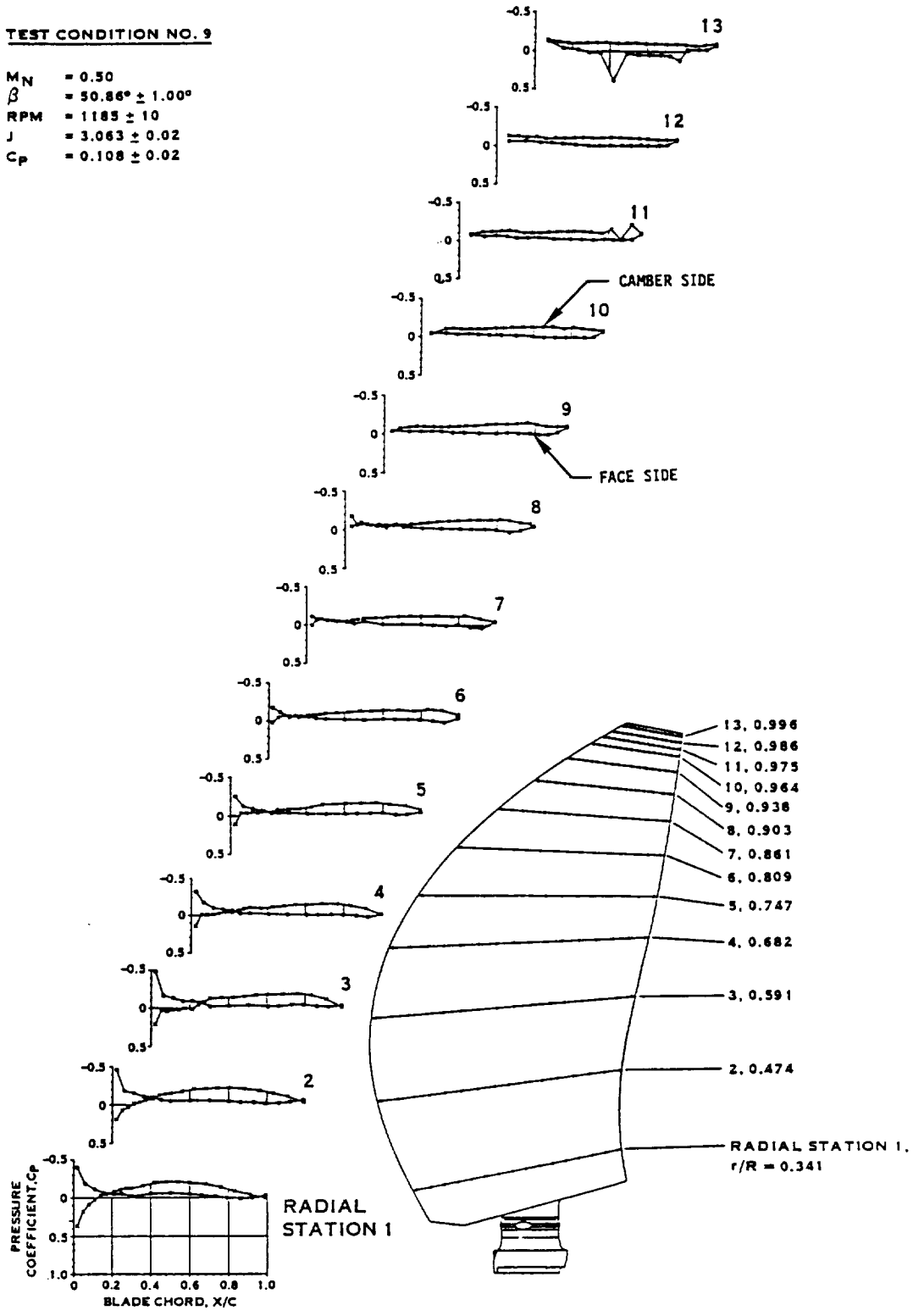

FIGURE 3.23 PRESSURE DISTRIBUTION, MACH .5, LOW POWER

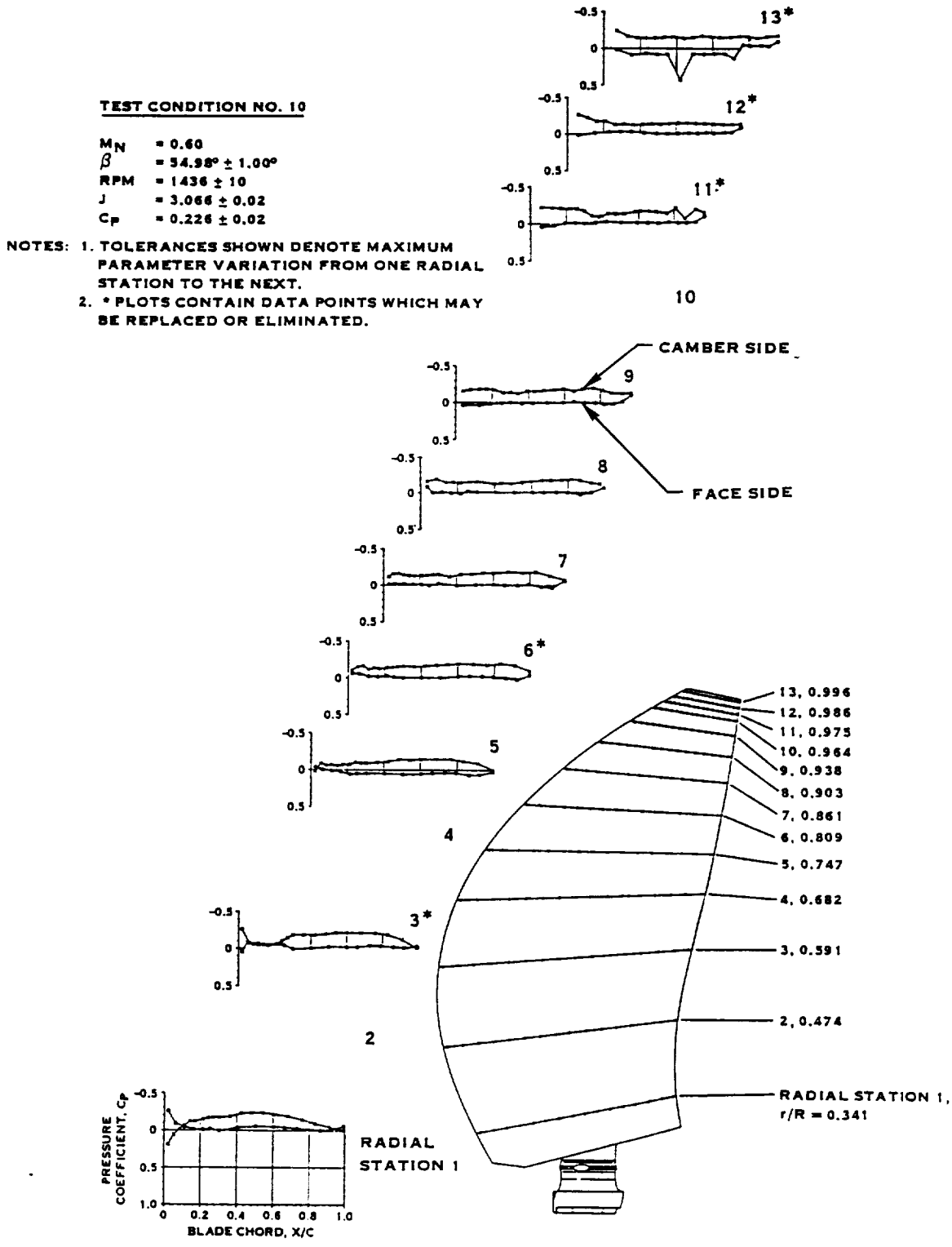

FIGURE 3.24 PRESSURE DISTRIBUTION, MACH. 5, INTERMEDIATE POWER

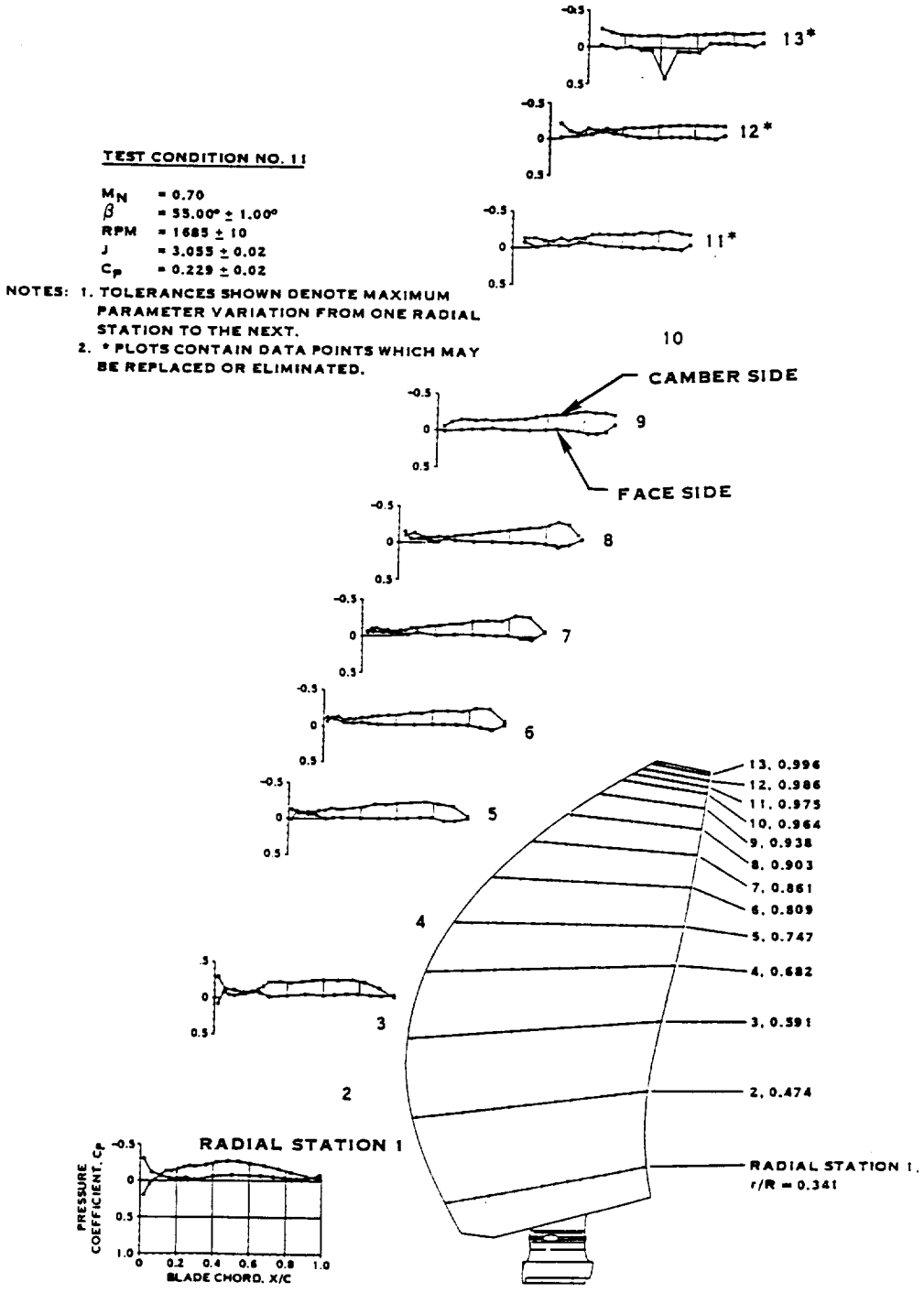

FIGURE 3.25 PRESSURE DISTRIBUTION, MACH. 5, HIGH POWER

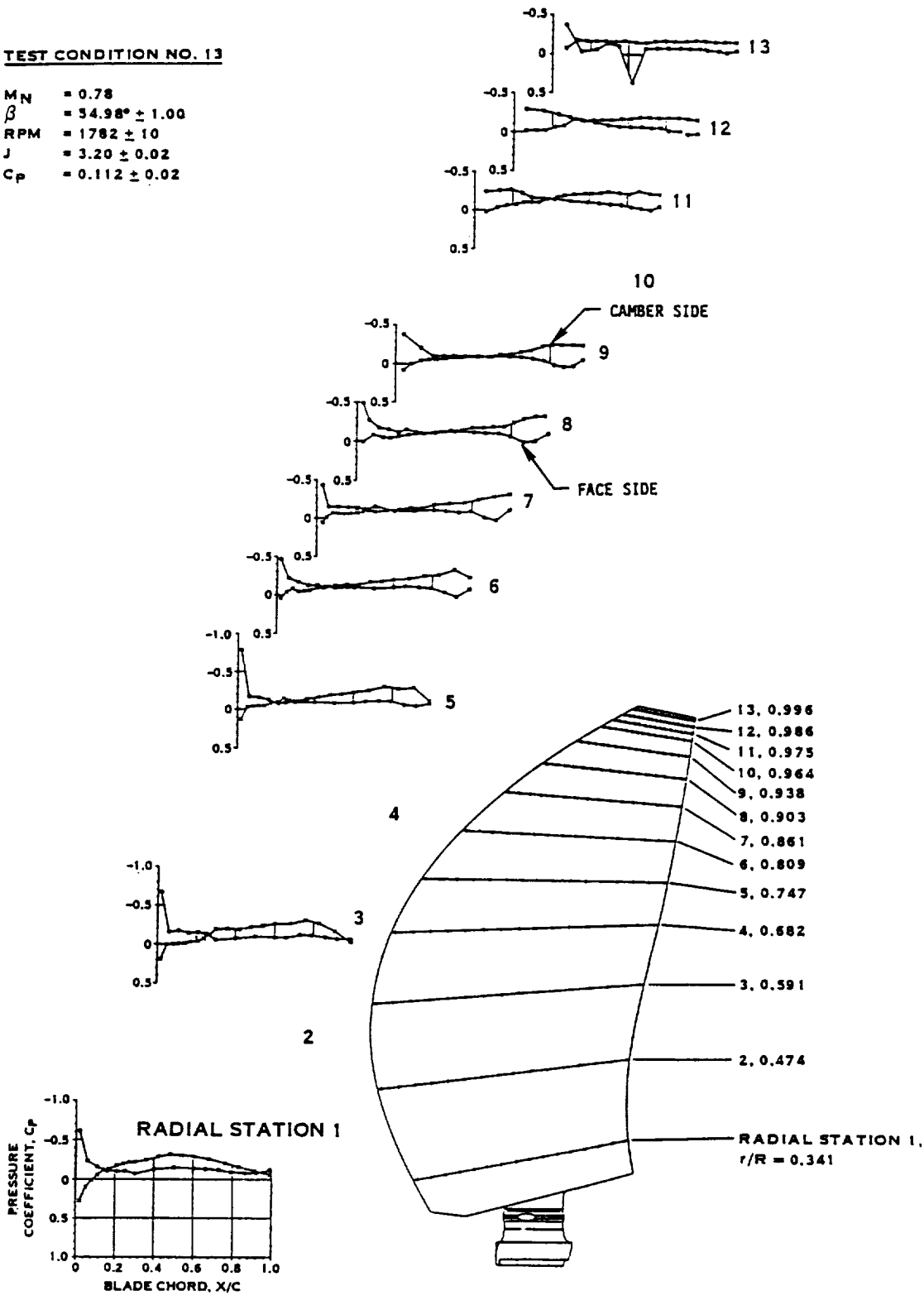

FIGURE 3.26 PRESSURE DISTRIBUTION, MACH. 78, LOW POWER

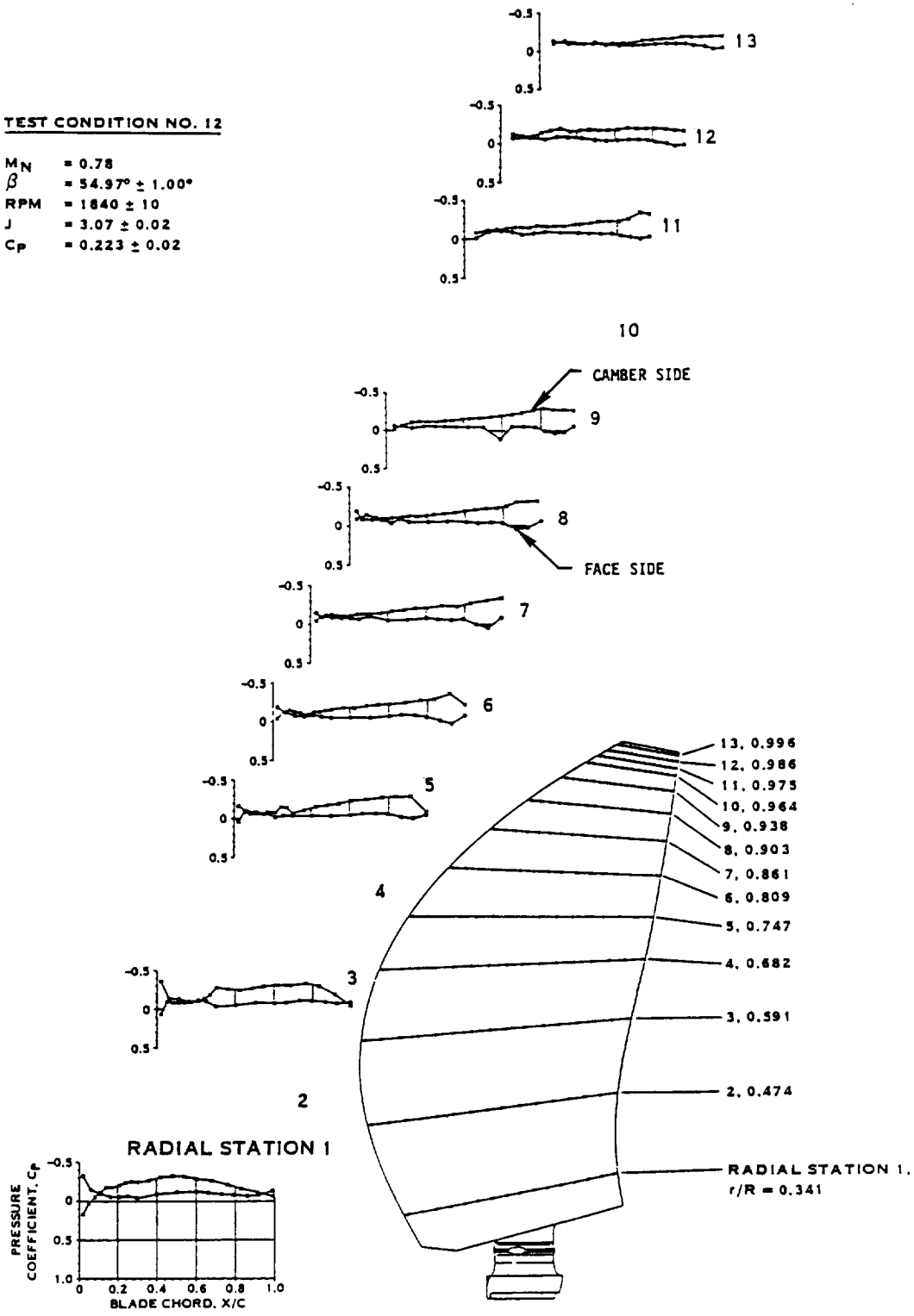

FIGURE 3.27 PRESSURE DISTRIBUTION, MACH. 78, INTERMEDIATE POWER

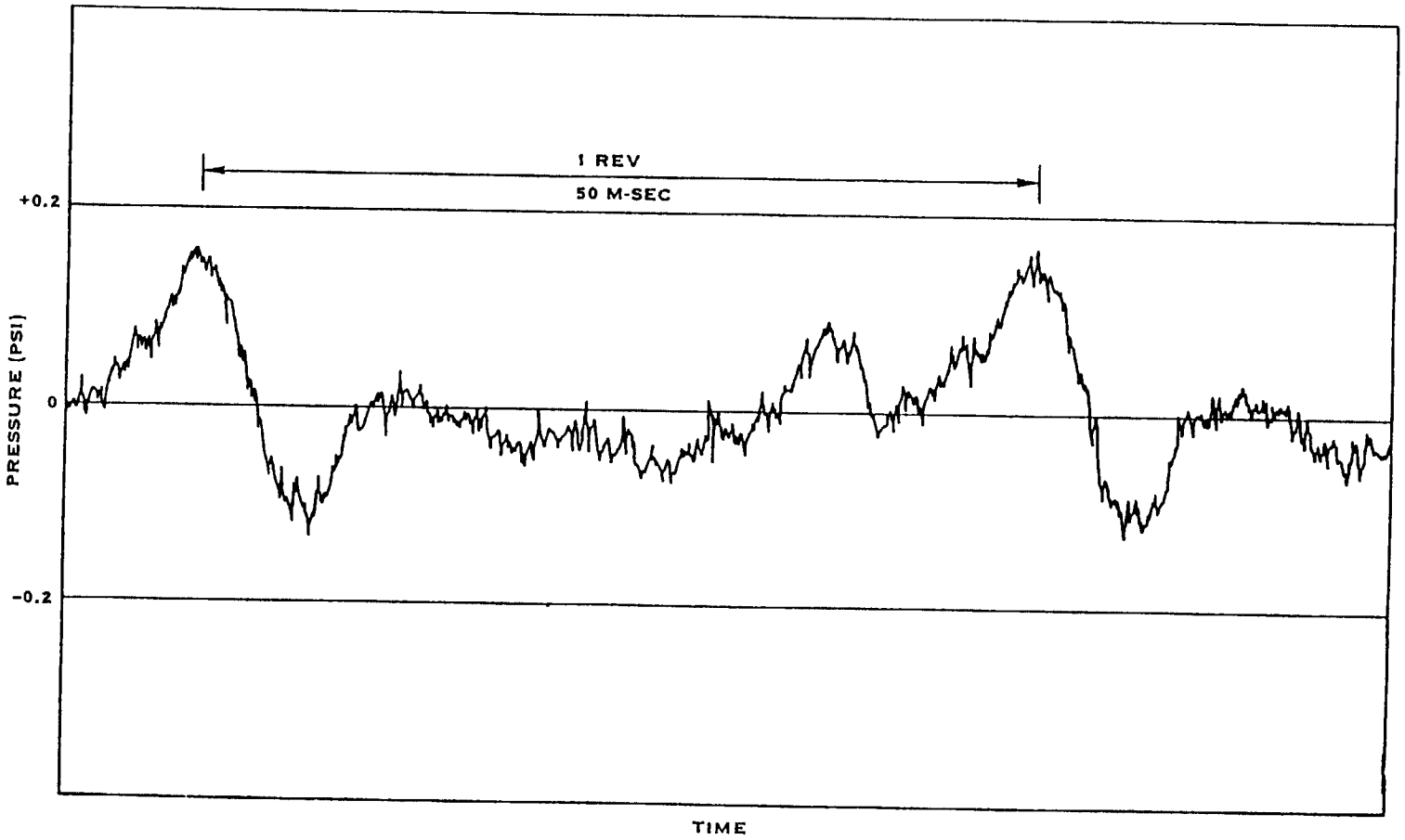

FIGURE 3.28 PRESSURE DATA, TRANSDUCER PT21C, PLATE OBSTRUCTION, β 3/4 = 32°, 1200 RPM

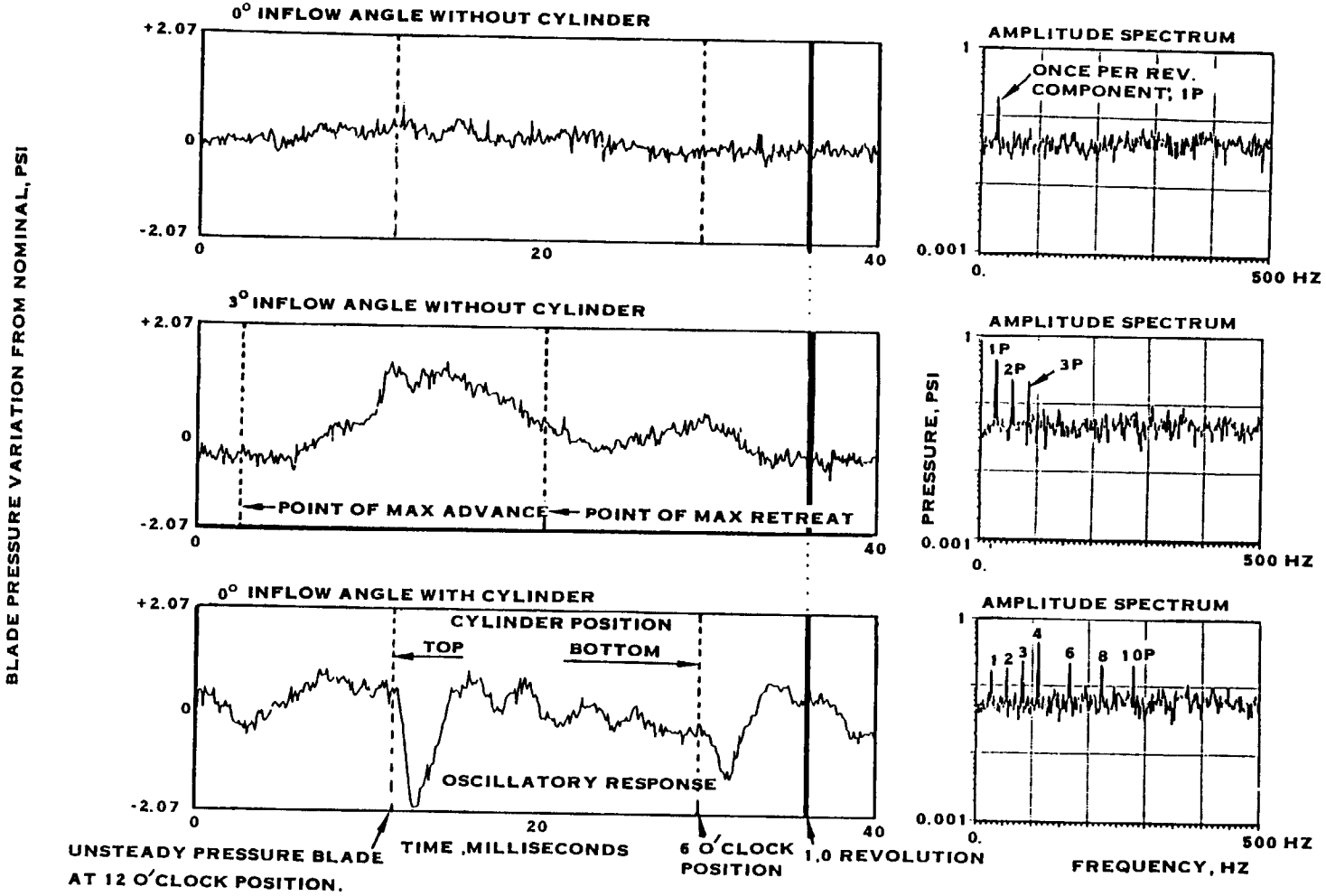

FIGURE 3.29 EXAMPLES OF THE MEASURED UNSTEADY PRESSURES

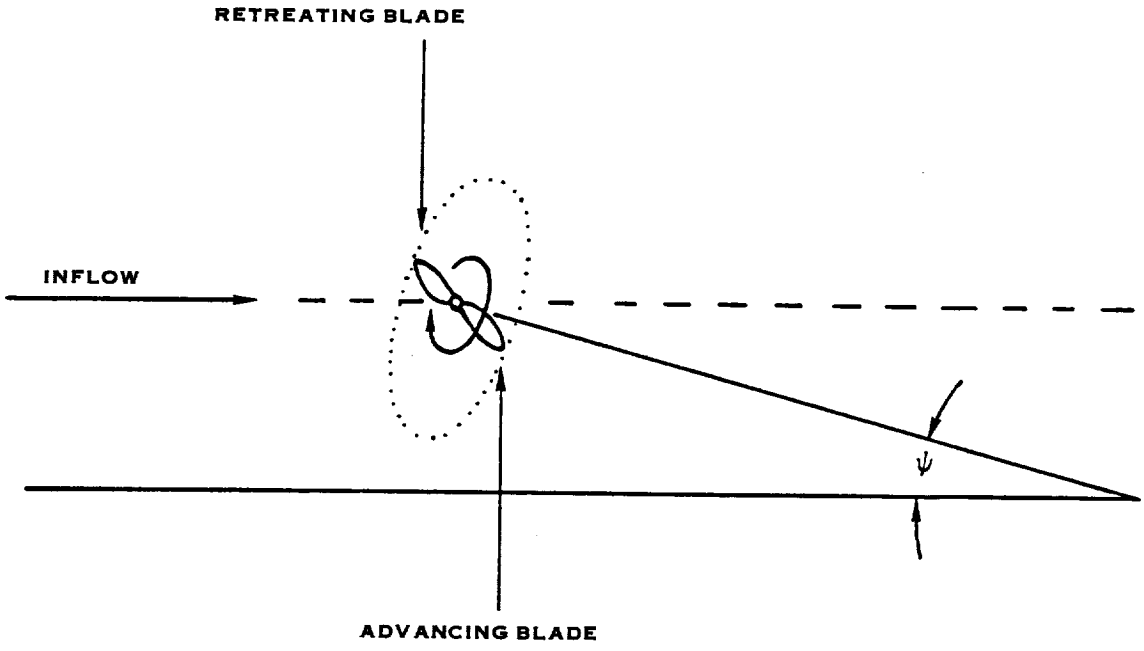

FIGURE 3.30 ILLUSTRATION OF THE TERMS "ADVANCING" AND "RETREATING" FOR ANGULAR INFLOW

4.0 AEROELASTICITY

The assessment of the aeroelastic response of a Prop-Fan blade in a real structure was a primary purpose of the Large Scale Advanced Prop-Fan program. The configuration of the Large Scale Advanced Prop-Fan was a radical departure from conventional propeller designs. The characteristics of the SR-7L Prop-Fan that represented unknowns from a structural dynamic viewpoint were the thin, highly swept, low aspect ratio blades and the large number of blades, which leads to close proximity of the aerodynamic surfaces and possible cascade interaction. All of these characteristics are essential to achieving the desired aerodynamic performance of the Prop-Fan at high subsonic Mach numbers. However, they also make the structural design more difficult.

The structural dynamic characteristics of the Prop-Fan that were investigated during the LAP program included the resonant modes and frequencies of the blades, the stall flutter boundaries, the response to an aerodynamic 1P forcing function, and the high speed stability of the Prop-Fan. These characteristics were evaluated during four program tests; the Retention Stiffness Test, the Wright Patterson Air Force Base Static Rotor Test, the Modane High Speed Wind Tunnel Test and the SR-7A Aeroelastic Model Wind Tunnel Test. Data from each test was correlated with predictions made using state of the art analytical tools. This provided an evaluation of the adequacy of the currently available methods for performing the aeroelastic design of Prop-Fans.

The purpose of the retention stiffness test was to experimentally determine the combined stiffness of the hub and blade retention. Retention stiffness has a great effect on blade resonant frequencies. The hub, blade retention, retention hardware and actuator dome were installed in an electric motor driven whirl rig with dummy blade stubs substituted for the blades. The stubs were designed to apply the same centrifugal force to the hub and retention as the blades. The test installation is depicted in Figure 4.1.

Rotation of the test assembly in the whirl rig results in excitation of the blade stubs due to random air turbulence. Strain gages were applied to the stubs to measure the in-plane and out-of-plane vibrational response to the excitation. Spectral analysis of the strain gage data allowed the natural frequencies of the blade stubs to be determined.

The test assembly natural frequencies are a function of the retention stiffness, the dynamic characteristics of the stubs and the Prop-Fan RPM. The stubs are essentially solid metal cylinders. As such they are simple structures that are easy to analyze. The stub natural frequencies are calculated and plotted as a function of retention stiffness for a range of rotational speeds. Therefore when the stub natural frequency is experimentally measured at a particular rotational speed, a retention stiffness corresponding to that natural frequency can then be determined.

The Static Rotor Test and High Speed Wind Tunnel Test were described in section 3.0 of this report. Much of the aeroelastic data was acquired concurrently with the aerodynamic performance data. The aeroelastic data was

acquired by extensive strain gaging of the blades. The blade strain gage arrangement used for the Static Rotor and High Speed Wind Tunnel Tests are shown in Figure 4.2.

The SR-7A Prop-Fan was a 2 foot diameter aeroelastically scaled model of the SR-7L. The aeroelastic scaling was achieved by matching the SR-7A blade mass and stiffness distributions to the SR-7L and scaling the SR-7A retention stiffness from the SR-7L by the ratio of the SR-7A to SR-7L blade loads. Testing of the SR-7A model was conducted in the NASA Lewis Research Center 9 x 15 Low Speed Wind Tunnel and the 8 x 6 High Speed Wind Tunnel. Static testing and testing over a range of Mach numbers from .05 to .8 was conducted. Aeroelastic data was acquired using strain gages attached to the blade structure as shown in Figure 4.3. The SR-7A aeroelastic model is shown installed in the 8 x 6 wind tunnel in Figure 4.4.

4.1 Retention Stiffness

4.1.1 Analysis

The design goal for the SR-7L Prop-Fan retention stiffness was to position the blade natural frequencies such that no 1-P critical speeds were present within the operating speed range and to provide specified critical speed margin for the 1P through 5P excitations as illustrated in Figure 4.5. The blade retention stiffness is influenced by the interaction of several of the Prop-Fan components. These components include the blade shank, the inner blade race, the retention ball bearing and the hub. These components are shown in Figure 4.6.

The retention stiffness was calculated using two approaches. In the first approach a two dimensional analysis was conducted for all of the components. The compliances determined from the 2-D analyses were then added reciprocally to obtain an overall retention stiffness. The barrel was modeled as three separate pieces; the arm, bridge and ring, which have stiffness that act in series. In the second approach the retention stiffness was determined using a three dimensional finite element model of the barrel.

The barrel stiffness and overall retention stiffness determined using the two different approaches are compared in Table 4.1.

TABLE 4.1

COMPARISON OF BARREL AND RETENTION STIFFNESS
CALCULATED WITH 2D AND 3D ANALYSIS

	IN-PLANE STIFFNESS (IN-LBS/RAD)		OUT OF PLANE STIFFNESS (IN-LBS/RAD)	
	2-D ANALYSIS	3-D ANALYSIS	2-D ANALYSIS	3-D ANALYSIS
Barrel Stiffness	$55X10^6$	$37X10^6$	$61X10^6$	$70X10^6$
Overall Retention Stiffness	$13.7X10^6$	$7.9X10^6$	$15.5X10^6$	$16.9X10^6$

4.1.2 Test Results

Figure 4.7 shows experimentally determined Prop-Fan in-plane and out-of-plane natural frequencies plotted as a function of RPM. The heat generated by rotation of the stubs in the test cell resulted in a rapid air temperature rise that precluded operation above 1599 RPM. However the smooth variation of natural frequency with speed allows extrapolation of the data to higher RPM's. The experimentally determined curves of natural frequency versus RPM are shown overlayed on the calculated curves of natural frequency versus retention stiffness in Figure 4.8. The intersections of these curves define the retention stiffness as a function of centrifugal load, which is plotted in Figure 4.9. The data is extrapolated out to a load of 369184N (83000 lbs) which corresponds to the design rotational speed of 1698 RPM.

The experimentally determined retention stiffnesses are compared to the stiffnesses determined by the two previously discussed analytical approaches in Table 4.2.

TABLE 4.2

COMPARISON OF MEASURED AND PREDICTED RETENTION STIFFNESS

	EXPERIMENT	2D ANALYSIS	3D ANALYSIS
In-Plane Stiffness (In-Lbs/Rad $X10^{-6}$)	11.2	13.7	7.9
Out of Plane Stiffness (In-Lbs/Rad $X10^{-6}$)	16.3	15.5	16.9

4.1.3 Summary of Results

Reasonable agreement was obtained between the experimentally determined out-of-plane stiffness and the out-of-plane stiffness calculated using both the 2-D and 3-D analysis. The experimentally determined in-plane stiffness fell midway between the stiffness calculated using the 2-D analysis and the stiffness calculated using the 3-D analysis. The measured stiffness were considered acceptable and should prevent significant infringement of any of the blade critical speeds upon the resonance avoidance zones. However, the variation between the 3D analysis and the experimental results is excessive for the in-plane stiffness. For applications where the critical speed placement is more sensitive to retention stiffness, a 42% variation may well be unacceptable. The results indicate that additional research effort is needed in the analytical area.

4.2 Resonant Frequencies and Mode Shapes

4.2.1 Analysis

The prediction and placement of the resonant frequencies of Prop-Fan blades are important aspects of the design analysis process. The first few integer orders of design rotational speed are important areas to avoid resonance because excitation forces for these are highest, decreasing inversely as P-order increases (reference Figure 4.5). Dynamic magnification, if insufficiently damped, could cause undesirable vibration and stresses. Furthermore, for an eight-bladed propeller, the 2-P, 3-P, 4-P, and 5-P modes of vibration are reactionless, that is, vibration loads at the blade shank are reacted internally through the hub, and no component of vibration is transmitted to the propeller shaft. Thus the pilot has no direct sensory feedback of the vibratory condition of the Prop-Fan. For this reason, specific bands of resonant frequency avoidance are specified. These frequency avoidance bands decrease in size with increasing P-order since the magnitude of the excitation decreases as P-order increases. The vibratory mode shapes corresponding to the predicted resonant frequencies at various operating conditions are also important for evaluating susceptibility to low speed stalled flutter and high speed unstalled flutter.

The SR-7L blade resonant frequencies and mode shapes were calculated using the NASTRAN eigenvalue solver. The mass, stiffness and differential stiffening matricies used in the solution were generated using the Hamilton Standard finite element code BESTRAN for the blade in its deflected shape. The stiffness matrix was formulated using an out-of-plane retention stiffness of 13.4×10^6 and an in-plane stiffness of 10.2×10^6, which were the original estimates. These stiffnesses vary from the experimentally determined stiffnesses in Table 4.2 by less than 20%. The resonant frequencies were calculated for eight operating conditions, which were a combination of flight and wind tunnel test cases. The first 5 resonant frequencies for each condition and the corresponding mode shapes are listed in Table 4.3.

TABLE 4.3

PREDICTED MODAL FREQUENCIES (HZ)
FOR DESIGN OPERATING CONDITIONS

CONDITION	MODE 1 FIRST FLATWISE BENDING	MODE 2 FIRST EDGEWISE BENDING	MODE 3 SECOND FLATWISE BENDING	MODE 4 FIRST TORSIONAL	MODE 5 THIRD FLATWISE BENDING
Design/Cruise	43.2	80.1	101.0	148.2	168.6
Take-Off/Climb	45.7	77.2	103.2	147.5	170.4
ONERA, 8 Blade	43.4	79.6	100.9	149.8	167.1
ONERA, 4 Blade	43.4	79.7	100.8	149.6	167.2
ONERA, 2 Blade	43.4	79.9	101.2	149.4	168.7
Static Thrust	46.4	76.3	103.1	148.4	169.6
Reverse Thrust	50.1	73.7	94.3	138.1	148.7
Cruise, Low RPM	38.8	77.6	95.6	143.2	155.9
Cruise, Hi RPM	44.0	80.7	101.9	149.0	169.4
Climb, Mid Altitude	44.1	78.9	102.0	148.8	169.5
Dive, Mid Altitude	44.7	77.0	102.2	150.1	168.6
Dive, High Altitude	44.0	77.3	101.6	149.5	168.2

The calculated modal frequencies for the required design conditions of design/cruise and take-off/climb are also plotted on a Campbell diagram in Figure 4.10. The Campbell diagram includes the integer order resonance avoidance bands specified in the design requirements. Static frequencies are also shown. These frequencies were calculated with a clamped blade shank, and therefore are not shown connected with the other modes that were calculated at speed. All resonance placement requirements were met except the second mode in the design cruise condition which impinges slightly on the 3P avoidance band. This was not considered to be of great concern.

The SR-7A blade natural frequencies and mode shapes were also calculated using the NASTRAN eigenvalve solver. The calculated SR-7A and SR-7L natural frequencies are compared on a modified Campbell Diagram in Figure 4.11. The diagram was modified to account for the difference in RPM between the SR-7A and SR-7L. This was accomplished by plotting frequency times tip radius versus propeller RPM times tip radius. In general the model natural frequencies were higher than the SR-7L natural frequencies. However, all of the first five SR-7A natural frequencies were within 10% of the SR-7L frequencies, which was considered acceptable. The comparison of the first five SR-7A mode shapes with the first five SR-7L mode shapes also showed acceptable similarity.

4.2.2 Test Results

The extensive amount of vibratory stress data taken during the Static Rotor Test of the SR-7L Prop-Fan allowed the blade natural frequencies to be plotted as a function of RPM and the effect of blade pitch angle on natural frequency to be determined. The natural frequencies were determined by spectral analysis of the vibratory data taken at each rotational speed. The natural frequencies are plotted versus RPM and compared to prediction in the Campbell plot of Figure 4.12. Good agreement was obtained between data and the calculated natural frequencies at the Prop-Fan design operating speed of 1698 RPM.

The data presented in the Campbell plot, Figure 4.12, is representative of all the blade angles tested and the condensed scale does not show the effect of blade angle on the blade natural frequency. To examine the blade angle effect the data was replotted versus blade angle in Figure 4.13 for three rotational speeds. Figure 4.13 shows the first and second flatwise bending modes decrease in frequency with increasing blade angle, the first edgewise mode increases in frequency with increasing blade angle, and the first torsional mode remains relatively unaffected by blade angle. These trends in frequency with blade angle are typical for rotating blades. The changes in frequency are caused by the orientation of the blade in the centrifugal field.

The centrifugal field produces a large out-of-plane centrifugal stiffening effect on the blade and a smaller in-plane centrifugal stiffening effect. When a blade is operating at low blade angle conditions, the flatwise natural modes of vibration are increased more than the edgewise modes by the larger out-of-plane centrifugal stiffening effect, because the flatwise motion is primarily out-of-plane. For flatwise modes, as the blade angle is increased the component of out-of-plane motion decreases and the in-plane motion increases so as to reduce the stiffening effect. This causes the blade natural frequency to decrease. The opposite is true for the edgewise natural modes of vibration which have more in-plane motion at low blade angles. Increasing the component of out-of-plane motion with increasing blade angle causes the edgewise mode to increase in frequency with blade angle.

Figure 4.13 also shows that frequency increases with increasing rpm.

The static frequences of the 24 SR-7L blades which were fabricated was experimentally determined immediately after manufacture. The results are tabulated in Table 4.4.

TABLE 4.4
SR-7L BLADE STATIC FREQUENCIES

Mode	Prediction	Limits of Experimentally Determined
1	33.95 Hz	32.4 - 34.07 Hz
2	78.1	76.35 - 80.97
3	137.8	131.2 - 138.3
4	140.9	134.4 - 140.4
5	162.0	154.2 - 162.8

The SR-7A blade natural frequencies derived from low and high speed wind tunnel data are plotted as a function of rotational speed in Figure 4.14 and 4.15. The experimentally determined natural frequencies are also compared to analytical predictions in the figures. In general the best spectral data was observed at low Mach number and high blade angle, where turbulence due to stall excited many modes. Except for the first mode, all of the modes seem to have a response frequency lower than the calculated values. This indicates that the model is slightly softer than anticipated.

The experimentally determined natural frequencies as a function of RPM are compared for the SR-7A and SR-7L in Figure 4.16. The difference in RPM between the SR-7A and SR-7L is again accounted for by plotting frequency times the blade tip radius versus RPM times the blade tip radius. It can be seen from this plot that for the first five vibratory modes, the natural frequencies of the SR-7A and SR-7L blades are for the most part within 10% of each other. This was one of the design requirements for the SR-7A aeroelastic Model.

4.2.3 Summary of Results

It can be concluded from the results that the BESTRAN and NASTRAN computer codes provide accurate predictions of natural frequencies fo the blade configuration and construction that is typical of Prop-Fan design. The results also confirmed the viability of the aeroelastic scaling techniques applied to the design of the SR-7A model and the usefulness of aeroelastic scale models in predicting the aeroelastic performance of a full scale Prop-Fan.

4.3 Stall Flutter Stability

Stall flutter is a vibratory phenomena that usually occurs when a propeller is operating at high power either statically or at a very low Mach number. The high angle of attack at which the blades must operate to absorb the power can lead to stall and flow separation which provides vibratory excitation of the blades. The response of straight blades in stall flutter is generally confined to a single vibratory mode, usually the torsional mode. The stress rise that occurs with the onset of stall flutter is typically gradual and reaches a limit amplitude.

4.3.1 Stall Flutter Stability Analysis

Theoretical analysis of stall flutter is not a well established procedure due to the complexity of the flow about a stalled blade. No attempt was made during the course of this program to improve the analytical tools available for evaluating the stall flutter stability of Prop-Fans. Two existing methods were used to evaluate the stall flutter stability of the SR-7L Prop-Fan. One was a semi-empirical formulation that has been incorporated in the Hamilton Standard aeroelastic stability analysis computer program. The other method was a purely empirical method used for conventional propeller stall flutter analysis.

The semi-empirical method uses combined bending and torsion modes, but does not couple the modes, since stall flutter is generally a single mode phenomenon. The unsteady airfoil coefficients are developed from steady state empirical airfoil data. The results from this analysis give the onset of stall flutter, not the magnitude of the response, because large amplitude stall flutter response is non-linear, while the analysis assumes a linear response.

Table 4.5 lists the conditions examined for stall flutter along with the resulting predictions. The predictions are in terms of blade angle because stall flutter occurs at high power when the blade is stalled and increasing power corresponds to increasing blade angle.

TABLE 4.5

STALL FLUTTER ONSET PREDICTION SUMMARY

	TAKE-OFF/ CLIMB	STATIC THURST	REVERSE
Speed, RPM	1698	1698	1698
Mach No.	0.2	0.0	0.0
Required Blade Angle, Deg.	38.0	33.0	-10.0
Flutter Blade Angle, Deg.	40.0	31.0	No Flutter
Flutter Mode of Vibration	4	4	No Flutter

The predictions show that stall flutter occurs at a lower blade angle than required by the static thrust. This prediction is illustrated by the damping plot of Figure 4.17. The fourth mode, which is the first torsional mode, becomes unstable at a blade angle of thirty one degrees. Instability is indicated by the negative viscous damping ratio encountered at that blade angle. When the Prop-Fan achieves a small amount of forward velocity, the stall flutter stability is greatly improved as seen in the damping plot for the takeoff and climb condition in Figure 4.18. No stall flutter was indicated for the reverse thrust condition.

Since the SR-7L blade has a distinct torsional mode, and stall flutter was predicted for this mode, a stall flutter parameter was applied to the blade. The stall flutter parameter is an empirical design factor that was developed for conventional propeller design to prevent the occurrence of torsional stall flutter. This parameter is calculated for a given configuration and plotted on a stall flutter design chart to see if torsional stall flutter is possible. The calculated stall flutter parameter for the SR-7L blade for a blade angle of 33.0 degrees is 1.35, which is well inside the stable region of a stall flutter design chart shown in Figure 4.19, indicating that no flutter will occur in the torsional mode. It should be noted that the calculated value is well outside the area for which empirical data exists.

The two methods used to predict the stall flutter stability of the SR-7L blade give different results. The first method, the semi-empirical method which predicted the blade angle when flutter would occur, shows stall flutter occurring in a mode that the second method, using the stall parameter, showed to be stable.

4.3.2 Stall Flutter Test

Evaluation of the stall flutter stability of the SR-7L was conducted during the Static Rotor Test at Wright Patterson Air Force Base. The stall flutter stability of the SR-7A aeroelastic model was evaluated in the 9 x 15 Low Speed Wind Tunnel at the NASA Lewis Research Center.

4.3.2.1 SR-7L Test

The stall flutter stability of the SR-7L was evaluated by running RPM traverses at a fixed blade angle. The first vibratory stress limit was encounted at a 32° blade angle. A map of the rotational speeds and blade angle at which stress limits were encountered is presented in Figure 4.20. A blade angle traverse was also attempted in an effort to circumvent the high stress region. As shown in Figure 4.20 the high stress boundary was encountered using this approach as well.

The blade vibratory stress limits were encountered in the blade tip region. The vibratory stress measured at the other locations remained below limits when the tip strain gages reached their respective limits. The high vibratory stress is characterized as buffet rather than flutter because the stress level and frequency content was unsteady in nature. The stress amplitude did not increase suddenly and no mode sustained a sinusoidal response.

The frequency content of the buffet vibratory stress was found not to be independent of the blade pitch angle. At a blade angle of 34° the dominant frequency was found to be 92.5 Hz, which corresponds to the second flatwise bending mode natural frequency. At blade angles above 39° the response frequency changed to 35 Hz which corresponds to the first flatwise mode of vibration.

The 32° blade angle at which the vibratory stress limits were encountered at 1698 RPM was very close to the 31° blade angle predicted by the semi-empirical method for the onset of stall flutter. However, the response mode encountered was different than predicted and the observed characteristic of the vibration did not indicate true stall flutter but buffet. Therefore the usefulness of the semi-empirical method in predicting the onset of stall flutter is questionable.

Although the buffet response was unsteady, spectral analysis indicated that all blades were vibrating at the same frequency. The data analysis showed no coherent inter-blade phase angle during buffet. To investigate why a lack of phase coherence existed with coherent frequency data, zoom spectral analysis was performed on the data to isolate the frequency content. Figure 4.21 shows the results of the zoom spectral analysis, which identified multiple frequency

response peaks in the data. The system is not vibrating at a single frequency. Multiple frequencies in the order of 92.5 Hz plus or minus 1 Hz exist. The multiple peaks show that the Prop-Fan is not responding in a single system mode, therefore no coherent inter-blade phase angle should exist.

4.3.2.2 SR-7A Test

Figure 4.22 shows the SR-7A vibratory strain boundaries, plotted as blade angle versus rotational speed, for a range of Mach numbers from 0 to .2. The boundaries represent the operating conditions at which the vibratory strains in the blade structure reached their predetermined limits. The boundaries for the Mach .15 and Mach .2 are shown as dashed lines since the vibratory strain limit was encountered at only one point below 9000 RPM. Figure 4.22 also indicates the predominant vibratory frequency occurring at various points along the vibratory strain boundaries and the vibratory modes with which they correspond. At high blade angle static conditions the blade vibratory strains are dominated by the first edgewise and second flatwise modes. The maximum response was observed at 328 Hz corresponding to the first edgewise mode. As previously discussed the stall buffet response mode of the SR-7L was found to be a function of blade angle. The SR-7L response frequency corresponded to the second flatwise mode at blade angles below 34° and the first flatwise mode at blade angles above 39°. Similar behavior was exhibited by the SR-7A aeroelastic model as illustrated by the change in response mode along the 0 Mach number vibratory strain boundary curve. For Mach numbers from .05 to .20 and high blade angle, the SR-7A blade buffet was dominated by higher frequency vibration corresponding to the blade second torsional mode.

Figure 4.22 indicates that an area of high vibratory strain was encountered at low blade angles for Mach numbers from 0 to .10. This behavior was not observed during Static Rotor Testing of the SR-7L Prop-Fan. The response frequency for the low blade angle was 590 Hz which corresponds to the first torsional mode. A possible explanation for the high response at low blade angle is wake flutter. Wake flutter is a self excited blade vibration believed to be caused by a given blade passing through the wake of the preceding blade. The theory of wake flutter is based on the idea of a blade natural mode being reinforced periodically by the wake pattern. It is therefore expected that such a flutter condition would occur at those rotational speeds where integral multiples of the rotational frequency are equal to a natural frequency of the blade. As seen in Figure 4.22 for a rotational speed of 7000 RPM the vibratory response was at 590 Hz. The 5P frequency at 7000 RPM is 583 Hz. Therefore these results compare favorably with the wake flutter theory. It is uncertain why the wake flutter phenomenon was observed during static testing of the SR-7A Aeroelastic Model but not during the SR-7L Static Rotor Test.

Figure 4.23 shows the vibratory strain boundaries for the SR-7A at 0° inflow angle and 0 Mach number overlayed on the vibratory strain boundaries determined for the SR-7L during the Static Rotor Test. For the high angle blade cases, good correlation was obtained between the SR-7A and SR-7L.

4.3.3 Summary of Results

The SR-7L Prop-Fan was prevented from absorbing full power during static operation due to high vibratory stress encountered by the blades. The nature of the vibratory stress was characterized as stall buffet rather than true stall flutter due to its unsteady character. The currently available analytical tools for predicting stall flutter were not found to be accurate when applied to Prop-Fans. Although testing allowed the characteristic of the stall buffet vibration to be well defined, the mechanism that causes it could not be isolated from the data taken. Since stall buffet could be an impediment to the certification of Prop-Fans for commercial use this is an area that deserves more attention.

The SR-7A aeroelastically scaled model was found to be a useful tool in simulating the stall flutter/buffet behavior of the full size Prop-Fan.

4.4 Unstalled Flutter Stability

4.4.1 Analysis

The unstalled or classical flutter stability analyses of the SR-7L and SR-7A Prop-Fans were accomplished using an analysis technique developed by Hamilton Standard to take into account the structural and aerodynamic complexities of Prop-Fans. The impetus for the development of this technique was the instability of the SR-5 Prop-Fan wind tunnel model which was observed during test in 1981. The instability was not predicted by methods available at that time. The analysis technique is described in detail in reference 5. The analysis method is a linear modal formulation with fully coupled mode shapes obtained from finite element analysis. The unsteady aerodynamic loads used in the formulation are based on linear compressible two dimensional theory, guided by model test data. The analysis did not consider blade tip losses and used a combination of cascade and isolated aerodynamic data to account for the variation in airfoil spacing between the blade root and tip. Cascade data was used for blade gap to chord ratios of two or less. This results in using cascade effects out to 80% of the blade radius and isolated effects for the remianing outboard 20%.

The design requirement for the SR-7L Prop-Fan was that no unstalled flutter instability exist anywhere in the operating envelope. Table 4.6 lists ten SR-7L operating conditions which were analyzed and the predicted Mach number for the onset of flutter for each condition. In each case the flutter Mach number was higher than the operating Mach number which indicated no flutter should occur. The analyzed conditions included the ONERA S1 wind tunnel operating condition. The eight-bladed wind tunnel condition was actually more severe than any condition within the design flight envelope established for the program.

TABLE 4.6

PREDICTED FLUTTER MACH NUMBER FOR TEN SR-7L OPERATION CONDITIONS

Case	Condition	Operating Mach No.	Altitude, Meters (Feet)	RPM	Flutter Mach No.	Flutter Mode
D1	Design/Cruise	.80	10,675 (35,000)	1,698	.95	3
D2	Take-off/Climb	.20	0 (0)	1,698	.60	3
1A	ONERA 8 blades	.80	4,270 (14,000)	1,698	.85	3
1B	ONERA, 4 blades	.80	4,270 (14,000)	1,698	1.00	2
1C	ONERA, 2 blades	.80	4,270 (14,000)	1,698	.95	2
4	Cruise Low RPM	.80	10,675 (35,000)	1,273	1.00	-
5	Cruise High RPM	.85	10,675 (35,000)	1,783	.92	3
6	Climb, Mid Altitude	.50	3,050 (10,000)	1,698	.76	3
7	Dive, Mid Altitude	.60	6,100 (20,000)	1,698	.92	3
8	Dive, High Altitude	.80	10,675 (35,000)	1,698	1.00	3

The unstalled flutter design requirement for the SR-7A aeroelastic model was to have the same predicted flutter Mach numbers as the SR-7L for equivalent operating condition. The SR-7A was analyzed for both the design cruise and take-off climb conditions and the results compared with the SR-7L. For the design cruise case the SR-7A was predicted to go unstable in mode three at Mach .95, which was the same as predicted for the SR-7L. The similarities between the SR-7L and SR-7A are illustrated in Figure 4.24. The zero damping value of mode three, the damping magnitude, the mode order and trends are very similar for both the SR-7A and SR-7L. For the take-off/climb condition a flutter Mach number of .56 was predicted for the SR-7A as compared to .6 for the SR-7L.

The SR-7A was also analyzed for the Mach .8 cruise condition in the NASA 8 X 6 wind tunnel. This condition tends to be more unstable due to the low density altitude (2292 meters) for the condition. The analysis showed the SR-7A to be marginally stable in mode two, up to Mach .8.

4.4.2 Test

As previously discussed, the SR-7L was analyzed for operation in the ONERA S1 wind tunnel at Mach .8, 1698 RPM and 4267 meters altitude. Due to operating limitations encountered in the wind tunnel, it was only possible to achieve Mach .73 in the wind tunnel with the eight blade Prop-Fan configuation. However operation was conducted at 1850 RPM at Mach .73. Therefore the combination of blade surface Mach number and density altitude resulted in predicted classical flutter stability equivalent to Mach .8. No sudden increase in blade stress, characteristic of flutter, was observed at this operating condition and the SR-7L was therefore found to be stable for this point as predicted.

Operation of the SR-7A was accomplished at Mach .9, 3284 meters altitude in the 8 X 6 wind tunnel. This was significantly above the condition that was analyzed; Mach .8, 2292 meters altitude. Stress data showed no indications of flutter for this condition although the case analyzed was predicted to be marginally stable.

4.4.3 Summary of Results

The classical flutter analysis program, which has been developed by Hamilton Standard for Prop-Fan unstalled stability prediction had previously correctly predicted unstalled flutter instability in Prop-Fan models. The program predicted stable operation of the SR-7L and SR-7A Prop-Fans within their design operating envelopes. This was verified by test during the LAP program, which indicates the analysis is conservative.

4.5 Prop-Fan Forced Vibratory Response

Operation of a Prop-Fan at a yaw angle with respect to the relative flow results in a once per revolution or 1P excitation of the Prop-Fan blades. The 1P excitation is caused by the variation in angle of attack experienced by the blades as they rotate through 360°. It is important to have the capability to calculate the 1P response so that the effect aircraft maneuvers have on blade stress levels can be determined.

4.5.1 Analysis

The 1P responses of the SR-7L and SR-7A Prop-Fans were determined using the finite element models of the SR-7L and SR-7A blades, which were constructed for the design phase of the program. The prediciton procedure began by calculating the steady centrifugal and aerodynamic loads and applying them to the finite element model. The steady aerodynamic loads were calculated using Hamilton Standard Program H444. It is an aerodynamic strip analysis based on Goldstein's vortex theory. A differential stiffening matrix was obtained

from the finite element analysis. The differential stiffening matrix was added to the structural stiffness matrix to account for the additional stiffness created by external loading of the blade. The aerodynamic loads associated with the non-uniform flow field were then applied to the model to determine the 1P response. The aerodynamic loads were determined using Hamilton Standard Program H337 which is an aerodynamic strip analysis employing a skewed wake theory. A Mohr's circle relationship was applied to the vibratory strains calculated using this analysis to determine strains in the directions of the blade strain gages for correlation with test data.

4.5.2 Test

The test installations for the SR-7L in the ONERA S1 wind tunnel and the SR-7A in the NASA Lewis 8 X 6 wind tunnel allowed canting of the rotor with respect to the relative air flow to create a once per revolution excitation of the blades. Therefore it was possible to simulate operating conditions for which analytical solutions for the 1P response had been determined. The 1P vibratory response of the blade was determined by spectral analysis of the strain gage data. Figures 4.25 and 4.26 show the variation of the SR-7L 1P blade shank bending moment response and the 1P blade root flatwise bending strain response as a function of power and Mach number for a 2-blade configuration. The data is compared with analytical predictions. The measured trends in 1P response corresponded well with prediction, however the magnitude of the measured response was significantly lower than was predicted. Table 4.7 shows a comparison of the measured and predicted 1P vibratory strains at several locations on the SR-7A blade for three selected operating conditions. Again there was a tendency to over-predict the 1P response.

4.5.3 Summary of Results

The analytical tools in place for calculating Prop-Fan 1P vibratory response predict trends as a function of parameters such as Mach number, power and RPM correctly. However improvement is needed in predicting the magnitude of the response.

TABLE 4.7

COMPARISON OF BESTRAN/NASTRAN PREDICTED SR-7A
1P VIBRATORY STRAINS WITH TEST DATA

Location of Strain Gage	Inflow < = 2.08° M = 0.6, RPM = 8004 SHP = 355, 3/4 = 51.85			Inflow < = 2.45° M = 0.8, RPM = 8004 SHP = 104, 3/4 = 54.5°			Inflow < = 2.13° M = 0.8, RPM = 8006 SHP = 417, 3/4 = 57.33°		
	GAGE STRAINS ±, IN/IN,			SHANK MOMENTS ± IN-LB					
	TEST	BESTRAN	BESTRAN / TEST	TEST	BESTRAN	BESTRAN / TEST	TEST	BESTRAN (NASTRAN)	BESTRAN / TEST
Shank Edgewise BG1-E	7	17	2.43	9	24	2.67	8	26 (23.4)	3.35
Shank Flatwise BG1-F	101	129	1.28	151	211	1.40	159	199 (199.5)	1.25
Mid-Blade Bending BG1-3	138	143	1.04	179	236	1.32	209	223 (223)	1.07
Tip-Bending BG1-4	119	87	0.73	82	147	1.79	149	136 (131)	0.91
Chordwise Bending BG1-5	30	29	0.97	12	33	2.78	17	20 (17)	1.17
Tip Shear BG1-6	91	126	1.38	86	174	2.04	99	198 (191)	2.00

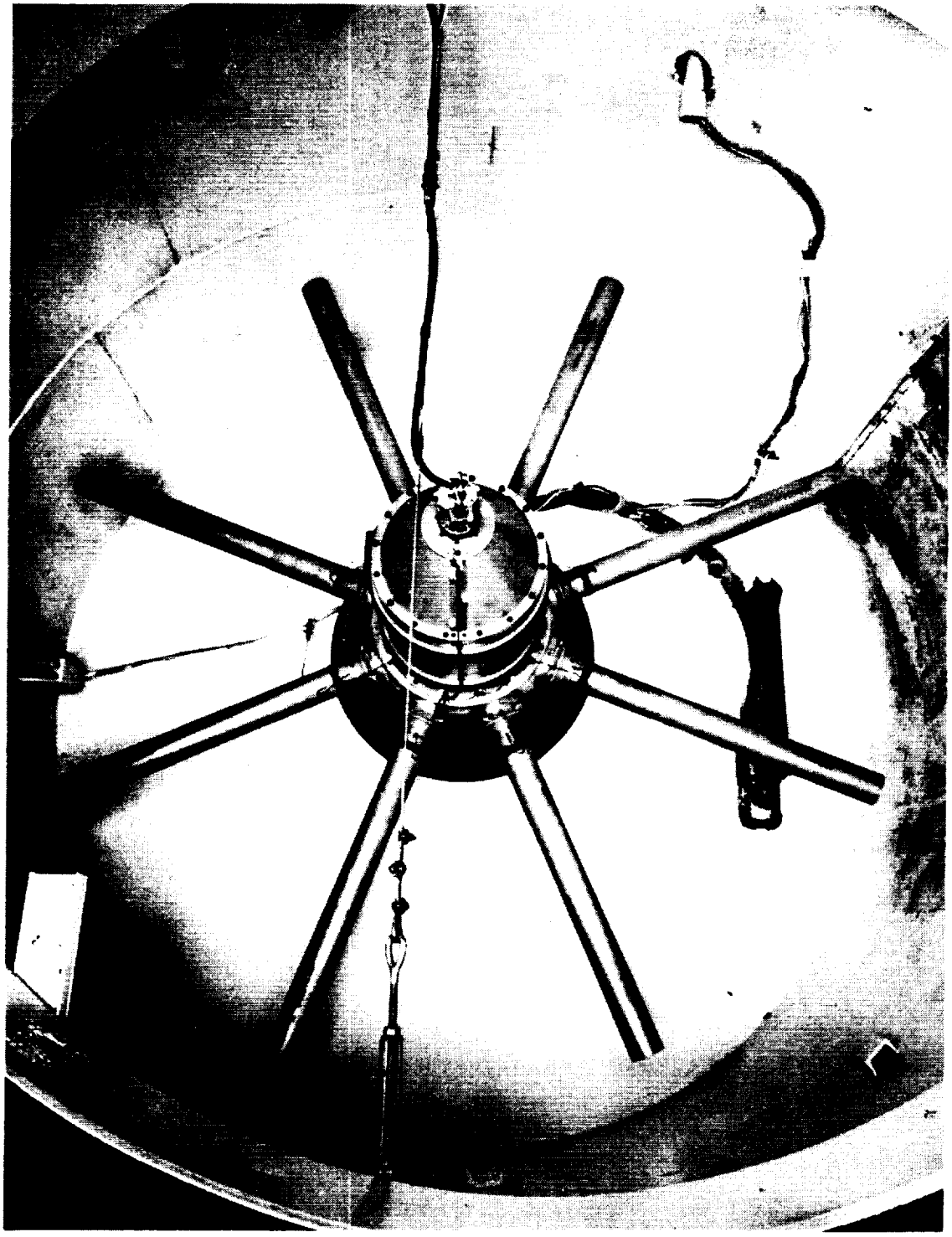

E-37996

FIGURE 4.1 RETENTION STIFFNESS TEST ARRANGEMENT

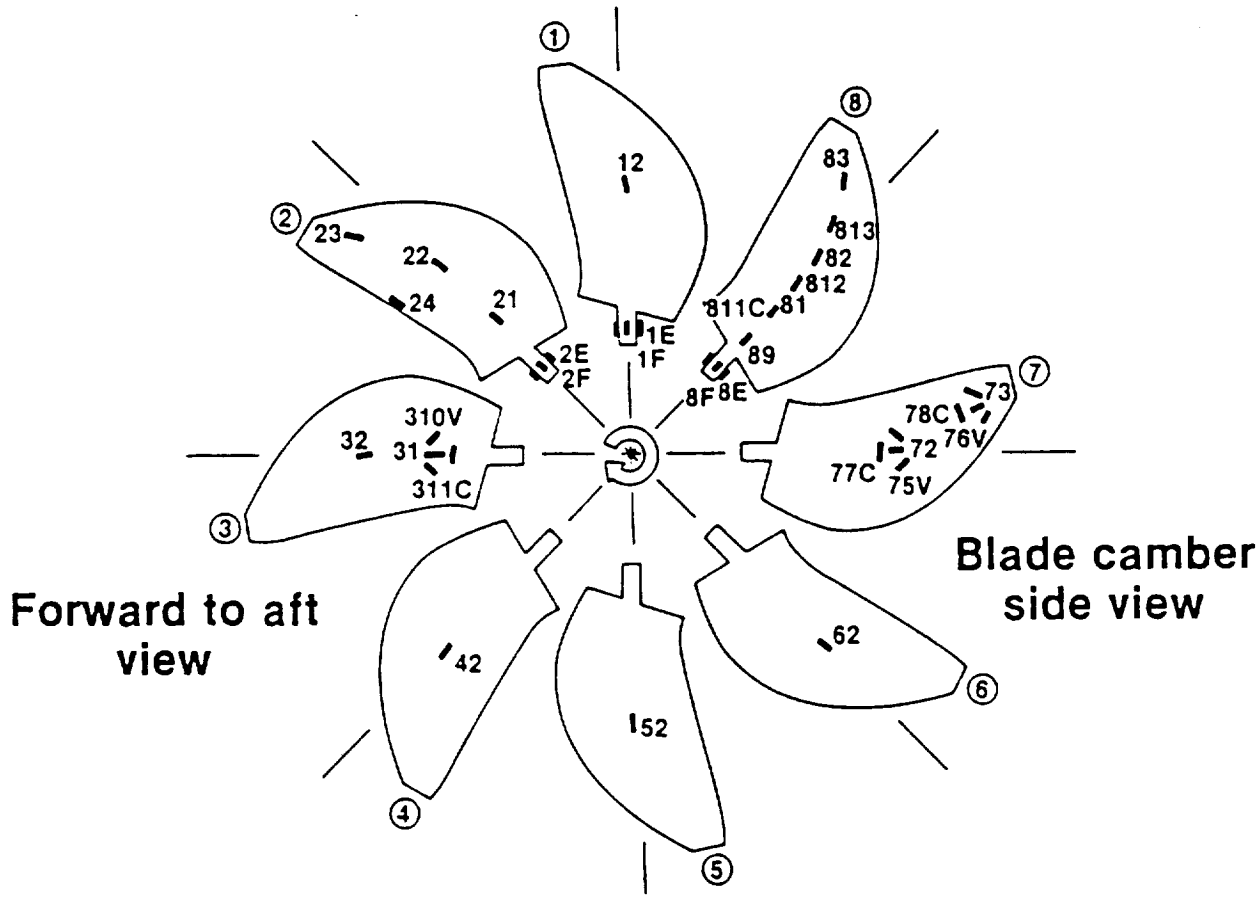

FIGURE 4.2 ACTIVE STRAIN GAGE ARRANGEMENT FOR SR-7L FLUTTER AND CRITICAL SPEED TESTING

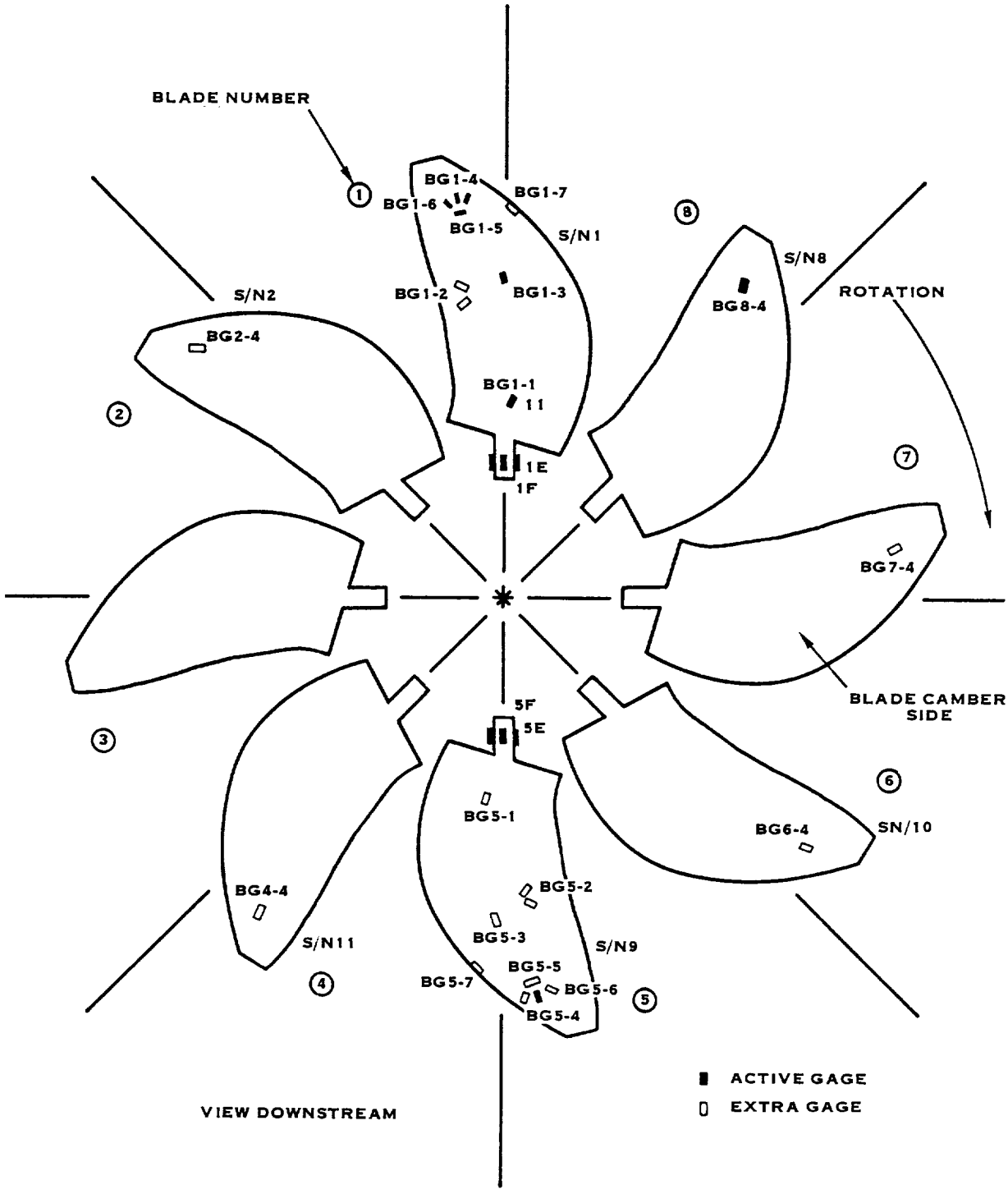

FIGURE 4.3 SR–7A STRAIN GAGE ARRANGEMENT

E-3798

FIGURE 4.4 SR-7A MODEL PROP-FAN IN 8 X 6 FOOT NASA-LEWIS WIND TUNNEL

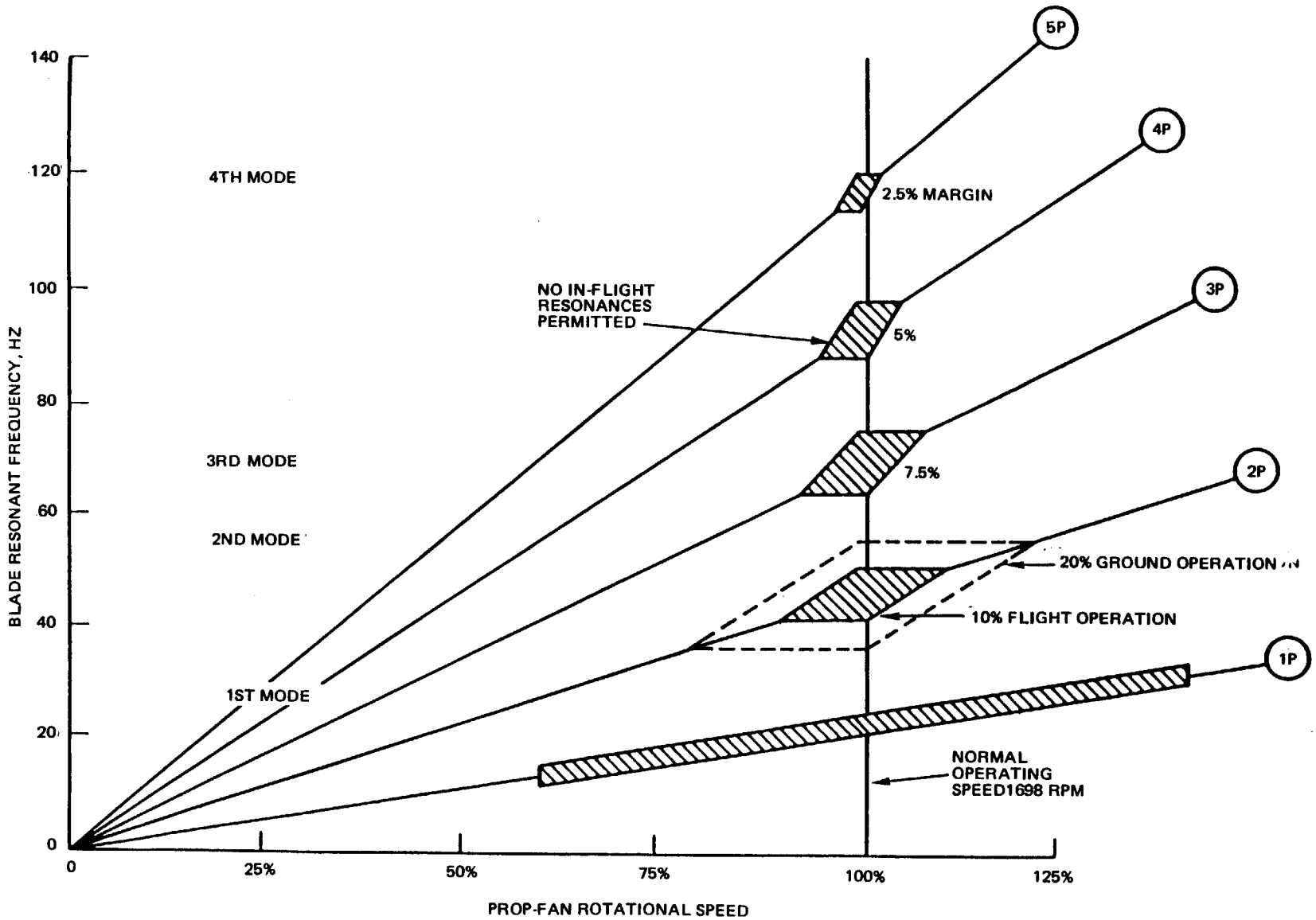

FIGURE 4.5 RESONANT FREQUENCY REQUIREMENTS

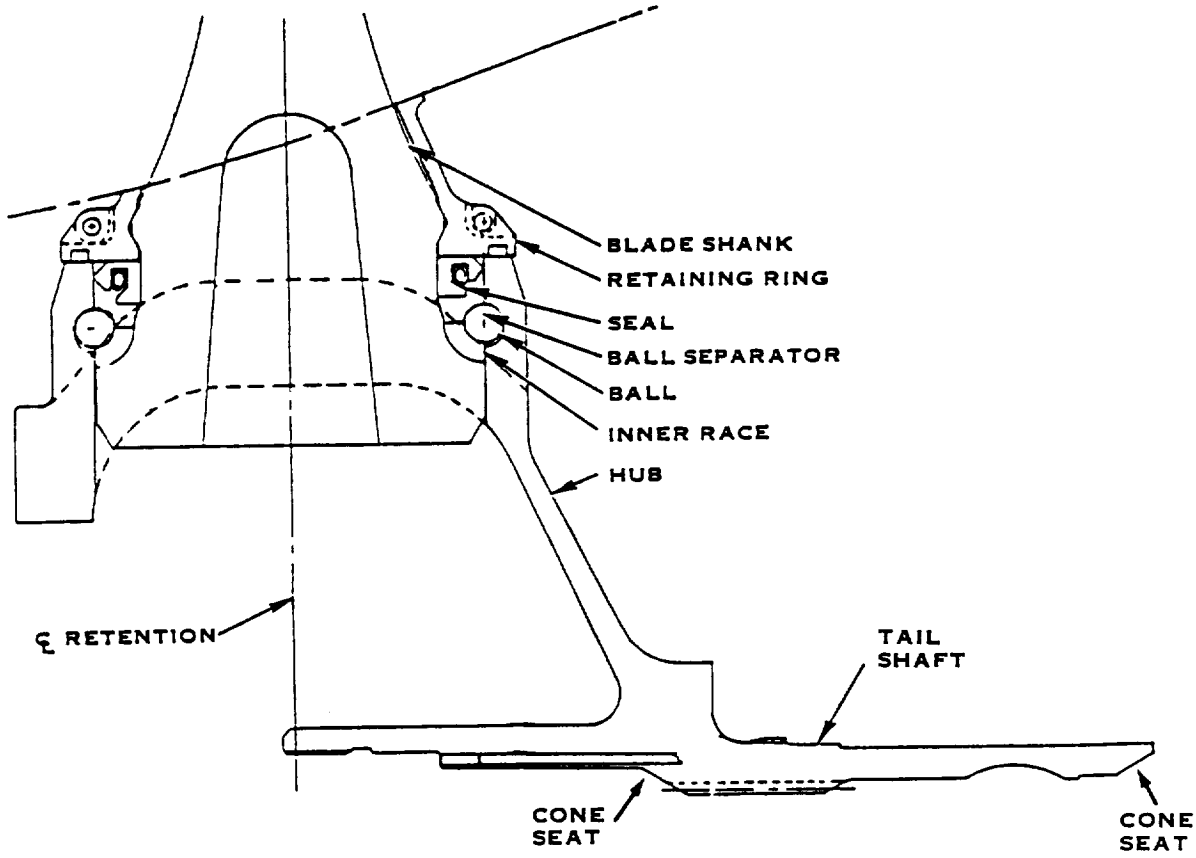

FIGURE 4.6 CROSS SECTION, LAP HUB AND BLADE RETENTION

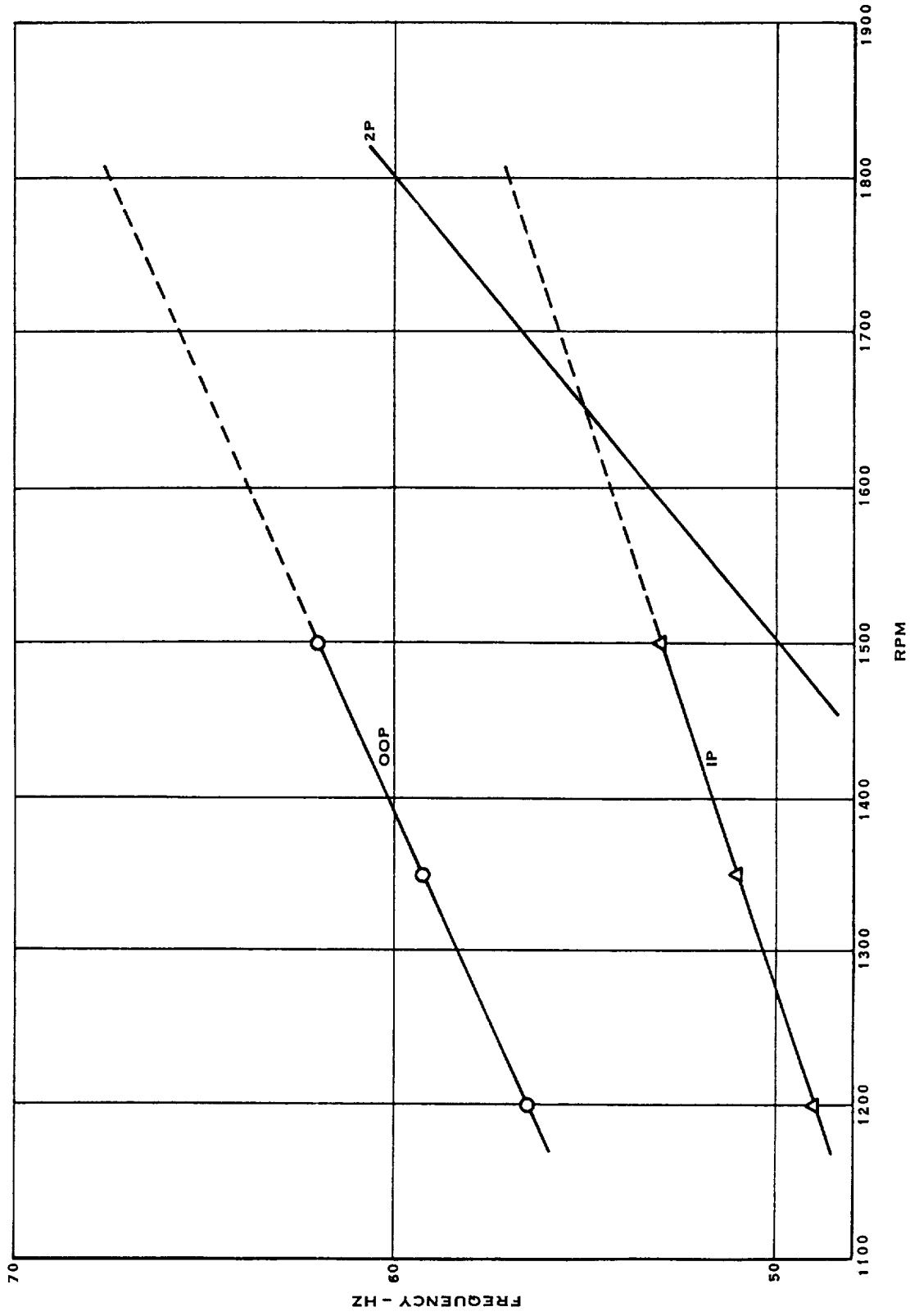

FIGURE 4.7 STUB NATURAL FREQUENCY VS. RPM

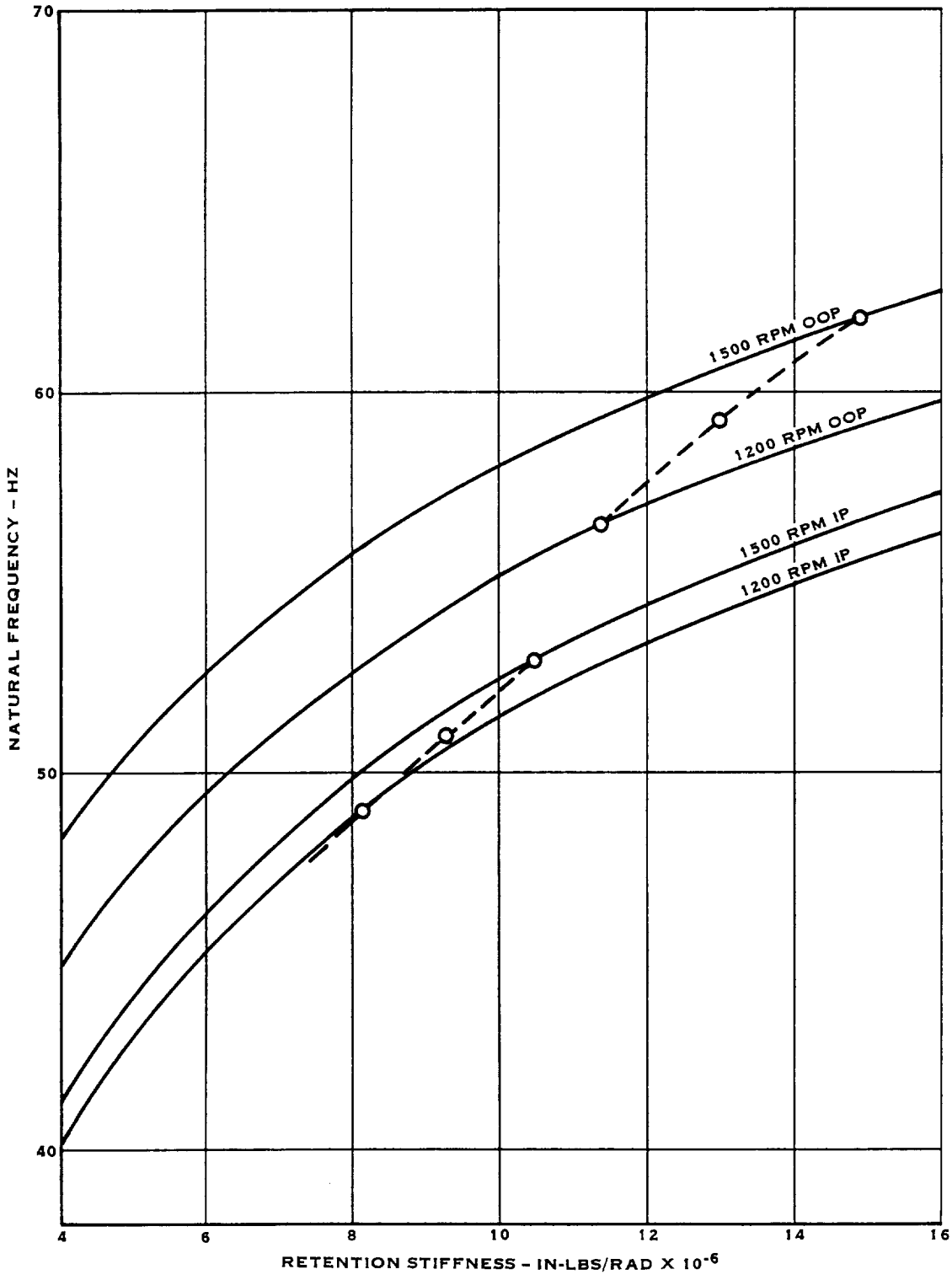

FIGURE 4.8 STUB NATURAL FREQUENCY VS. RETENTION STIFFNESS

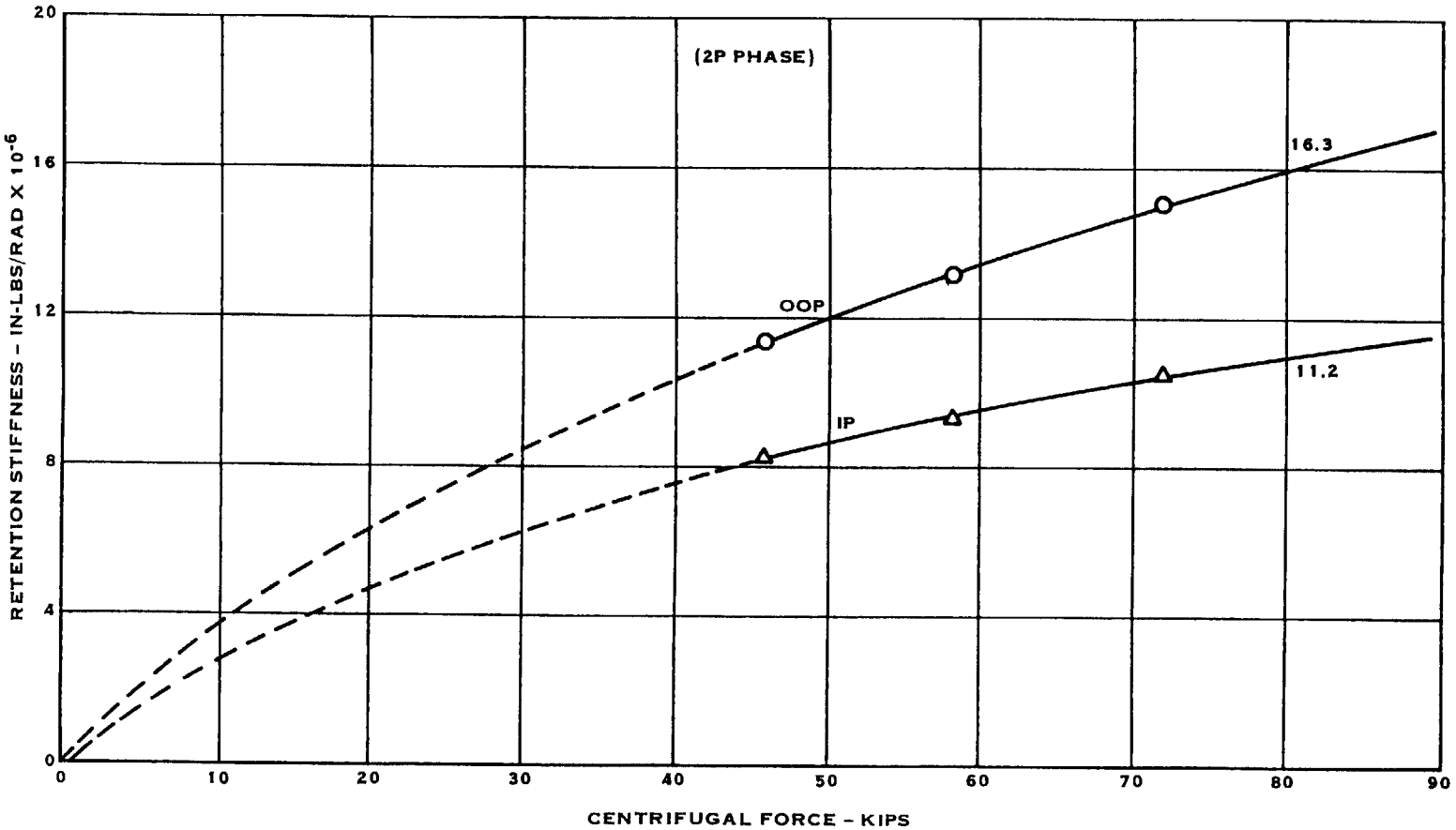

FIGURE 4.9 RETENTION STIFFNESS VS. CENTRIFUGAL LOAD

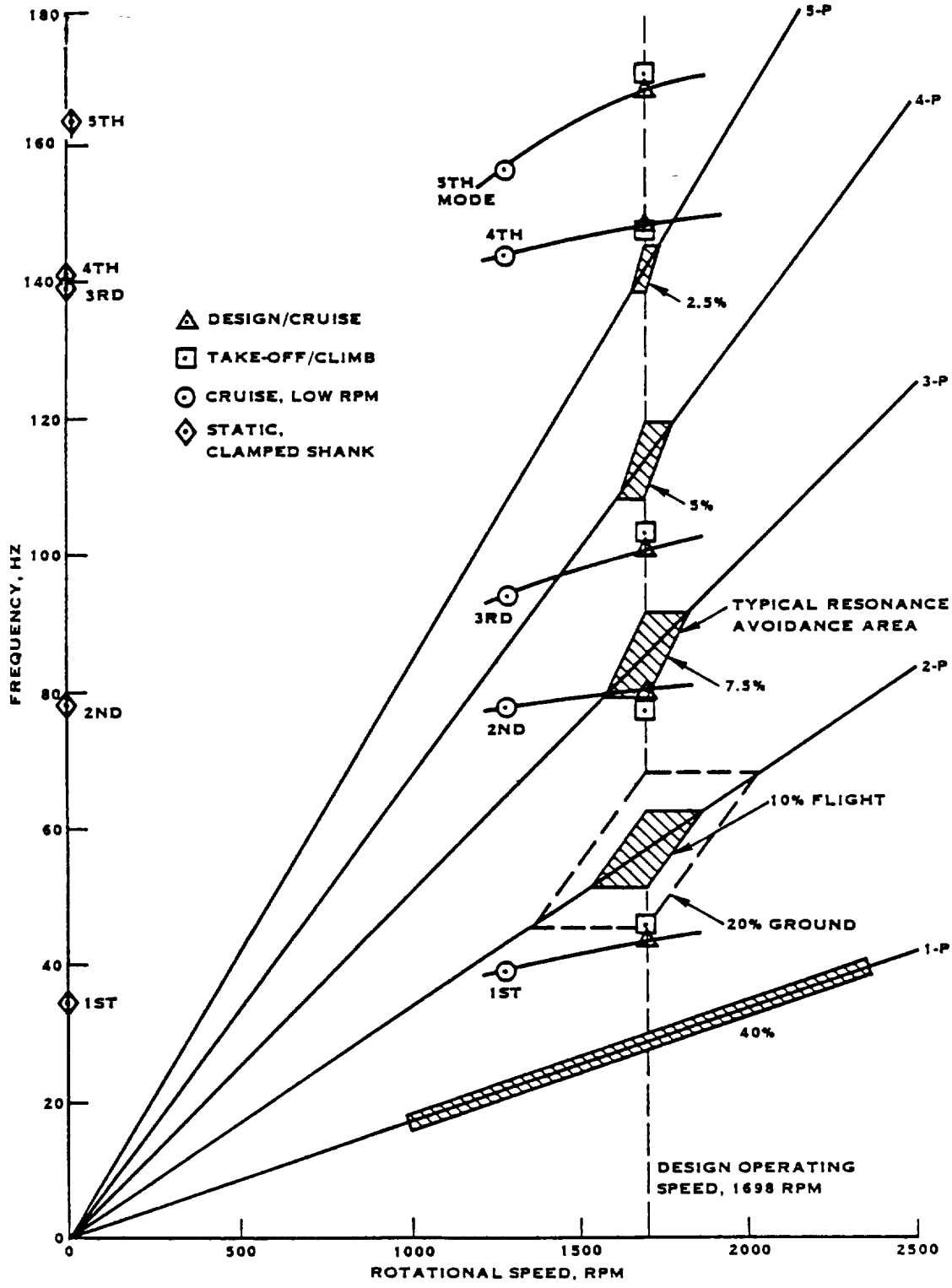

FIGURE 4.10 SR–7L CALCULATED MODAL FREQUENCIES

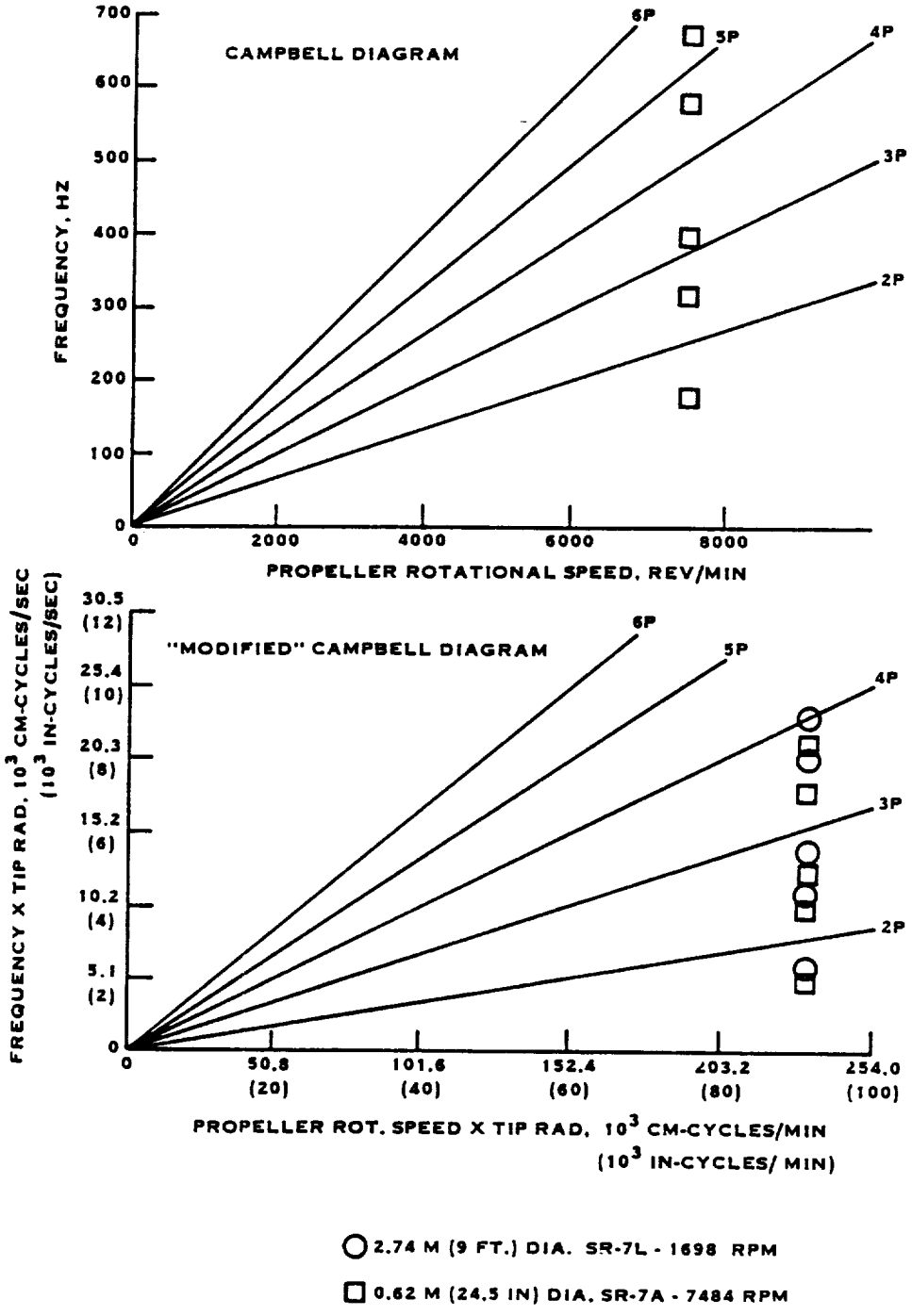

FIGURE 4.11 COMPARISON OF SR–7A AND SR–7L CALCULATED NATURAL FREQUENCIES ON MODIFIED CAMPBELL DIAGRAM

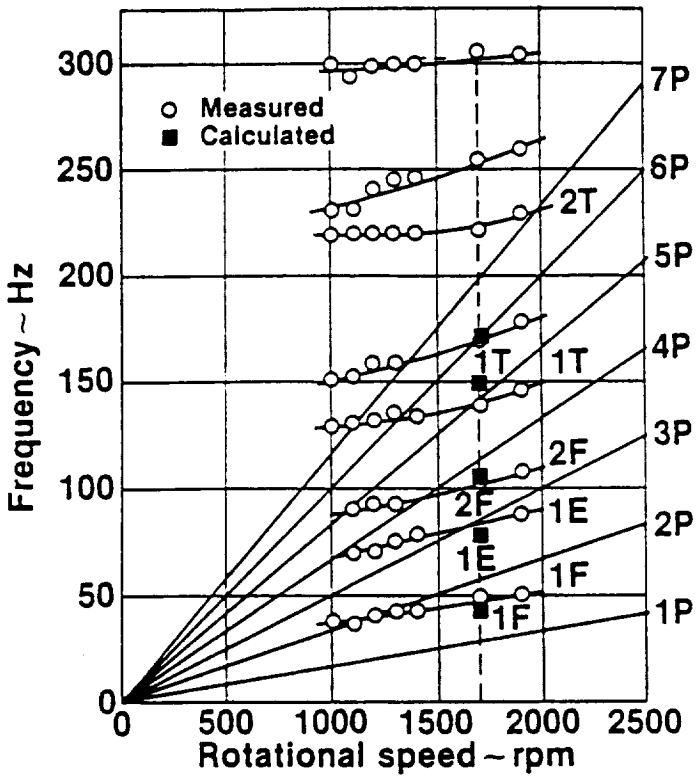

FIGURE 4.12 SR–7L BLADE NATURAL FREQUENCIES DERIVED FROM STATIC TEST DATA

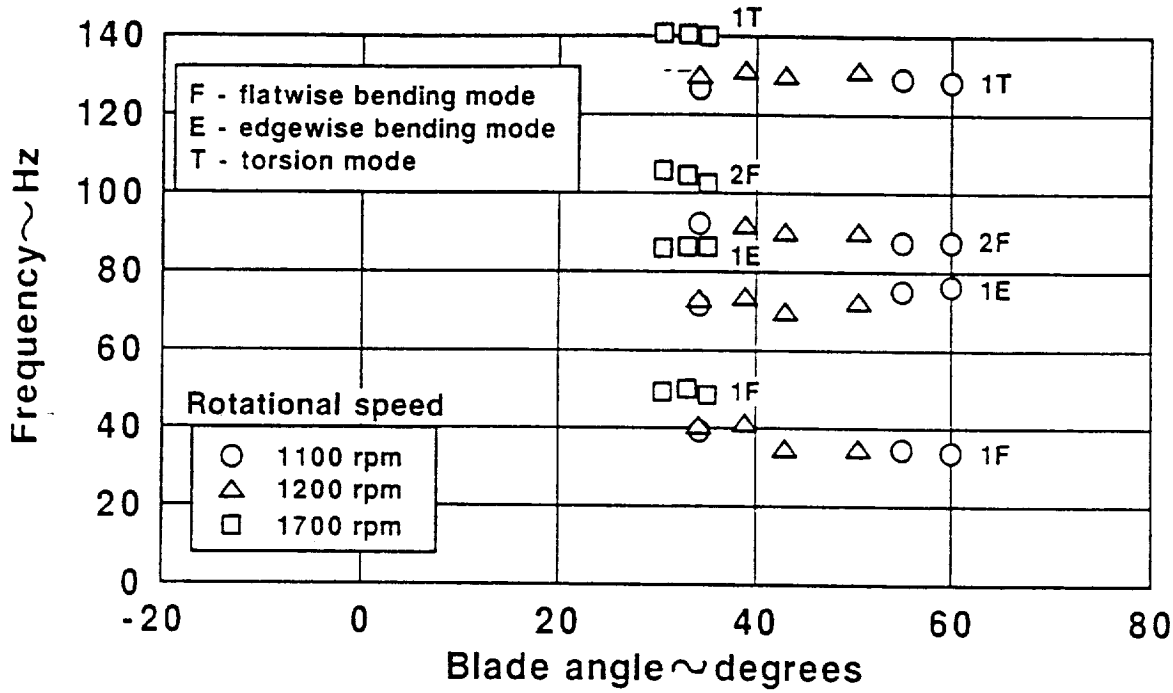

FIGURE 4. 13 THE EFFECT OF BLADE ANGLE ON BLADE NATURAL FREQUENCY FOR THE SR-7L

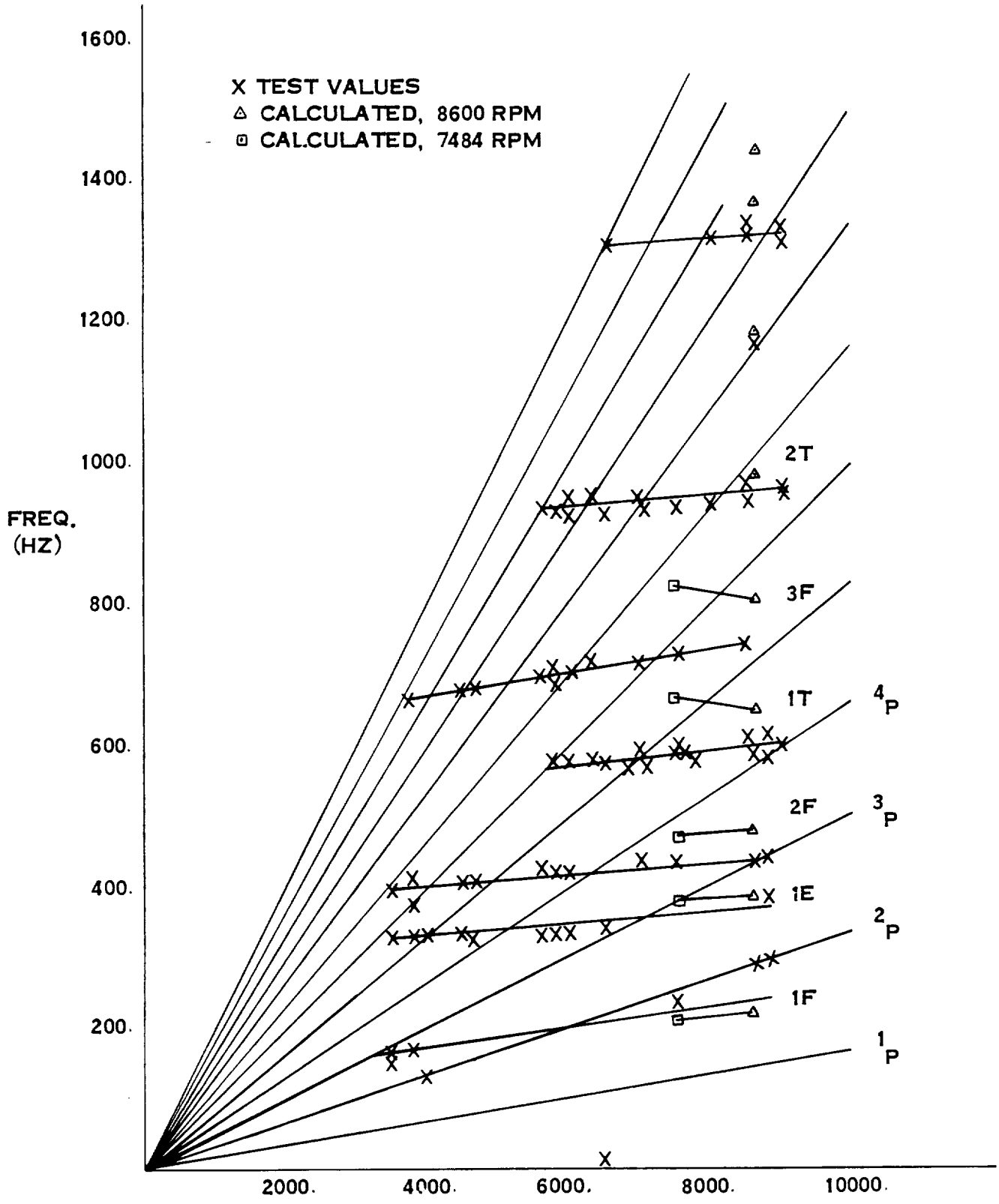

FIGURE 4.14 SR–7A BLADE NATURAL FREQUENCY VS. RPM DERIVED FROM LOW SPEED WIND TUNNEL DATA

E-38093

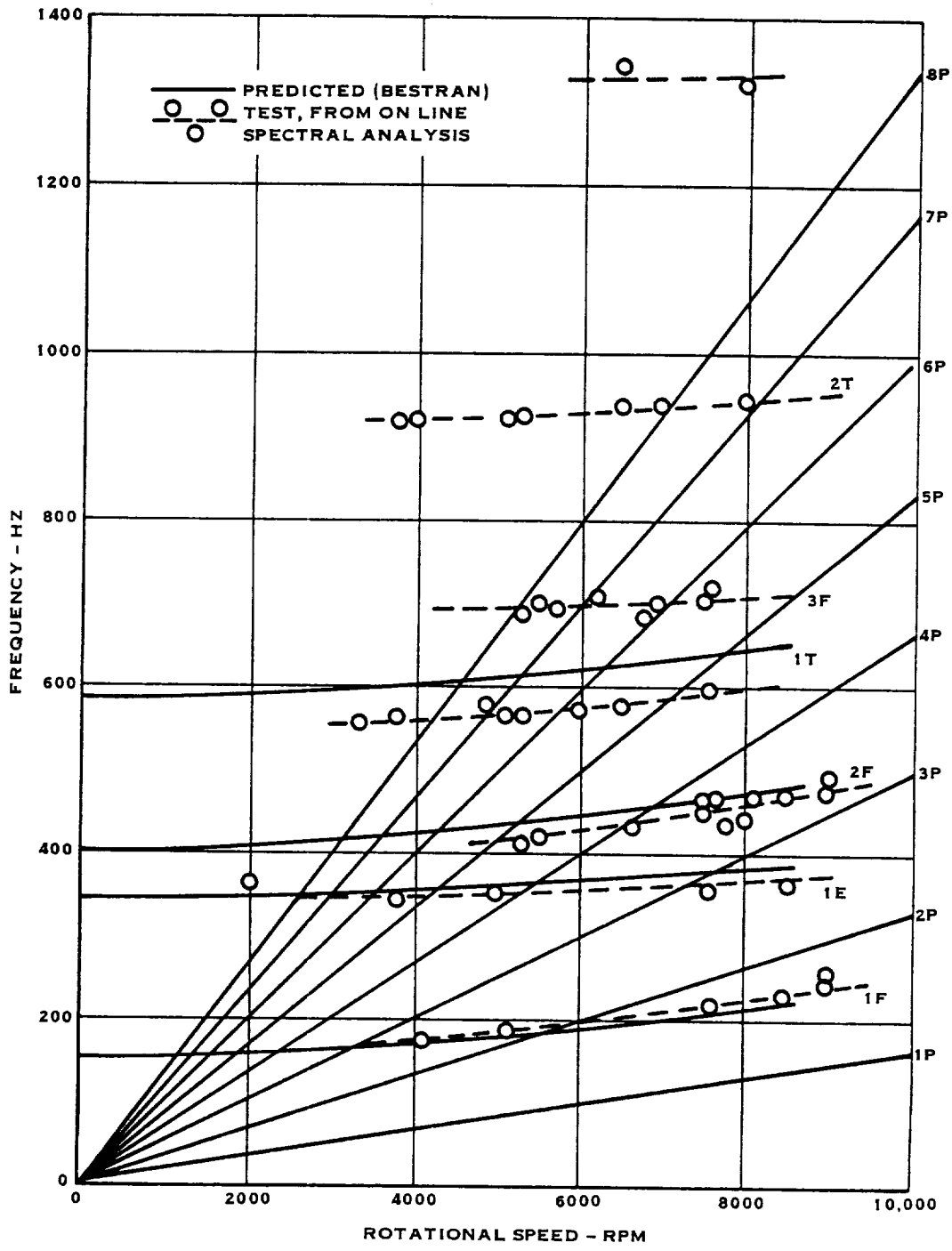

FIGURE 4. 15 SR–7A BLADE NATURAL FREQUENCY VS. RPM DERIVED FROM HIGH SPEED WIND TUNNEL DATA

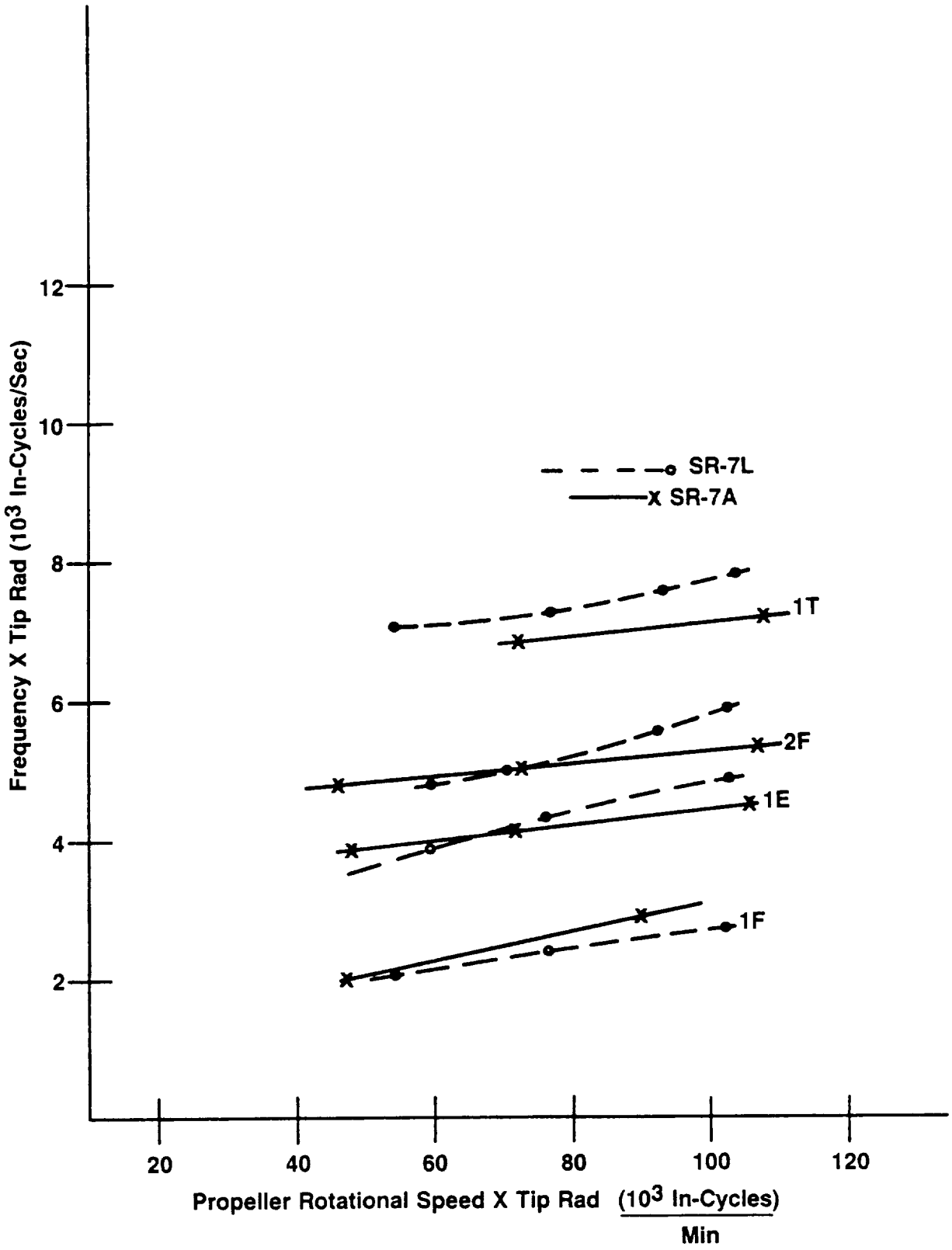

FIGURE 4.16 COMPARISON OF EXPERIMENTALLY DETERMINED SR–7A AND SR–7L NATURAL FREQUENCIES

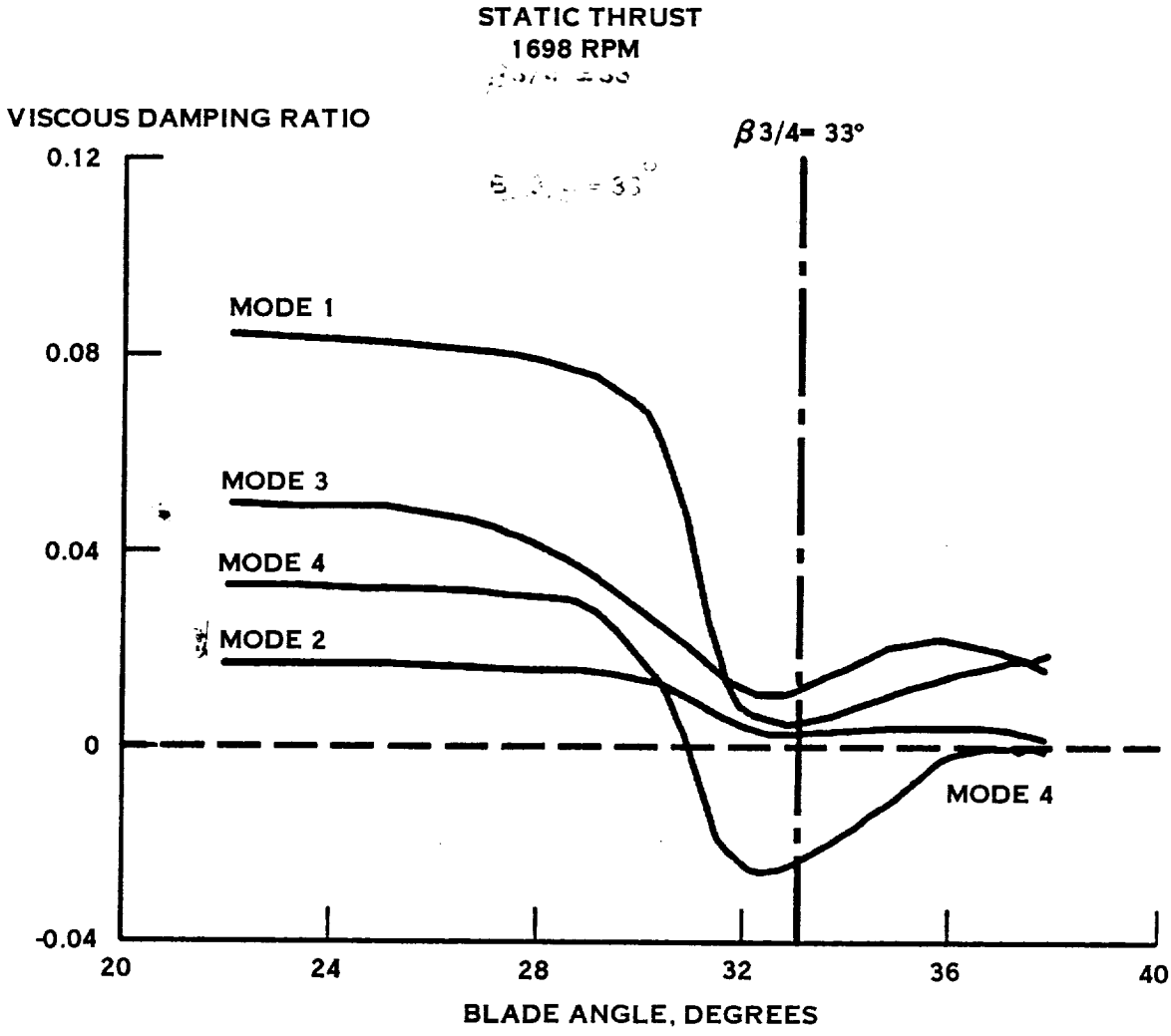

FIGURE 4.17 SR-7L STALL FLUTTER STABILITY

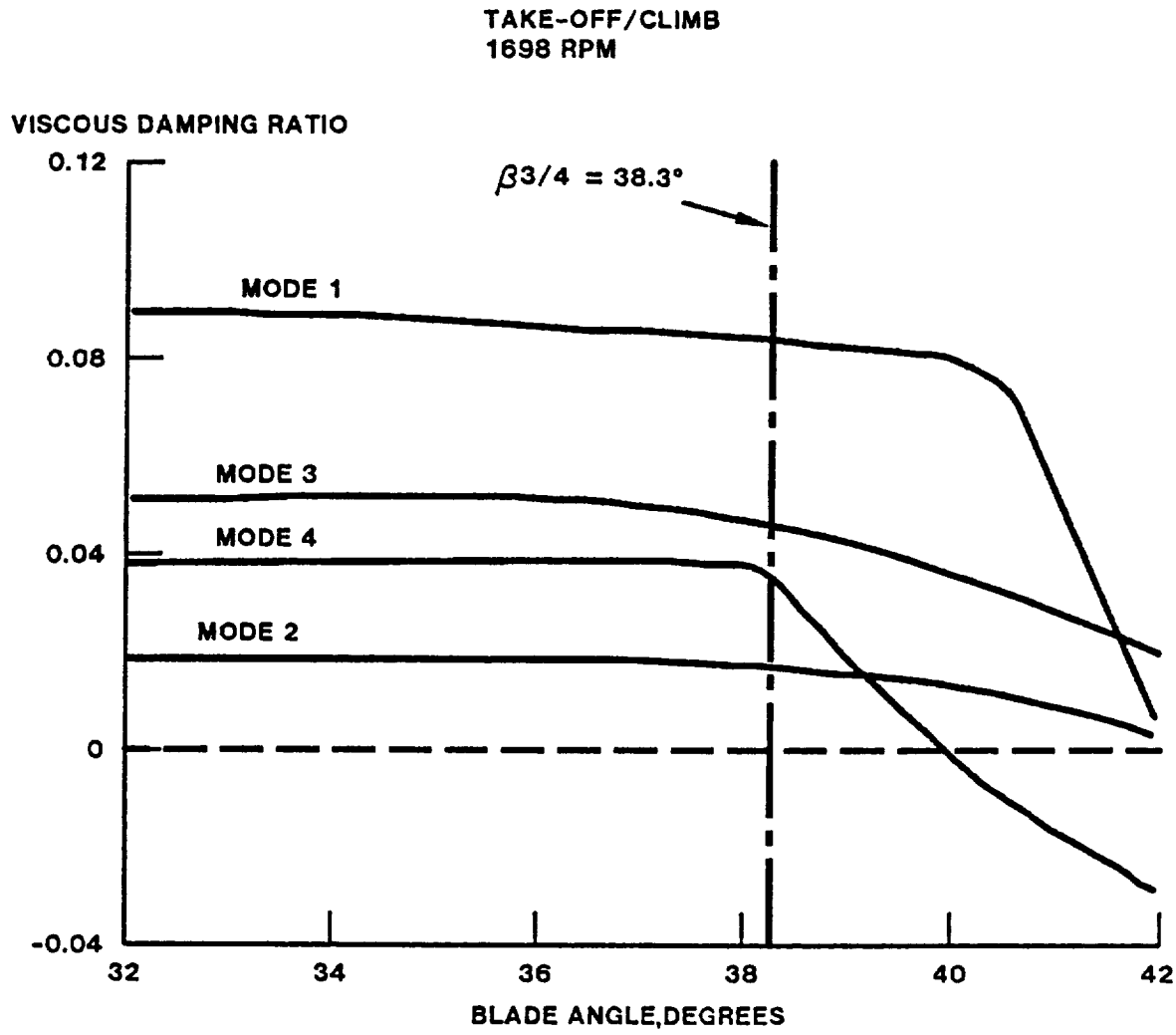

FIGURE 4.18 SR-7L STALL FLUTTER STABILITY

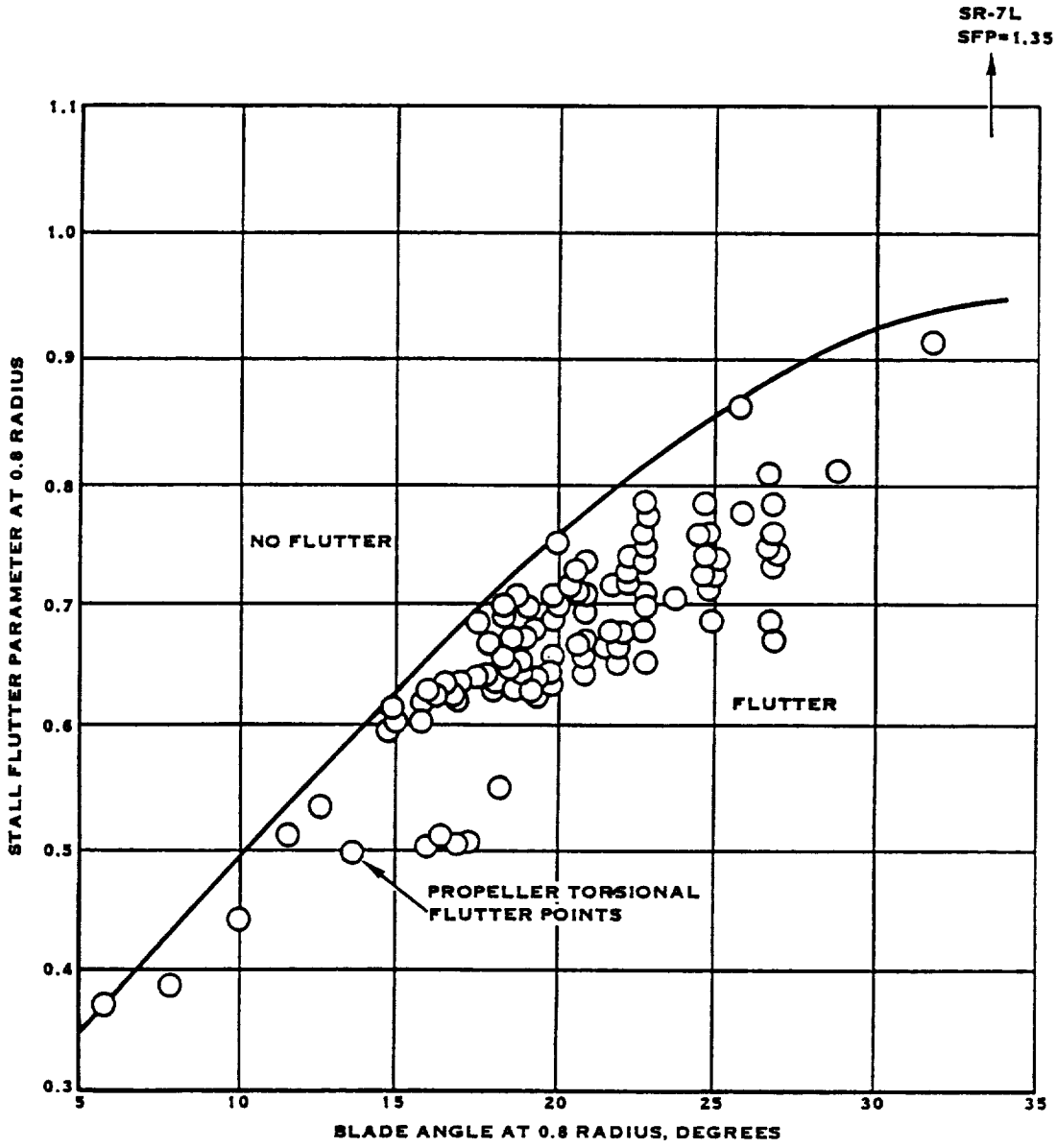

FIGURE 4. 19 STALL FLUTTER DESIGN CHART

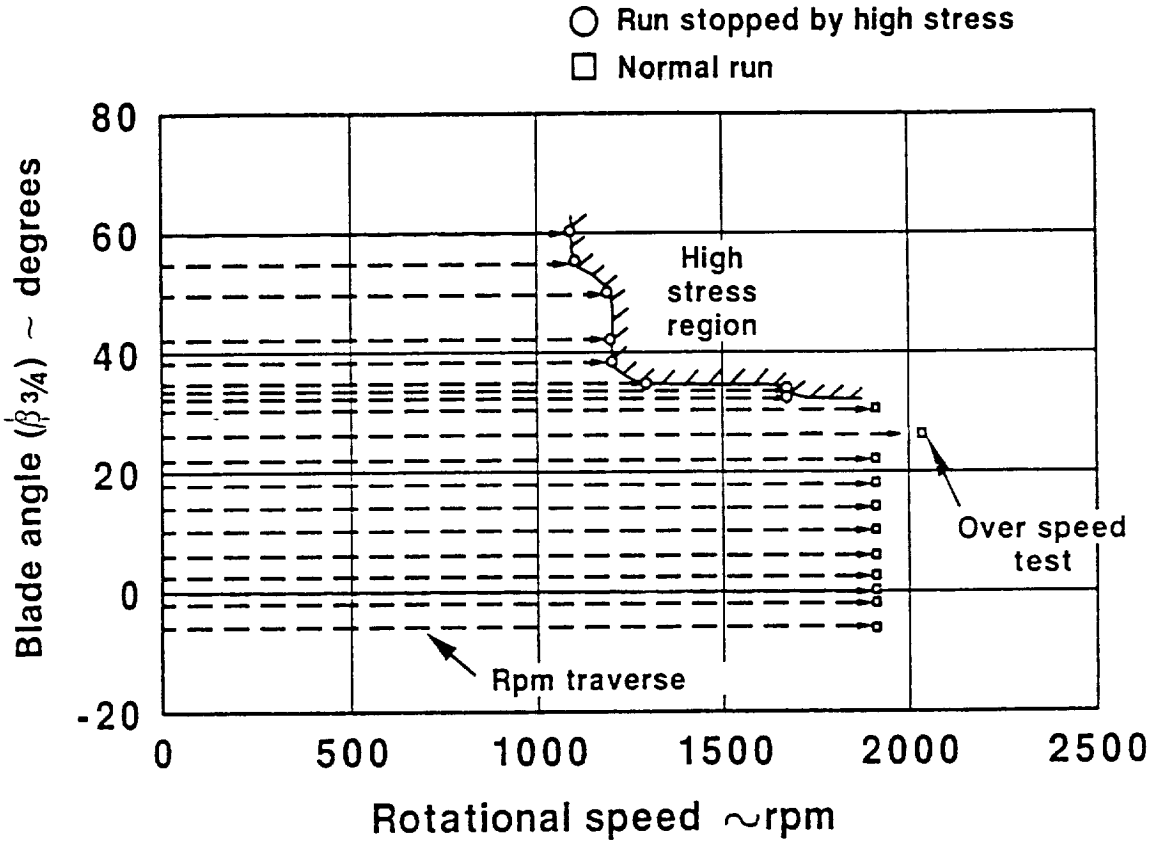

FIGURE 4.20 SR-7L STATIC ROTOR TEST HIGH VIBRATORY STRAIN OPERATING LIMITS

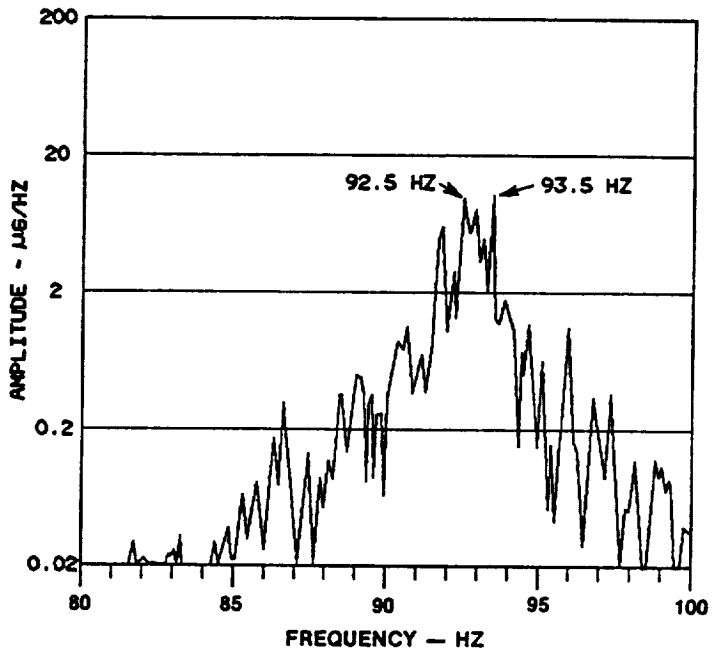

FIGURE 4.21 ZOOM SPECTRAL ANALYSIS OF THE MID—BLADE BENDING GAGE (72) FOR 1300 RPM, 34.2° BLADE ANGLE

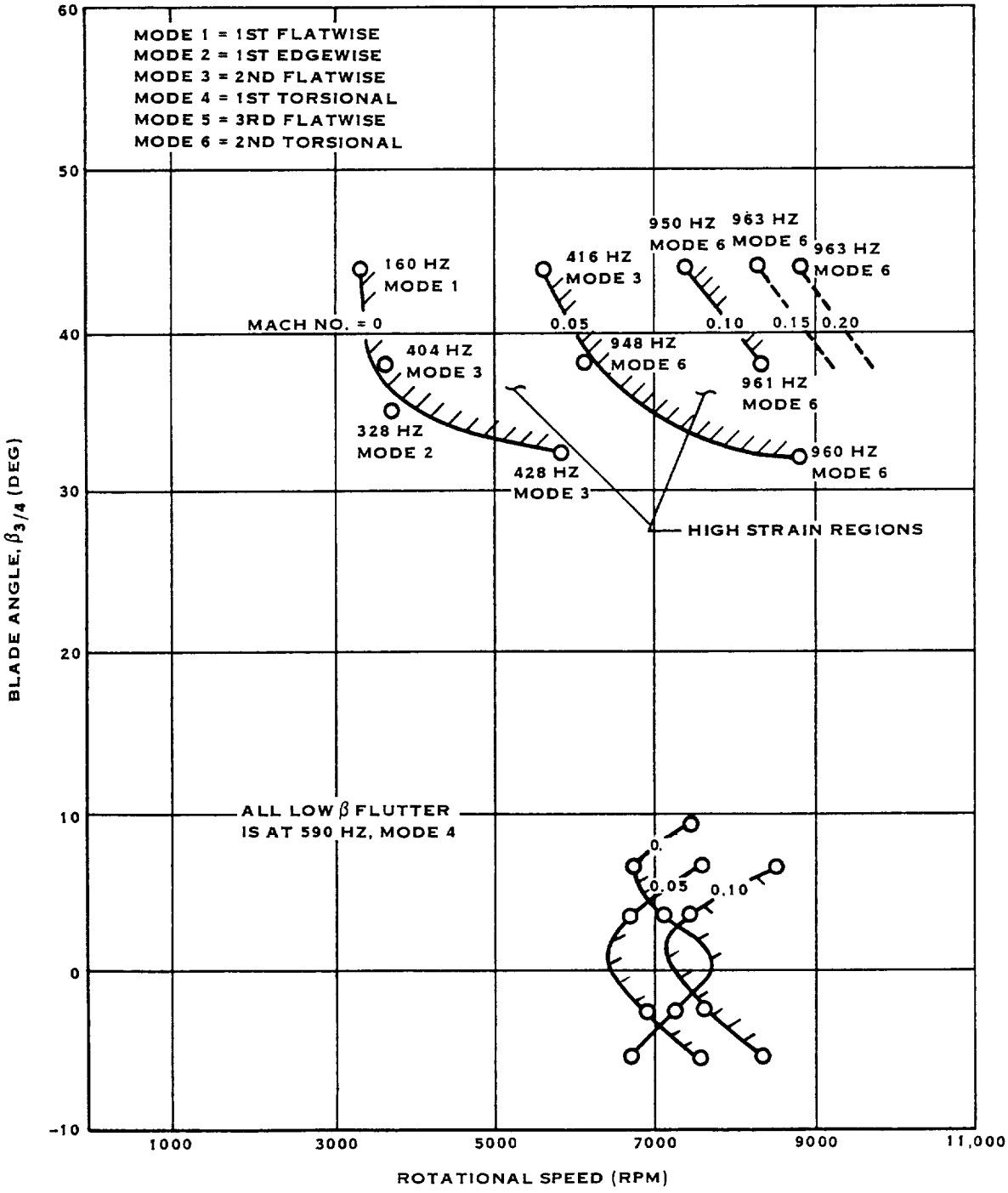

FIGURE 4.22 SR–7A HIGH VIBRATORY STRAIN OPERATING LIMITS

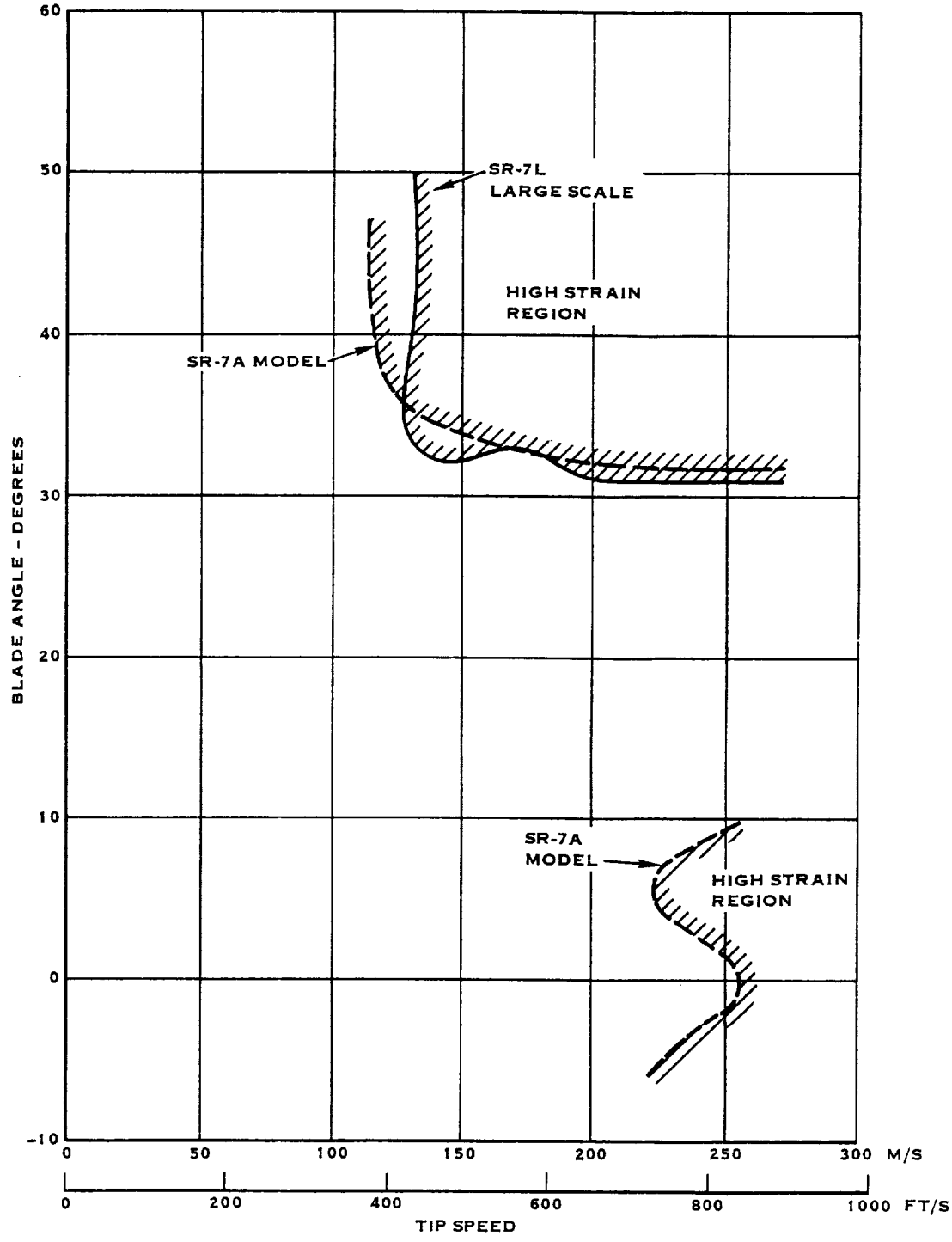

FIGURE 4.23 COMPARISON OF HIGH VIBRATORY STRAIN OPERATING BOUNDARIES FOR SR–7A AND SR–7L

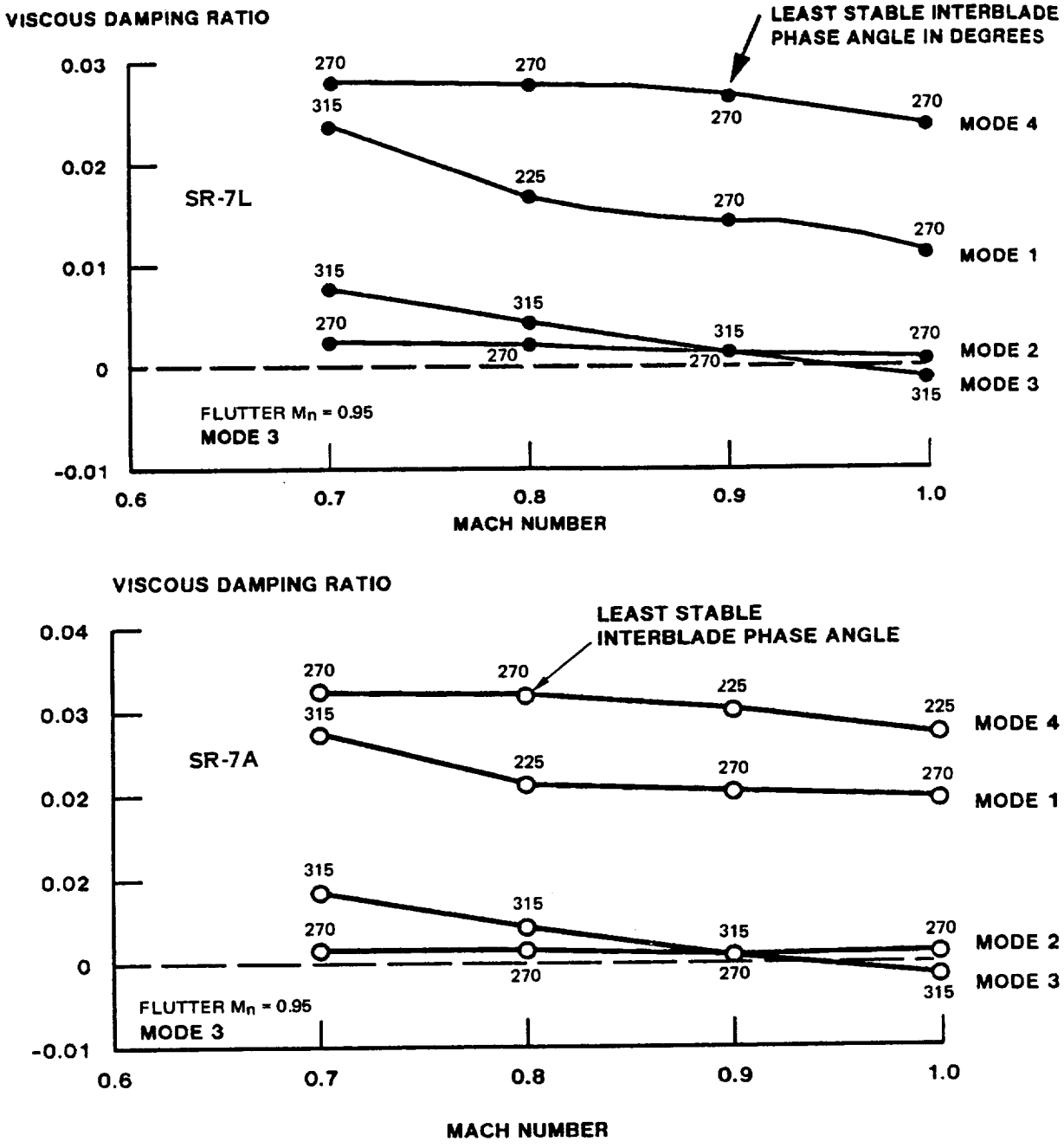

FIGURE 4.24 COMPARISON OF PREDICTED UNSTALLED STABILITY AT MACH 0.8 DESIGN CRUISE CASE FOR SR-7L AND SR-7A PROP-FANS

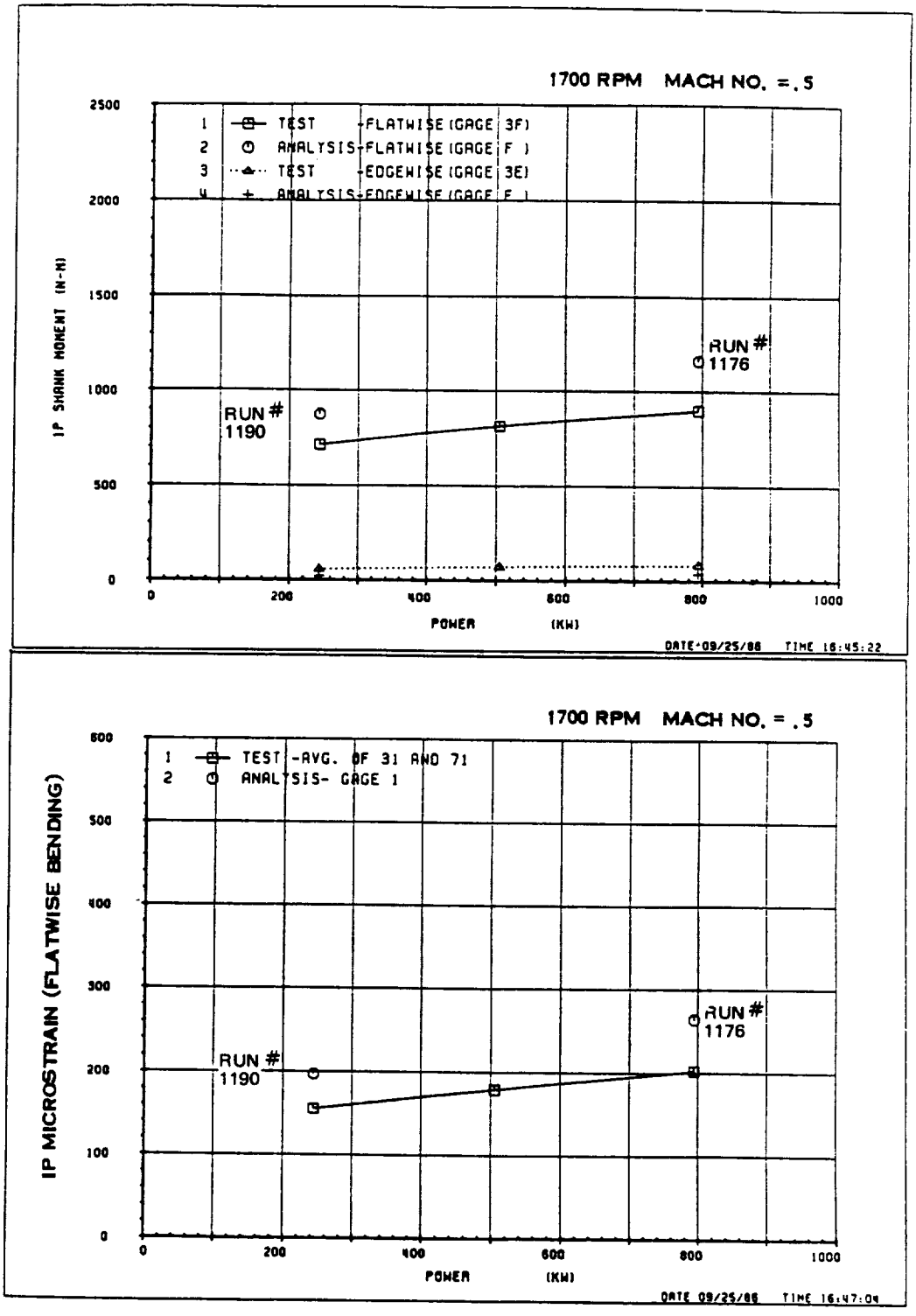

FIGURE 4.25 SR-7L TEST VS ANALYSIS-EFFECT OF POWER ON 1P RESPONSE

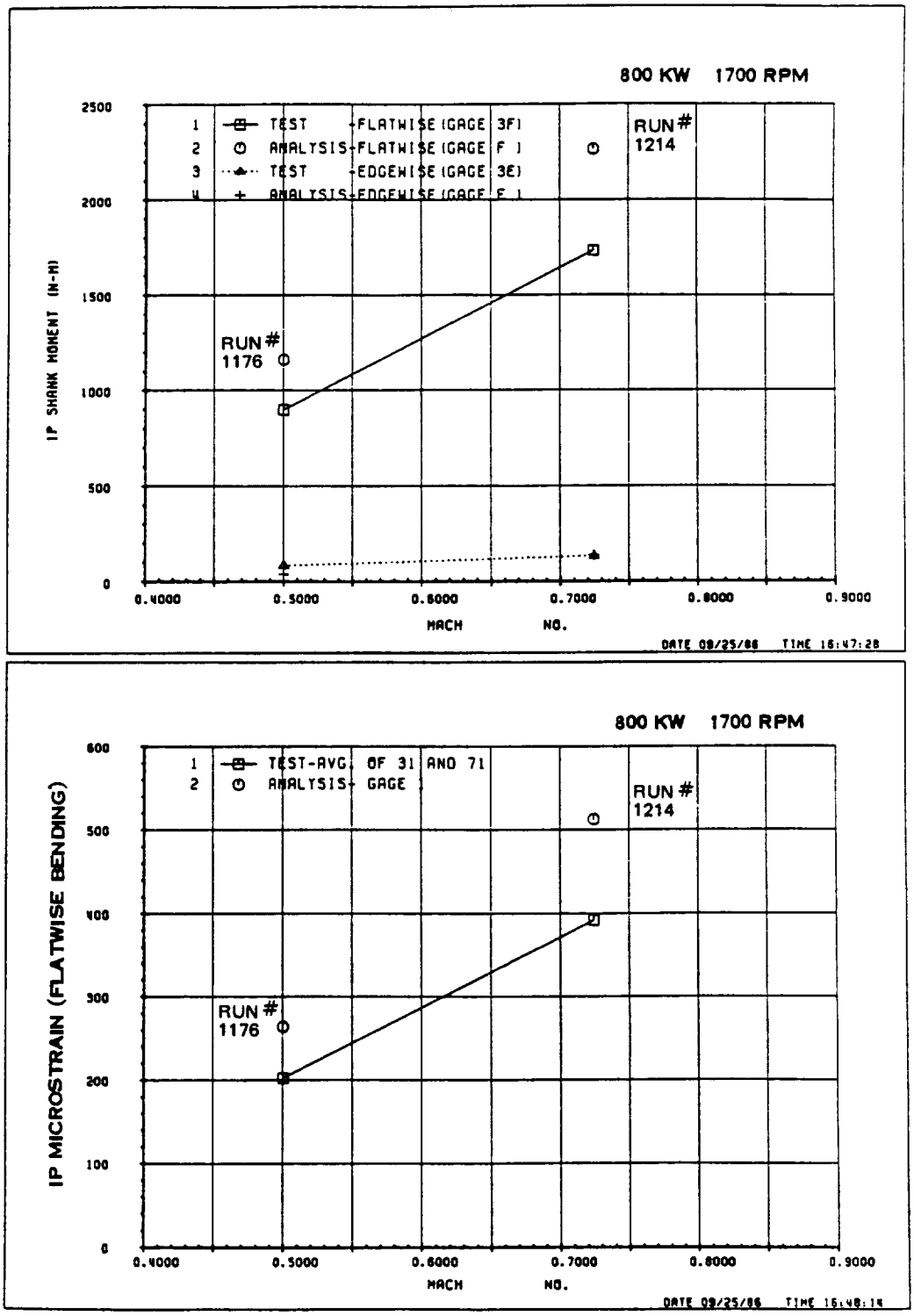

FIGURE 4.26 SR-7L TEST VS ANALYSIS-EFFECT OF MACH NO. ON 1P RESPONSE

5.0 ACOUSTICS

The acoustic design of the SR-7L Prop-Fan blade was conducted during the preliminary design study contract NAS3-22394 which preceded the Large Scale Advanced Prop-Fan Program. The results of the acoustic design were reported in Reference 1. No acoustic testing of either the SR-7L or SR-7A Prop-Fans was conducted during the LAP program. Extensive evaluation of the acoustic performance of the SR-7L Prop-Fan is planned for the follow on NASA Prop-Fan Test Assessment (PTA) program. The PTA program will include the acquistion of extensive near field and far field acoustic data with the Prop-Fan mounted on a Gulfstream II aircraft and operating over a range of representative flight conditions. Near field data will be acquired using microphones mounted on the wing and fuselage of the aircraft and in the aircraft cabin. Testing will be conducted over a range of Mach numbers from .2 to .85, altitudes from 1524 m (5,000 ft.) to 1219 m (40,000 ft.), tip speeds from 183 m/sec (600 ft./sec.) to 256 m/sec. (840ft./sec.) and a range of powers from 440 KW to 4476 KW. Far field data will be acquired from ground based microphones with the aircraft simulating takeoff and climb operating conditions at 305 m (1,000 ft.) above ground level. Hamilton Standard will make analytical predictions of the near field and far field noise levels for selected test points so that the accuracy of the analytical methods can be evaluated by comparison of predictions with data.

Although there was no direct effort to acquire acoustic data during the Large Scale Advanced Prop-Fan Program the blade surface steady pressure measurements, which are discussed in Section 3.2 of this report, did provide insights into the sources of noise generated by Prop-Fans. These insights are related to the discovery of the existence of vortex flow on the surface of the Prop-Fan blades.

5.1 Effect of Vortex Flow on Prop-Fan Noise

Propeller noise calculation is based on the evaluation of the integrals of source terms on the blade surface. The linear sources are given by the blade geometry for thickness, noise and by the blade pressure distribution for loading noise. Aerodynamic methods to determine blade loading for Prop-Fans are for the most part based on the assumption of fully attached flow. Noise prediction using this assumption have been good at high tip speeds where thickness noise is dominant. But at low speed high power coefficient conditions, typical of Prop-Fan take-off, calculations tend to under-predict noise levels. This was illustrated by testing of the SR-3 Prop-Fan model in the United Technologies Research Center Acoustic wind tunnel.

An explanation of the under-prediction of noise levels for low speed high power conditions may be found in the existence of blade tip vorticies at these conditions. The existence of the blade tip vortex was uncovered from SR-7L blade surface steady pressure data. This phenomena was discussed in Section 3.2.2 of this report. The lift distribution dropping to zero at the tip causes a spanwise flow component outward on the face side of the blade and

inboard on the camber side. Under ideal conditions the flow stays attached as it wraps around the tip. If the lift is too high the flow separates and forms a vortex on the camber surface. This vortex produces extra lift at the tip, beyond what would be predicted by potential flow.

Analytical methods have been developed to consider the noise source resulting from the radial flow and tip vortex. This methology is discussed in Reference 6. The conclusions of the analysis indicate that the additional tip loading resulting from the tip vortex produces dipole radiation that has an important influence on noise. At low speeds, typical of take-off, this noise source radiates in phase with the thickness noise and makes a significant contribution to the overall noise level. At higher speeds, this source is out of phase with thickness noise and may actually provide an overall noise reduction.

6.0 MATERIALS AND FABRICATION TECHNIQUES

The SR-7L and SR-7A Prop-Fans were designed and fabricated without the use of exotic materials or the development of significant new manufacturing technology. The thin, highly swept Prop-Fan blades were fabricated using the aluminum spar, fiberglass shell, foam fill construction that has been service proven in Hamilton Standard's commercial and military propellers. The integrity of Prop-Fan blades fabricated using these materials and manufacturing techniques was demonstrated by fatigue testing of the blades and by the rotating tests run during the course of the program. The remaining Prop-Fan components were also constructed from materials that are common to other Hamilton Standard commercial and military propellers and using fabrication methods that are standard in the aerospace industry. The fact that Prop-Fan technology could be implemented using currently available materials and manufacturing techniques makes a strong case for the readiness of this technology for commercialization.

The manufacturing techniques employed in the fabrication of the SR-7L and SR-7A Prop-Fans are briefly described in the following sections.

6.1 Manufacturing

6.1.1 SR-7L Blade Fabrication

The SR-7L blade was manufactured using a vacuum injection fabrication method. The injection molding process inherently results in repeatable blades since the airfoil is produced by matched dies fabricated from a close tolerance master blade.

Manufacture of the blade began with fabrication of the spar. The spar is an aluminum forging, which was finish machined to obtain the proper airfoil contour and shank configuration. The low blade thickness to chord ratio, swept leading edge and the large amount of blade twist increased the complexity of the spar fabrication process. In the injection molding process urethane foam was formed around the spar in matched dies. Fiberglass cloth was laid up over the spar/foam assembly, a formed sheath was positioned over the outboard leading edge, and an integral de-icing heater was assembled to the inboard leading edge. Both the spar and sheath were previously coated with adhesive in areas which form a bond joint at assembly. This assembly was placed in a two-piece female die and epoxy resin was injected into the fiberglass and cured at an elevated temperature. A blade is shown being removed from the resin injection dies in Figure 6.1.

The high temperature cure not only cures the epoxy resin but provides it with elevated temperature resistance needed during operation. All of the high temperature cures during the blade manufacture were accomplished with the blade restrained in matched dies to preclude any airfoil distortion. Following the final resin cure in the injection molding die, the blade was not exposed to temperatures greater than those experienced in operation. Inspection of the airfoil was accomplished using airfoil templates to confirm conformance to the

aerodynamic shape. The complete blade aerodynamic shape; contour, angle, leading edge alignment, face alignment, thickness and width were inspected at each design station. The blade was then painted with erosion coating.

6.1.2 SR-7L Hub Fabrication

The LAP hub was fabricated using conventional techniques which are used in the manufacture of Hamilton Standard's propeller hubs. The hub was fabricated from a steel forging which was heat treated to obtain the desired mechanical properties. A wood pattern of the hub was fabricated and the external contour of the hub was hydrotelled using the wood pattern as the master. The eight holes for the blades were bored and the races were rough machined. The races were hardened using a carburization process and then finish ground. A development program was conducted to determine the optimum parameters for the carburization process.

6.1.3 SR-7L Spinner Fabrication

The shell of the LAP spinner was fabricated using an injection molding technique and hard tooling. Fiberglass cloth was layed up on a male mandrel, the female mandrel was placed on top and resin was injected into the tooling. The front and mid-spinner bulkheads were fabricated by laying up fiberglass cloth over rigid foam forms and then bonding these assemblies to the ID of the spinner shell. The rear spinner bulkhead was also fabricated by injection molding using hard tooling. The interconnecting platforms between the front and rear spinners were injection molded using soft tooling. Hard tooling was required for the spinner shell and aft bulkhead because of the complexity of their shapes.

6.1.4 SR-7L Pitch Control and Actuator

The pitch control and actuator were fabricated using conventional techniques which are commonly used in aerospace manufacturing. Many of the components were acquired from vendors who produce similar production hardware for Hamilton Standard. Some of the control components are common with a military control or were fabricated by modifying existing 54460 control components.

6.1.5 SR-7A Aeroelastic Model Blade Fabrication

Fabrication of the SR-7A blade began with the manufacture and preparation of the titanium blade spar. The spars were machined using a 6X tracing master, constructed from stacked airfoil templates, to guide the grinding operation. The spar contours were inspected using 10X comparator charts. The bonding surface of the spar was prepared by passivation and application of an epoxy based adhesive. After cure the adhesive coated surfaces were abraded by sand blasting to enhance bonding.

The next step in the fabrication process was construction of the spar/foam sub-assembly. This was accomplished using a foaming mold. The foaming mold defined the leading and trailing edge foam cavities, held the spar in the correct spatial orientation with respect to the leading and trailing edge foam

pieces and provided holes for injection and venting of the foam. The foaming mold is depicted in Figure 6.2. The airfoil surfaces of the foam mold were coated with epoxy based adhesive, which was partially cured.

The mold was then bolted together with the spar properly aligned in the mold cavity. Foam was injected into the leading and trailing edge cavities under vacuum and the assembly was cured in an oven. The assembly was extracted from the mold and the flashing was removed by a hand operation. The spar/foam sub-assembly is shown in Figure 6.3.

The shell was constructed using the resin injection mold shown in Figure 6.4. A layup of dry glass cloth and unidirectional graphite fibers were cut and stitched for both the face and camber sides of the blade. The face and camber shell pads were then located on the spar/foam assembly and sewn in place. This assembly was placed in the resin injection mold. Epoxy resin was injected into the mold and the resin was cured in an oven. The blade assembly was removed from the mold, trimmed and painted with erosion coating. Non-destructive testing of the blades included X-ray and tap testing to detect the pressure of any foam voids and delaminations.

The fabrication of the SR-7A blade tooling did represent an advancement in manufacturing efficiency. Previous to the SR-7A, the construction of foam and resin injection tooling began with the fabrication of airfoil masters. The masters were defined by a series of points along the airfoil surface at several discrete radial stations. These points were faired to obtain the blade master shape. The foaming and resin injection dies were then machined by hydrotell from the master. In the case of the SR-7A blade a CATIA data base was constructed for the SR-7A blade shape. The CATIA data base defined every point on the aerodynamic surface of the SR-7A blade. By use of a CAD/CAM computer, proper offsets from the SR-7A blade shape were calculated to define the foaming and resin injection die contours mathematically. This information was then transmitted directly to numerically controlled milling equipment that was used to machine the dies. This eliminated the need to create the master.

ORIGINAL PAGE
BLACK AND WHITE PHOTOGRAPH

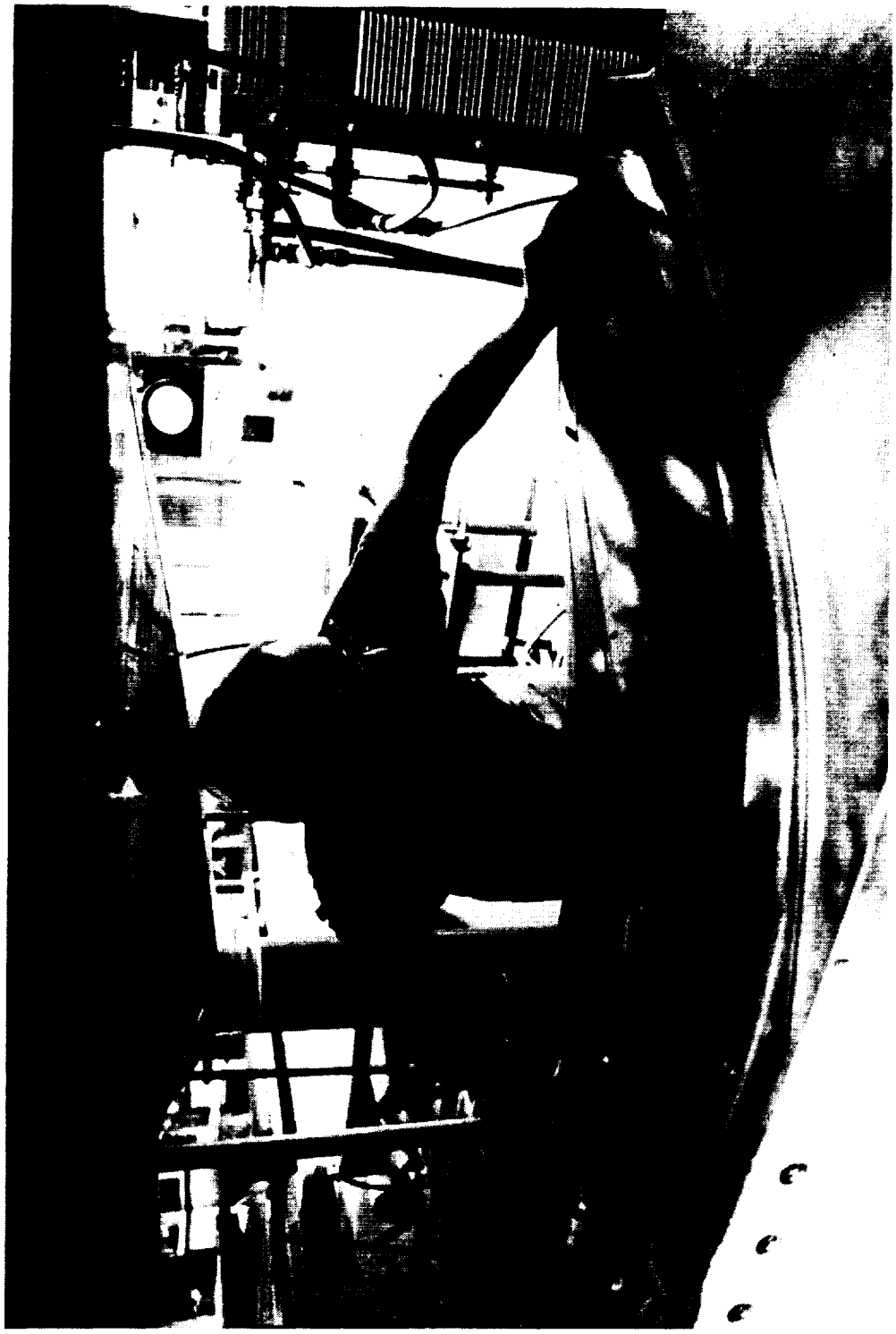

E-37993

FIGURE 6.1 SR-L BLADE IN RESIN INJECTION DIE

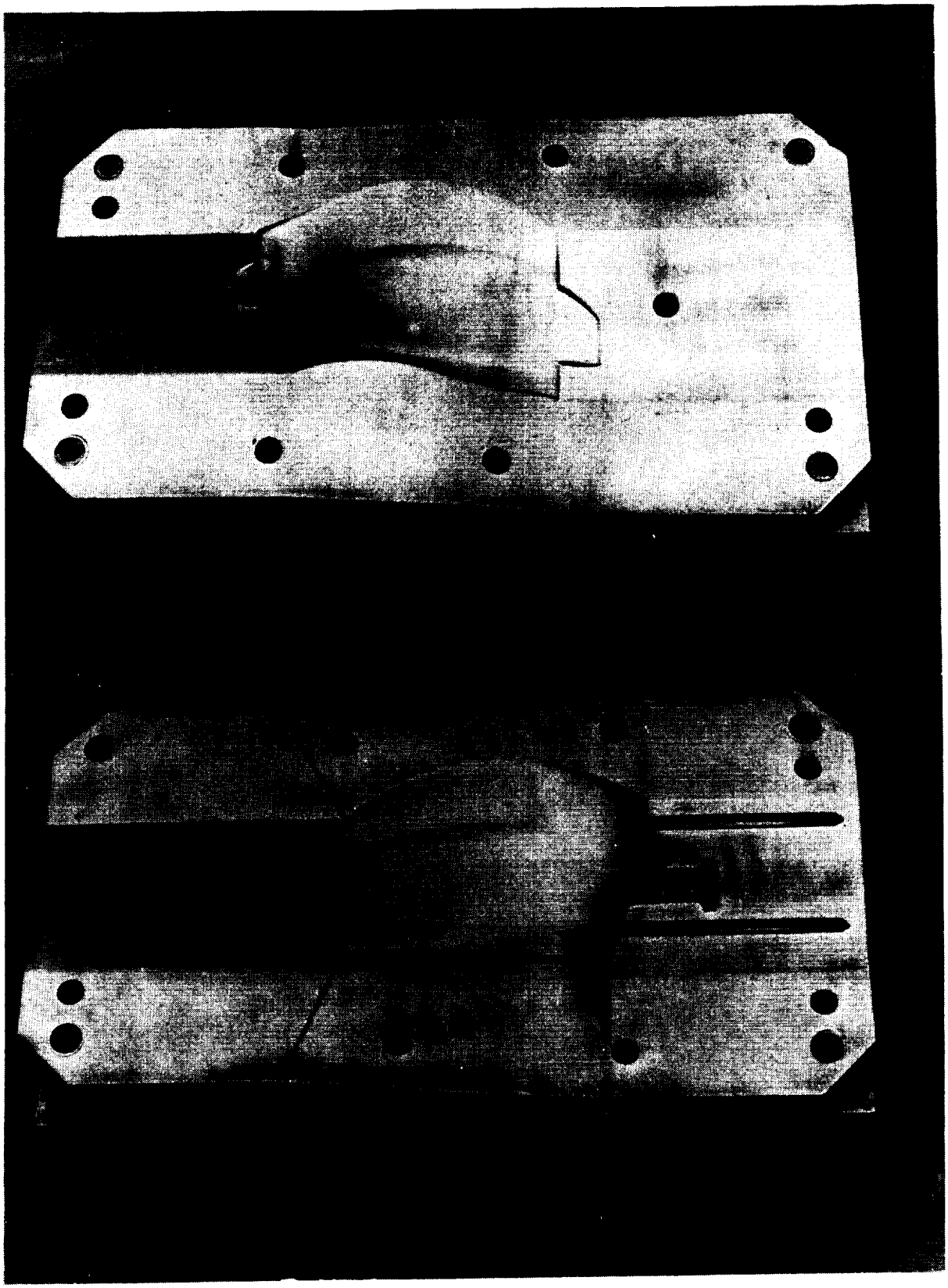

FIGURE 6.2 SR–7A FOAMING MOLD E–37989

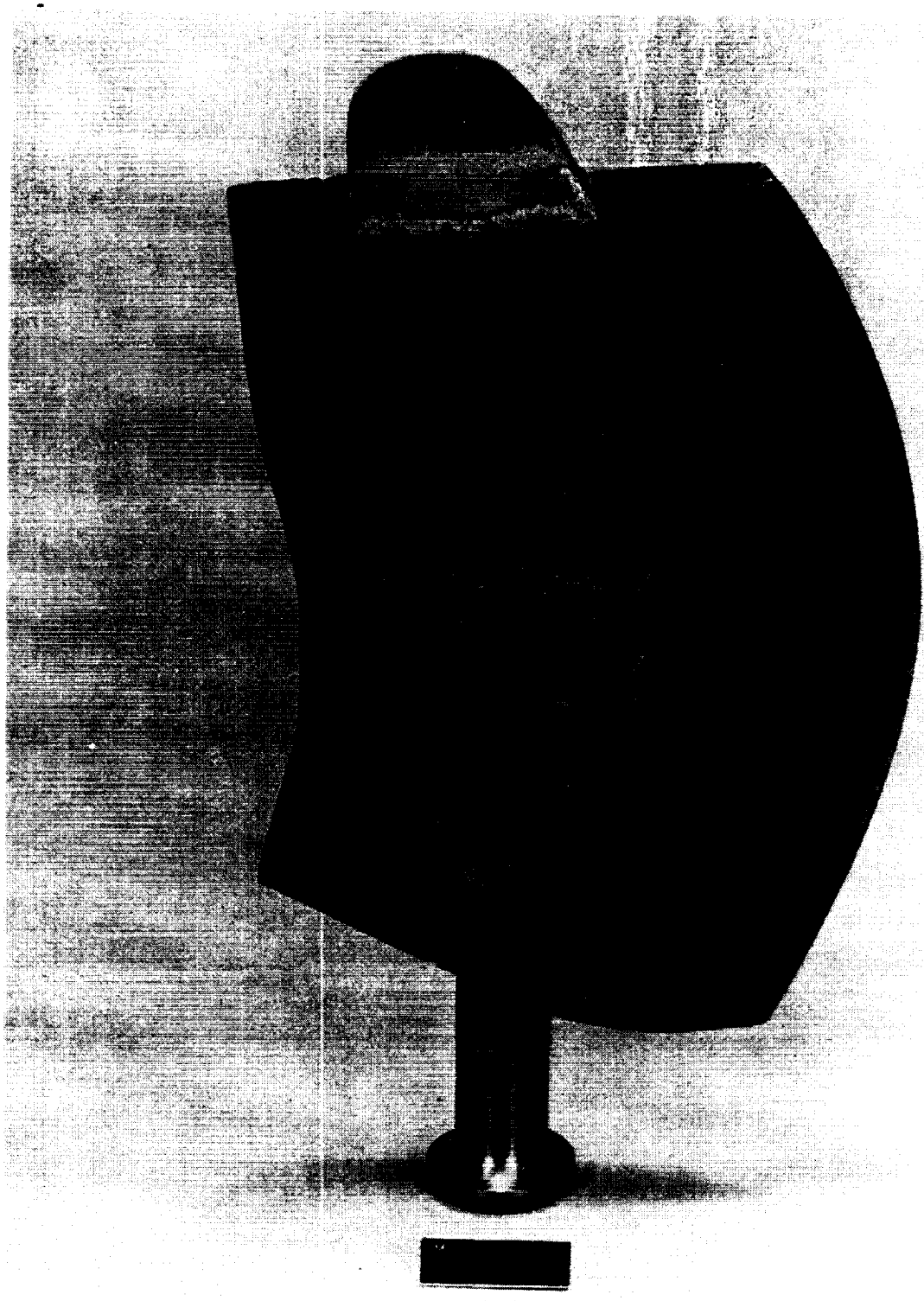

E-37992

FIGURE 6.3 SR-7A SPAR/FOAM ASSEMBLY

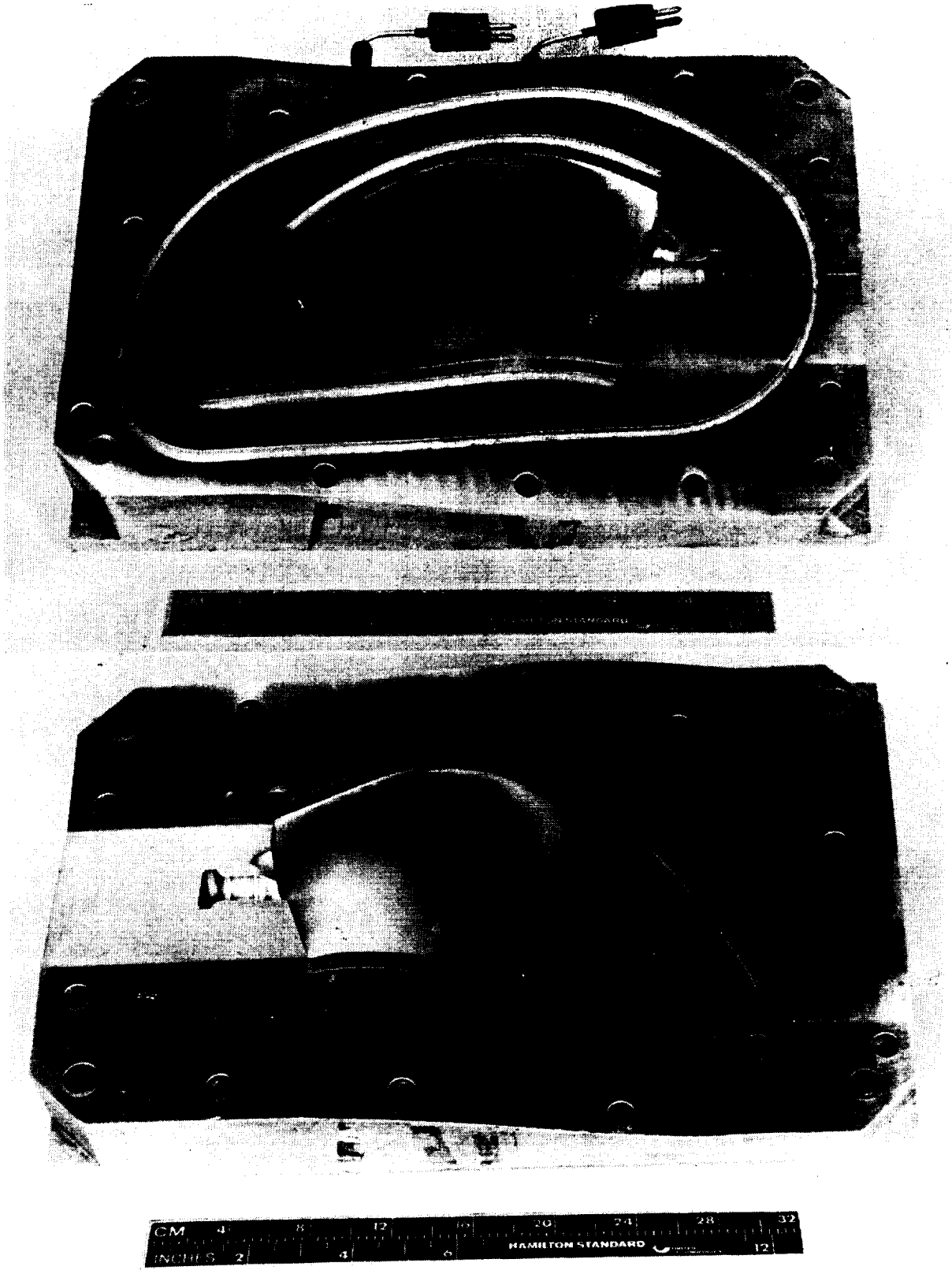

FIGURE 6.4 SR-7A RESIN INJECTION MOLD E-37991

7.0 CONCLUSIONS AND RECOMMENDATIONS

The Large Scale Advanced Prop-Fan Program has added significantly to the understanding of the aerodynamics and aeroelastic performance of single rotation Prop-Fans. No significant acoustic research was conducted during the LAP program. The blade surface pressure data acquired may significantly improve the understanding of blade surface aerodynamics and may lead to further improvements in aerodynamic, acoustic and structural response analysis. The LAP program also verified that Prop-Fan technology can be implemented using state-of-the-art materials and fabrication techniques.

The conclusions and recommendations derived from the LAP program in the areas of aerodynamics, aeroelasticity, acoustics, and materials and fabrication are presented below.

7.1 Conclusions

* The static aerodynamic performance of the SR-7L Prop-Fan corresponded well with analytical predictions for blade angles below 30°. At blade angles above 30° the measured thrust produced and power absorbed were lower than predicted. Blade surface pressure measurements also indicated that the loading distribution on the SR-7L blade was different than expected based on analysis.

* Good agreement between measured and predicted aerodynamic performance for the SR-7L was obtained for operating points in the range from Mach .2 to Mach .73 that were run in the ONERA S1 wind tunnel. This is attributed to the aerodynamic analytical techniques being more accurate at operating conditions where the blade angle of attack is well away from stall. Analysis of blade surface pressure data taken in the wind tunnel at high Mach numbers may further improve the accuracy.

* Reasonable agreement between the measured and predicted blade retention stiffness for the SR-7L Prop-Fan was obtained. However, the variation of the measured and predicted in-plane stiffness using a 3D method was excessive for applications where critical speed placement is more sensitive to retention stiffness.

* A stall buffet phenomena, resulting in high vibratory blade stress, was experienced during high power static operation of the SR-7L Prop-Fan. The onset of the buffet was found to correspond with the point at which measured and predicted static aerodynamic performance begin to diverge. The cause of the stall buffet was not isolated but one hypothesis is that it results from separation caused by the collapse of the blade tip vortex at high blade angles.

* Testing of the SR-7L and SR-7A Prop-Fans indicate that the Large Scale Advanced Prop-Fan is free of stall and unstalled flutter over its entire design operating envelope above Mach 0.2.

* The aeroelastic performance of the SR-7A scale model was found to correspond well with that of the SR-7L Prop-Fan. This verified that the scaling techniques used in the design of the SR-7A model were valid and that aeroelastic models can be used to predict the structural dynamic behavior of full size Prop-Fans.

* The presence of blade tip vorticies indicated in the blade surface pressure data acquired from testing of the SR-7L may be a significant source of Prop-Fan noise at high power, low velocity operating points.

* The successful implementation of Prop-Fan technology in the Large Scale Advanced Prop-Fan, using state-of-the-art materials and fabrication techniques, indicates the readiness of this technology for commercial or military application.

7.2 Recommendations

* Static test results showed that the aerodynamic performance of the SR-7L Prop-Fan was not accurately predicted for high power cases. The measured blade loading distribution was also not accurately predicted by analysis. More effort is needed to improve the analytical tools used to predict Prop-Fan static aerodynamic behavior.

* Experimental determination of the SR-7L blade retention in-plane stiffness revealed a 42% difference from the value calculated by a 3D analysis. Additional research is necessary to improve the accuracy of the analysis.

* The stall buffet phenomena observed during Static Rotor Testing of the SR-7L prevents the Prop-Fan from absorbing full power at design RPM due to high vibratory blade stress. Additional research is necessary to understand the mechanisms causing this phenomena and to design single rotation Prop-Fans that avoid it.

* The LAP High Speed Wind Tunnel test resulted in the acquisition of extensive blade surface pressure data. This data affords the opportunity to significantly improve the analytical tools used in aerodynamics, acoustics, and structural design. Predictions of the SR-7L blade surface pressure distribution, derived from various analytical techniques should be correlated with this data to determine how these techniques could be refined to improve their accuracy.

8.0 LIST OF SYMBOLS

BF - Buoyancy Force, N
C_N - Normal Force Coefficient
C_P - Power Coefficient = $\frac{P}{\rho o\ N^3\ D^5}$

C_T - Thrust Coefficient = $\frac{T}{\rho o\ N^2\ D^4}$

C_{TNET} - Net Thrust Coefficient = $\frac{T_{APP} - BF}{\rho o\ N^2\ D^4}$

D - Diameter, m
J - Advance Ratio = $60\ \frac{V}{ND}$
M - Mach Number
N - Rotational Speed
P - Power, Watt
R - Radius, m
r/R - Fractional radius
SHP - Shaft Horsepower
T - Thrust, N
V - Velocity, m/sec
- Blade Angle, deg
- Mass Density, Kg/m^3

Subscripts

APP - Apparent
N - Number
NET - Net
o - Free Stream
T - Thrust
TNET - Net Thrust

9.0 REFERENCES

1. Billman, L. C., et al, Large Scale Prop-Fan Structural Design Report, NASA CR 174992/174993.

2. Campbell, W. A., Arseneaux, P. J., Wainauski, H. S., Large Scale Advanced Prop-Fan (LAP), High Speed Wind Tunnel Test Report, NASA CR 182125.

3. DeGeorge, C. L., Turnberg, J. E. and Wainauski, H. S., Large Scale Advanced Prop-Fan (LAP), Static Rotor Test Report, NASA CR 180848.

4. Goldstein, S., On the Vortex Theory of Screw Propellers, Proc. Roy. SOC. (1924).

5. Turnberg, J., "Classical Flutter Stability of Swept Propellers", AIAA 83-0847-CP

6. Hanson, D. B., "Propeller Noise Caused by Blade Tip Radial Forces.", AIAA-86-1892.

1. Report No.	2. Government Accession No.	3. Recipient's Catalog No.
NASA CR 182142		

4. Title and Subtitle	5. Report Date
Large Scale Advanced Prop-Fan (LAP) Technology Assessment Report	SEPT. 1988
	6. Performing Organization Code: 73030
7. Author(s): C. L. De George	8. Performing Organization Report No.: HSER 11804
9. Performing Organization Name and Address: Hamilton Standard Division, UTC, P.O. Box 1000, Windsor Locks, CT	10. Work Unit No.: 535-03-01
	11. Contract or Grant No.: NAS3-23051
12. Sponsoring Agency Name and Address: NASA-LEWIS RESEARCH CENTER, 21000 Brook Park Road, Cleveland, Ohio 44135	13. Type of Report and Period Covered: Contractor Report
	14. Sponsoring Agency Code

15. Supplementary Notes

Project Managers: J. Notardonato, I. Sumner, D. Sagerser
Advanced Turboprop Project Office
NASA-Lewis Research Center, Cleveland, Ohio

16. Abstract

This report describes the technologically significant findings and accomplishments of the Large Scale Advanced Prop-Fan (LAP) program in the areas of aerodynamics, aeroelasticity, acoustics and materials and fabrication. The extent to which the program goals related to these disciplines were achieved is discussed, and recommendations for additional research are presented.

The Large Scale Advanced Prop-Fan program consisted of the design, manufacture and testing of a near full-scale Prop-Fan or advanced turboprop capable of operating efficiently at speeds to Mach .8. An aeroelastically-scaled model of the Large Scale Advanced Prop-Fan was also designed and fabricated. The goal of the program was to acquire data on Prop-Fan performance that would indicate the technology readiness of Prop-Fans for practical applications in commercial and military aviation.

17. Key Words (Suggested by Author(s))	18. Distribution Statement
Prop-Fan Aerodynamics Aeroelasticity Acoustics	THIS DOCUMENT WILL REMAIN UNDER DISTRIBUTION LIMITATION UNTIL SEPT. 1989.

19. Security Classif. (of this report)	20. Security Classif. (of this page)	21. No. of Pages	22. Price*
UNCLASSIFIED	UNCLASSIFIED	100	

[redacted]

NASA-C-168 (Rev. 10-75)

25. STIMS 1X ACC# 8810397 IPS-FILE ADABAS # = 237150

FICHE AVAIL	= OK	HARD COPY AVL	= OK	COPYRIGHT	= N
ORIG AGENCY	= NASA	RECEIPT TYPE	= REG	ACQUIS TYPE	= REG
DOCUMENT CLASS	= TRP	ACCESS LEVEL	= 0	ACCESS RESTR	= UNRES
LIMITATION CAT	= NONE	DOCUMENT SEC	= NC	TITLE SECURITY	= NC
SUBJECT CATGRY	= 07	SPECIAL HANDL	=	PAGE COUNT	= 00102
INC AUTHOR LST	= N	INC CNTRCT LST	= N	LANGUAGE	= EN
COUNTRY ORIGIN	= US	COUNTRY FINANC	= US	ABSTRACT PREP	= AUT
PUB DATE	= 19880900	CORP SOURCE	= HD213210		

TITLE = Large scale advanced prop-fan (LAP) technology ass
TITLE = essment report
AUTHOR = DEGEORGE, C. L.
CONTRACT NUM = NAS3-23051
SUPP RESEARCH = 535-03-01
REPORT NUM = NASA-CR-182142
REPORT NUM = NAS 1.26:182142
REPORT NUM = HSER-11804
MAJOR TERMS = AEROACOUSTICS
MAJOR TERMS = AEROELASTICITY
MAJOR TERMS = ENGINE DESIGN
MAJOR TERMS = PROP-FAN TECHNOLOGY
MINOR TERMS = FABRICATION
MINOR TERMS = PROPELLER EFFICIENCY
MINOR TERMS = SCALE MODELS
MINOR TERMS = TURBOPROP ENGINES
ABST AUTHOR = Author
FORM OF INPUT = HC

ABSTRACT = The technologically significant findings and accom
plishments of the Large Scale Advanced Prop-Fan (L
AP) program in the areas of aerodynamics, aeroelas
ticity, acoustics and materials and fabrication ar
e described. The extent to which the program goals
related to these disciplines were achieved is dis
cussed, and recommendations for additional researc
h are presented. The LAP program consisted of the
design, manufacture and testing of a near full-sca
le Prop-Fan or advanced turboprop capable of opera
ting efficiently at speeds to Mach .8. An aeroelas
tically scaled model of the LAP was also designed
and fabricated. The goal of the program was to acq
uire data on Prop-Fan performance that would indic
ate the technology readiness of Prop-Fans for prac
tical applications in commercial and military avia
tion.

********** END OF ADABAS RECORD # 237150 **********